

OPTICAL AND ELECTRICAL CHARACTERIZATION OF $\text{Ga}_{0.75}\text{In}_{0.25}\text{Se}$ LAYERED
SINGLE CRYSTALS

A THESIS SUBMITTED TO
THE GRADUATE SCHOOL OF NATURAL AND APPLIED SCIENCES
OF
MIDDLE EAST TECHNICAL UNIVERSITY

BY

MEHMET IŞIK

IN PARTIAL FULFILLMENT OF THE REQUIREMENTS
FOR
THE DEGREE OF DOCTOR OF PHILOSOPHY
IN
PHYSICS

JANUARY 2013

Approval of the thesis:

OPTICAL AND ELECTRICAL CHARACTERIZATION OF $\text{Ga}_{0.75}\text{In}_{0.25}\text{Se}$ LAYERED SINGLE CRYSTALS

submitted by **MEHMET IŞIK** in partial fulfillment of the requirements for the degree of **Doctor of Philosophy in Physics Department, Middle East Technical University** by,

Prof. Dr. Canan Özgen
Dean, Graduate School of **Natural and Applied Sciences**

Prof. Dr. Mehmet Zeyrek
Head of Department, **Physics**

Prof. Dr. Nizami Hasanli
Supervisor, **Physics Dept., METU**

Examining Committee Members

Prof. Dr. Tofiq Memmedli
Physics Dept., Gazi University

Prof. Dr. Nizami Hasanli
Physics Dept., METU

Assoc. Prof. Dr. Enver Bulur
Physics Dept., METU

Prof. Dr. Ramazan Aydın
Electrical and Electronics Engineering Dept., Atilim University

Assoc. Prof. Dr. Hatice Kökten
Physics Dept., METU

Date:

I hereby declare that all information in this document has been obtained and presented in accordance with academic rules and ethical conduct. I also declare that, as required by these rules and conduct, I have fully cited and referenced all materials and results that are not original to this work.

Name, Last Name : Mehmet Işık

Signature :

ABSTRACT

OPTICAL AND ELECTRICAL CHARACTERIZATION OF $\text{Ga}_{0.75}\text{In}_{0.25}\text{Se}$ LAYERED SINGLE CRYSTALS

Işık, Mehmet
Ph. D., Department of Physics
Supervisor: Prof. Dr. Nizami Hasanli

January 2013, 93 pages

In the present thesis, optical and electrical properties of $\text{Ga}_{0.75}\text{In}_{0.25}\text{Se}$ layered single crystals have been studied.

The optical properties of the crystals have been investigated by means of visible and infrared reflectivity and transmittance, ellipsometry, Raman spectroscopy, photoluminescence (PL) and thermoluminescence (TL) measurements. The analysis of the absorption data at room temperature revealed the existence of indirect transitions in the crystal. Moreover, the rate of change of the band gap energy with temperature was calculated from the analysis of the temperature dependence of transmission measurements. The spectroscopic ellipsometry measurements on $\text{Ga}_{0.75}\text{In}_{0.25}\text{Se}$ crystals were also performed to get detailed information about the real and imaginary parts of the pseudodielectric function, pseudorefractive index and pseudoextinction coefficient. The critical point analysis of the second derivative spectra of the dielectric function was done to reveal the interband transition energies. The vibrational spectra of $\text{Ga}_{0.75}\text{In}_{0.25}\text{Se}$ crystals were studied by means of infrared reflectivity and transmittance and Raman scattering. The refractive and absorption indices, the frequencies of transverse and longitudinal optical modes, high- and low-frequency dielectric constants were obtained from the analysis of the IR reflectivity spectra. PL experiments were carried out as a function of temperature and excitation laser intensity to get detailed knowledge about the recombination levels in $\text{Ga}_{0.75}\text{In}_{0.25}\text{Se}$ crystals. The observed emission bands in PL spectra were interpreted as the transitions from donor levels to an acceptor level.

Electrical characterization of the crystal have been performed using dark electrical conductivity, space charge limited current, photoconductivity and thermally stimulated current (TSC) measurements. The detailed information about the localized levels in the band gap has been obtained from the analysis. The photoconductivity measurements were performed to determine the dominant recombination mechanism in the crystal.

Defect centers in the crystal were characterized from TSC and TL measurements accomplished in the low temperature range. The activation energies, attempt-to-escape frequencies, concentrations and capture cross sections of the traps were calculated from the analysis of the experimental data.

Keywords: Semiconductor Crystals, Optical Properties, Electrical properties, Defects.

ÖZ

Ga_{0,75}In_{0,25}SE KATMANLI TEK KRİSTALLERİNİN OPTİKSEL VE ELEKTRİKSEL KARAKTERİZASYONLARI

Işık, Mehmet
Doktora, Fizik Bölümü
Tez Yöneticisi: Prof. Dr. Nizami Hasanlı

Ocak 2013, 93 sayfa

Sunulan tezde, Ga_{0,75}In_{0,25}Se katmanlı tek kristallerinin optiksel ve elektriksel özellikleri çalışıldı.

Kristalin optiksel özellikleri görünür ve kızılötesi yansıma ve geçirgenlik, elipsometri, Raman spektroskopisi, fotoluminesans (PL) ve termoluminesans (TL) ölçümleri sayesinde incelendi. Oda sıcaklığındaki absorpsiyon datasının analizleri kristal içerisinde dolaylı geçişlerin varlığını açıkladı. Ayrıca, bant enerjisinin sıcaklık ile değişim oranı sıcaklığa bağlı geçirgenlik ölçümlerinin analizlerinden hesaplandı. Ga_{0,75}In_{0,25}Se kristalinin spektroskopik elipsometri ölçümleri, psödodielektrik fonksiyonunun reel ve sanal kısımları, psödokırıcılık indisi ve psödösönme katsayısı hakkında daha detaylı bilgi almak için gerçekleştirildi. Dielektrik fonksiyonunun ikinci türevinin spektrasının kritik nokta analizleri bant arası geçiş enerjilerinin bulunması için yapıldı. Ga_{0,75}In_{0,25}Se kristallerinin titreşimsel spektrumu kızılötesi yansıtıcılık ve transmitans ve Raman saçılımı aracılığı ile çalışıldı. Kırıcılık ve absorpsiyon indisleri, enine ve boylamasına optik modların frekansları, yüksek ve düşük frekans dielektrik sabitleri kızılötesi yansıtıcılık spektrumunun analizlerinden elde edildi. Ga_{0,75}In_{0,25}Se tek kristallerinin rekombinasyon merkezleri hakkında detaylı bilgi elde etmek için sıcaklığa ve uyarma lazer yoğunluğuna bağlı PL deneyleri gerçekleştirildi. PL spektrasında gözlemlenen emisyon bandları donör seviyesinden alıcı seviyesine geçiş olarak yorumlandı.

Kristalin elektriksel karakterizasyonu karanlık elektriksel iletkenlik, sınırlı boşluk yükü akımı, fotoiletkenlik ve ısıluvarılmış akım (TSC) ölçümleri kullanılarak gerçekleştirildi. Band boşluğu içerisindeki lokalize seviyeler hakkında detaylı bilgiler analizlerden elde edildi. Fotoiletkenlik ölçümleri kristal içerisindeki dominant rekombinasyon mekanizmalarına karar vermek için gerçekleştirildi.

Kristal içerisindeki kusur merkezleri düşük sıcaklık aralığında gerçekleştirilen TSC ve TL ölçümleri ile karakterize edildi. Tuzakların aktivasyon enerjileri, kaçış frekansları, konsantrasyonları ve yakalama kesit alanları deneysel datanın analizlerinden hesaplandı.

Anahtar Kelimeler: Yarıiletken kristaller, Optiksel özellikler, Elektriksel özellikler, Kusurlar.

ACKNOWLEDGEMENTS

First, I would like to express my sincere gratitude to my supervisor Prof. Dr. Nizami Hasanli for his invaluable guidance and support during my graduate career. I have learned a great deal both professionally and personally from him. He has been supportive at all stages of my graduate life more than I had ever expected and beyond his role as a professor and supervisor.

I would like to thank Assoc. Prof. Dr. Enver Bulur for his support and suggestions in this work. It is hardly possible to be guided by such an experienced researcher.

I wish to thank my committee members Prof. Dr. Tofiq Memmedli, Prof. Dr. Ramazan Aydın and Assoc. Prof. Dr. Hatice Kökten for their assistances.

I am also thankful to Prof. Dr. Raşit Turan (METU), Prof. Dr. Süleyman Özçelik (Gazi University), Prof. Dr. Atilla Aydınli (Bilkent University) and Assist. Prof. Dr. Filiz Korkmaz Özkan (Atılım University) for letting me perform my experiments in their laboratories.

I would like to thank Prof. Dr. Atef Qasrawi for his invaluable support and incentive during my graduate education.

I would like to express my special thanks to Dr. İpek Güler. She was so helpful, kindles and collaborative when I need a help about my experiments. I would also like to express my appreciation to S. Şebnem Çetin for her worthy sharing about the ellipsometry measurements.

My special thanks to Atılım Physics Group members and technician İbrahim Aydemir for his big assistance with all types of technical problems.

Finally, my most sincere gratitude and appreciation go to my family and especially to my lovely wife Duygu. It is a big chance to have such a supportive, understanding, lovely and patient wife. Without her I would never able to finish my work so comfortable.

To My Father

TABLE OF CONTENTS

ABSTRACT	iv
ÖZ	v
ACKNOWLEDGEMENTS	vi
TABLE OF CONTENTS	viii
LIST OF TABLES	x
LIST OF FIGURES	xi

CHAPTER

1. INTRODUCTION.....	1
1.1. Previous Studies on Ga _x In _{1-x} Se	4
1.2. Present Study	4
2. THEORETICAL APPROACH	6
2.1. Introduction.....	6
2.2. Electronic Properties of Semiconductors	6
2.2.1. Band Structure of Semiconductors	6
2.2.2. Defects.....	9
2.2.3. Intrinsic and Extrinsic Semiconductors.....	11
2.3. Theoretical Approach to Characterization Techniques.....	13
2.3.1. X-ray Diffraction	13
2.3.2. Energy Dispersive Spectral Analysis	15
2.3.3. Optical Absorption, Transmission and Reflection	15
2.3.3.1. Absorption	15
2.3.3.2. Reflection	15
2.3.3.3. Transmission	16
2.3.4. Ellipsometry	17
2.3.4.1. p- and s-polarized light waves	17
2.3.4.2. Measured values in ellipsometry	19
2.3.4.3. Pseudodielectric function	20
2.3.4.4. Critical Point Analysis	20
2.3.5. Infrared Spectroscopy	20
2.3.5.1. Fourier Transform Infrared Measurements	21
2.3.5.2. Raman Spectroscopy	21
2.3.5.3. Kramers-Kronig Dispersion Relations	22
2.3.6. Thermally Stimulated Current and Thermoluminescence.....	22
2.3.6.1. Electronic Transitions in TSC and TL Methods.....	22
2.3.6.2. Theoretical Approach	24
2.3.6.3. Curve Fitting	28
2.3.6.4. Initial Rise Method	30
2.3.6.5. Peak Shape Method	30
2.3.6.6. Differential Analysis Method	30
2.3.6.7. Various Heating Rate Method	31
2.3.7. Photoluminescence Experiments	31
2.3.7.1. Recombination Mechanisms	32
2.3.7.2. Laser Excitation Power Dependence of Photoluminescence Peak Energy	34
2.3.7.3. Temperature Dependence of Photoluminescence	35
2.3.8. Electrical Measurements	36

2.3.8.1. Electrical Conductivity	36
2.3.8.2. Space Charge Limited Currents	36
2.3.8.3. Photoconductivity	37
3. EXPERIMENTAL TECHNIQUES	38
3.1. Introduction	38
3.2. Energy Dispersive Spectral Analysis	38
3.3. X-ray Diffraction Experiments	38
3.4. Transmission and Reflection Experiments	40
3.5. Ellipsometry Experiments	41
3.6. Infrared and Raman Spectroscopy Measurements	41
3.7. Photoluminescence Experiments	41
3.8. Electrical Measurements	42
3.9. Thermally Stimulated Current Experiments	44
3.10. Thermoluminescence Experiments	45
3.11. Photoconductivity Decay Experiments	47
4. RESULTS AND DISCUSSION	48
4.1. Introduction	48
4.2. X-ray Diffraction and Energy Dispersive Spectral Analysis	48
4.3. Transmission and Reflection Experiments	50
4.4. Ellipsometry Measurements	55
4.5. Infrared and Raman Spectroscopy Measurements	59
4.6. Photoluminescence Measurements	64
4.7. Temperature Dependence of Dark Electrical Resistivity	69
4.8. Space Charge Limited Current Analysis	70
4.9. Temperature Dependence of Photocurrent Measurements	72
4.10. Thermally Stimulated Current Measurements	74
4.11. Thermoluminescence Measurements	78
5. CONCLUSION	83
REFERENCES	86
CURRICULUM VITAE.....	91

LIST OF TABLES

TABLES

Table 2.1	Characteristics of the seven crystal classes.....	14
Table 3.1	The applied currents between contact pairs, measured potential differences between neighboring contacts and corresponding resistances	43
Table 4.1	X-ray powder diffraction data for $\text{Ga}_{0.75}\text{In}_{0.25}\text{Se}$ crystal	50
Table 4.2	Critical point energies for $\text{Ga}_{0.75}\text{In}_{0.25}\text{Se}$ and GaSe single crystals.....	58
Table 4.3	The frequencies of IR and Raman modes (cm^{-1}) of GaSe, InSe and $\text{Ga}_{0.75}\text{In}_{0.25}\text{Se}$ crystals, and attributions of IR transmittance minima due to two-phonon absorption processes in $\text{Ga}_{0.75}\text{In}_{0.25}\text{Se}$ crystal.....	63
Table 4.4	The activation energy (E_t), capture cross section (S_t), attempt-to-escape frequency (ν) and concentration (N_t) of observed trap of $\text{Ga}_{0.75}\text{In}_{0.25}\text{Se}$ crystal from TSC measurements	77
Table 4.5	The activation energy (E_t), capture cross section (S_t) and attempt-to-escape frequency (ν) of observed traps of $\text{Ga}_{0.75}\text{In}_{0.25}\text{Se}$ crystal from TL measurements.....	80

LIST OF FIGURES

FIGURES

2.1 (a) Schematic representation of the dependence of potential energy of an electron in a one-dimensional crystal lattice. (b) Kronig-Penney model approximation to the realistic potential energy.....	7
2.2 The extended-zone representation of the dependence of energy on k -vector.....	8
2.3 Simple diagram of the reduced-zone representation.....	8
2.4 Schematic diagram of (a) direct and (b) indirect band structures.....	9
2.5 Representation of different point defect types in the semiconductors.....	10
2.6 (a) Edge dislocation; (b) Screw dislocation.....	11
2.7 The doped Silicon crystals with (a) Phosphor atom (n-type doping), (b) Boron atom (p-type doping).....	12
2.8 Representation of the (a) donor and (b) acceptor levels in the forbidden energy gap.....	13
2.9 Representation of x-ray diffraction by a crystal lattice.....	14
2.10 Reflection of p- and s- polarized light waves.....	17
2.11 Representation of magnetic and electric fields in the p- and s-polarization.....	18
2.12 The processes in the FTIR measurements	21
2.13 Possible electronic transitions in the TSC and TL techniques. (a) band-to-band excitation; (b) and (e) electron and hole trapping, respectively; (c) and (f) electron and hole release; (d) and (g) indirect recombination; (h) direct recombination. Solid circles, open circles and arrows represent electrons, holes and transitions, respectively.....	23
2.14 Simple diagram of the band structure consisting one electron and one hole trap	24
2.15 Representation of the (a) excitation, (b) thermalization and (c) recombination mechanisms in the energy band gap structure.....	32
2.16 Possible transitions in the band structure.....	32
2.17 Schematic diagram of the absorption transitions in (a) direct band gap semiconductors and (b) indirect band gap semiconductors.....	33
3.1 Schematic representation of scanning electron microscope.....	39
3.2 Simple schematic representation of XRD experiment.....	39

3.3	Simple schematic representation of (a) transmission (b) reflection experimental set-up	40
3.4	Simplified block diagram of the PL measurement set-up.....	42
3.5	Representation of the contacts on arbitrary shaped van der Pauw geometry	43
3.6	Simple representation of the sample with sandwich configuration.....	44
3.7	Simplified block diagram for TSC experimental set-up.....	45
3.8	Simplified block diagram of the TL experimental set-up.....	46
3.9	Simplified block diagram of photoconductivity decay experimental set-up.....	47
4.1	Energy dispersive spectroscopic analysis of Ga _{0.75} In _{0.25} Se crystal.....	49
4.2	X-ray powder diffraction pattern of Ga _{0.75} In _{0.25} Se crystal.....	49
4.3	The spectral dependence of transmission for Ga _{0.75} In _{0.25} Se crystal in the temperature range of 10–300 K. Inset: The spectral dependence of reflectivity at room temperature.....	51
4.4	The dependence of $(ahv)^{1/2}$ on photon energy in the temperature range of 10–300 K.....	52
4.5	The indirect band gap energy as a function of temperature. The circles are experimental data and the solid line represents the fit according to equation 2.111.....	53
4.6	The variation of refractive index as a function wavelength at room temperature. Inset: The circles show experimental data. The solid line represents the fit according to equation 2.19 in the low energy region.....	54
4.7	Plot of $(n^2-1)^{-1}$ vs. $(hv)^2$ in the $hv < E_g$ range at room temperature. Open circles are experimental data and the solid line represents the fit using equation 2.14.....	54
4.8	The spectrum of the ϵ_1 in the 600–1100 nm wavelength range at room temperature. The inset represents the spectrum of the ϵ_2 in the same range.....	55
4.9	(a) The spectra of the pseudodielectric function of Ga _{0.75} In _{0.25} Se. Solid and dot-dashed curves represent the real and imaginary part spectra, respectively. (b) The spectra of the refractive index and extinction coefficient Solid and dot-dashed curves represent the refractive index and extinction coefficient spectra, respectively.....	56
4.10	The spectral dependence of reflectivity R of Ga _{0.75} In _{0.25} Se crystal.....	57
4.11	Second-energy derivative of the dielectric function of Ga _{0.75} In _{0.25} Se. Stars and open circles represent the second-energy derivative spectra of the real and imaginary part of the dielectric function, respectively. The solid and dot-dashed curves show the fit to the experimental data.....	58
4.12	Sketch of the electronic energy band structure of Ga _{0.75} In _{0.25} Se crystal near the bandgap at the Brillouin zone center	59
4.13	The spectral dependencies for Ga _{0.75} In _{0.25} Se crystal: (a) Infrared reflectivity; (b) ϵ_2 and $\text{Im}(1/\epsilon)$; (c) Optical constants n and k	60
4.14	Unpolarized Raman scattering spectrum of Ga _{0.75} In _{0.25} Se crystal	61

4.15 Infrared transmittance spectrum of Ga _{0.75} In _{0.25} Se crystal	62
4.16 PL spectra of Ga _{0.75} In _{0.25} Se crystal in the 7–59 K temperature range and 580–670 nm wavelength region with excitation laser intensity of $L = 1.40 \text{ W cm}^{-2}$	64
4.17 Deconvolution of the PL spectrum into Gaussian lineshapes at $T = 7 \text{ K}$	65
4.18 Temperature dependencies of observed A- and B-band intensities for Ga _{0.75} In _{0.25} Se crystal. Circles and triangles are experimental data. Solid curves show the theoretical fits using equation 2.109. Inset: Temperature dependence of emission band energies	66
4.19 PL spectra of Ga _{0.75} In _{0.25} Se crystal for different excitation laser intensities at $T = 7 \text{ K}$	67
4.20 Dependence of emission band energies on excitation laser intensity at $T = 7 \text{ K}$. Stars are experimental data. Solid curves represent the theoretical fit using equation 2.105. Inset: Dependence of PL intensities at the emission band maximums versus excitation laser intensity at $T = 7 \text{ K}$. The solid lines show the theoretical fit using equation 2.104	68
4.21 Proposed energy band diagram for Ga _{0.75} In _{0.25} Se crystal	69
4.22 Temperature dependence of resistivity of Ga _{0.75} In _{0.25} Se crystal. The inset shows the linear fit (solid line) of the experimental data (circles)	70
4.23 The variation of current density as a function of applied voltage. Inset shows the $\ln(\theta) - T^{-1}$ variation. Circles are experimental data and solid line is the linear fit	71
4.24 The $\ln(J) - \ln(V)$ characteristics in the SCL region	72
4.25 Variation of I_{ph} with F at different temperatures for Ga _{0.75} In _{0.25} Se crystals	73
4.26 The temperature dependence of photocurrent at various illumination intensities	73
4.27 TSC spectra of Ga _{0.75} In _{0.25} Se crystal for various illumination times. Inset: the dependence of peak maximum current on illumination time. The dash-dotted lines are only guides for the eye	74
4.28 Typical experimental TSC curves of Ga _{0.75} In _{0.25} Se crystal under opposite bias voltage. Circles and stars represent the experimental data obtained at illumination of positive and negative contacts, respectively	75
4.29 Experimental TSC spectrum of Ga _{0.75} In _{0.25} Se crystal with heating rate of 0.8 K/s. Open circles are experimental data. Solid curve shows the fit to the experimental data	76
4.30 Thermally stimulated current vs. $1000/T$. The circles present the experimental data and the line represents the theoretical fit using initial rise method	76
4.31 Derivative of the thermally stimulated current. Open circles are experimental data and the line is the tangent at $T_m = 156.7 \text{ K}$	77
4.32 Photoconductivity decay curve for the Ga _{0.75} In _{0.25} Se crystal. Open circles are experimental data. Solid line shows the fit to the experimental data	78
4.33 TL curves of Ga _{0.75} In _{0.25} Se crystals for different illumination times at a constant heating rate $\beta = 1.0 \text{ K/s}$. Inset: Maximum value of TL intensity as a function of illumination time. The dash-dotted line is only guide for the eye	79

- 4.34 Experimental TL curve of $\text{Ga}_{0.75}\text{In}_{0.25}\text{Se}$ crystal with heating rate $\beta = 1.0$ K/s and decomposition of this curve into four separate peaks. Open circles are experimental data. Dashed curves represent decomposed peaks. Solid curve show total fit to the experimental data80
- 4.35 TL intensity vs. $1000/T$ for observed peaks in TL spectra of $\text{Ga}_{0.75}\text{In}_{0.25}\text{Se}$ crystal. Open circles are experimental data and solid lines are the fitted straight lines81
- 4.36 Experimental TL glow curves of $\text{Ga}_{0.75}\text{In}_{0.25}\text{Se}$ crystal before (stars) and after (circles) thermal cleaning for a heating rate of $\beta = 1.0$ K/s. Inset: Experimental TL curve after thermal cleaning and decomposition of this curve into two separate peaks. Open circles are experimental data. Dashed curves represent decomposed peaks. Solid curve show total fit to the experimental data.....82
- 4.37 Experimental TL curve of $\text{Ga}_{0.75}\text{In}_{0.25}\text{Se}$ crystal with different heating rates. Inset: $\ln(T_m^2/\beta)$ versus $1000/T_m$ for different heating rates. Open circles are experimental data and solid line shows the theoretical fit to the experimental data82

CHAPTER 1

INTRODUCTION

Semiconductors are materials which have band gap energies between those of insulators and conductors. In the last forty years, researches on the semiconductor materials and devices picked up. The usage areas of the semiconductor devices have been increasing, especially in the electronic circuits and photo-electronic applications. The most attractive property of the semiconductor materials is the possibility of controlling their physical properties in the desired way. The elements of the III, IV, V, VI groups and compounds produced from the combination of these elements with each other are the most used materials in the semiconductor device applications. Therefore, the characterization of these elements and compounds provide important contributions to the semiconductor technology.

Among the many important semiconducting compounds, the A^{III}B^{VI} type has become very attractive due to their structural, optical and electrical properties. GaSe and InSe layered crystals are used in many areas such as solar cells, optoelectronic device applications, nonlinear optical applications. The feasibility of mixed crystals in a large range of compositions allows varying in a wide range of some parameters like the band gap energy, conduction type, photosensitivity, carrier mobility, etc. GaSe and InSe compounds form a restricted series of mixed crystals Ga_xIn_{1-x}Se. Saintonge and Brebner showed that the quality of Ga_xIn_{1-x}Se mixed crystals becomes very poor as x approaches to some solubility limits [1]. Their growth experiences revealed these limits as $0 \leq x \leq 0.2$ and $0.75 \leq x \leq 1$. In the present thesis, we have performed our studies focusing on the optical and electrical properties of Ga_{0.75}In_{0.25}Se ($x = 0.75$) crystal. Among Ga_xIn_{1-x}Se mixed crystals in the limits of solubility ($0.75 \leq x \leq 1$), this crystal is the most distinctive one showing properties like GaSe. Moreover, the trapping centers existed in the undoped crystals which are important for functioning of optoelectronic devices, were studied by means of thermally stimulated current (TSC) and thermoluminescence (TL) experiments.

In the literature, there are many studies on the constituent compounds, GaSe and InSe, but few papers concerning the characterization of the Ga_xIn_{1-x}Se mixed crystals. Firstly, it will be worthwhile to give information about the results of the researches on the constituent crystals GaSe and InSe, and then on Ga_xIn_{1-x}Se mixed crystals.

GaSe and InSe layered semiconductor crystals are characterized by a highly anisotropic bonding forces. The reason of this high anisotropy comes from the fact that the bonding within the layers is rather stronger than bonding perpendicular to layers. In GaSe and InSe, the forces corresponding to interlayer interaction are predominantly van der Waals type [2]. On the other hand, covalent bonding forces are effective within the layers. GaSe and InSe crystal structures consist of four monatomic sheets in the order Se-Ga-Ga-Se and Se-In-In-Se, respectively [3-8]. A single layer is hexagonally ordered and c -axis is perpendicular to the layers.

The lattice parameters a and c of the hexagonal structure of GaSe crystals were calculated as 0.375 and 1.595 nm, respectively [9]. The optical properties of GaSe crystals have been extensively studied in the literature. Karabulut et al. found the direct band gap energy of the undoped GaSe crystals as 1.985 eV at room temperature [10]. In Ref. [11], it was shown that as grown GaSe is a p-type semiconducting material having an indirect band gap with energies of 2.065 and 2.075 eV at 77 and 4.2 K, respectively.

Optical characterization studies on GaSe single crystals were extended using ellipsometry and electroreflectance measurements. Ellipsometry measurements revealed the spectral dependencies of the components of the pseudodielectric function, pseudorefractive index and pseudoextinction coefficient [12]. Moreover, the results of the analysis on the second-energy-derivative spectra of the pseudodielectric function showed the presence of seven critical points in the electronic band structure of the GaSe crystals.

The temperature dependencies of the Raman-active mode frequencies and linewidths in GaSe were studied in the frequency range of $10\text{-}320\text{ cm}^{-1}$ [13]. The measurements performed in the $15\text{-}300\text{ K}$ temperature range showed that the optical phonon lines softens and broadens with increasing temperature. Analysis revealed that Raman frequency shift and broadening of linewidths are well described by considering the thermal-expansion, pure-temperature (phonon-phonon coupling) and crystal disorder contributions.

PL measurements were carried out by Aydinli et al. on the undoped semiconducting GaSe [14]. The experiments performed in the $10\text{-}300\text{ K}$ range resulted with two wide bands. The temperature dependence of the emitted intensities revealed the presence of two shallow acceptor levels at 14 and 76 meV . Authors inferred that there exist two deep donor levels at 163 and 264 meV .

In Ref. [15], TSC measurements were studied in the temperature range of $10\text{-}300\text{ K}$ to characterize the trapping centers in undoped GaSe crystals. The results showed the presence of three centers with activation energies of 0.02 , 0.10 and 0.26 eV . Moreover, the capture cross sections, trap concentrations and attempt-to-escape frequencies of the levels were determined.

The electrical characterization of GaSe crystals have also been examined to get detailed information about the usage importance of the crystals in photoelectric applications. Manfredotti et al. carried out their electrical measurements in the temperature range of $77\text{-}850\text{ K}$ [16]. The resistivity of the studied crystals varied from 10^2 to $10^6\text{ }\Omega\text{cm}$ depending on growth conditions.

InSe, the minor constituent of $\text{Ga}_{0.75}\text{In}_{0.25}\text{Se}$, has also been characterized to study the structural, optical and electrical properties.

C. De Blasi et al. [17] studied electrical properties of undoped n-type InSe crystals by carrying out resistivity, Hall effect and space-charge-limited-current (SCLC) measurements in the temperature range of $100\text{-}300\text{ K}$. The results of the measurements revealed two donor levels located at about 0.10 and 0.34 eV . It was also shown that the donor level at 0.34 eV affects the SCLC at room temperature. The room temperature Hall mobility of the InSe crystals was found as $400\text{ cm}^2/\text{Vs}$.

Ellipsometry measurements on single crystals InSe were carried out in the energy range of $1.5\text{-}9.2\text{ eV}$ [18]. The spectra of pseudodielectric function and pseudorefractive index were given as a result of these experiments. Moreover, the critical point analysis was accomplished on the second derivative spectra of the pseudodielectric function. The analysis revealed the presence of twelve critical point energies in the studied energy range.

Kundakci et al. investigated the Urbach tail and electric field influence on optical properties of InSe crystals [19]. The band gap energies at 10 K were found as 1.358 eV and 1.348 eV under 0 and 30 V applied voltages, respectively. The temperature dependencies of the Urbach energy and steepness parameter were also determined.

Abay et al. carried out PL experiments on n-InSe crystals in the temperature range of $10\text{-}210\text{ K}$ [20]. Four peaks at 1.334 , 1.306 , 1.288 and 1.232 eV were observed at 10 K . These peaks were attributed to radiative recombination of the direct free exciton, an impurity-band transition, a donor-acceptor recombination channel and the transition within an impurity-vacancy complex, respectively.

TSC measurements were also performed on the InSe crystals to characterize the trapping centers [21]. The analysis of the measurements carried out in the temperature range of $50\text{-}300\text{ K}$ brought out three trapping centers located at 60 , 160 and 340 meV below the conduction band. Their capture cross sections, concentrations and attempt-to-escape frequencies were also determined.

GaSe and InSe are important materials in fields of both fundamental research and technical applications because of their characteristic properties. In addition to the above given

characterizations of GaSe and InSe, there are also some studies concerning the technological applications of the crystals.

Sigetomi et al. studied the electrical and photovoltaic properties of undoped and Cu-doped *p*-GaSe/*n*-InSe heterojunction [22]. Transport and phototransport properties were investigated using capacitance-voltage, current-voltage, and the spectral response of short-circuit current measurements. The efficiency parameters under illumination were estimated using open-circuit voltage and short-circuit current. The low resistivity of Cu-doped GaSe is an effective property for the electrical and photovoltaic properties of GaSe/InSe heterojunctions.

Iwamura et al. investigated the configuration dependence of the absorption edge shift of GaSe crystal due to the applied electric field [23]. They have also described the switching characteristics and proposed a device in which 100% intensity modulation of light from a He-Ne laser (632.8 nm) can be made possible by a new GaSe device driven directly by a transistor. The absorption edge was 623 nm without applying voltage to the sample. When the voltages of 10-20 V were applied to the sample, it was observed that absorption edge moves toward longer wavelength. The shift for 20 V applied voltage was observed as 20 nm (63 meV). Since the absorption edge moved to wavelength longer than 632.8 nm, the authors proposed a light modulator for the He-Ne laser.

Far-infrared conversion applications of GaSe crystal have been investigated in Ref. [24]. Crystals transmitted light between 0.65 to 18 μm range which is wider and more appropriate than the range of other nonlinear optical materials, such as AgGaSe_2 , ZnGeP_2 , Tl_3AsSe_3 crystals. Moreover, measurements of second harmonic conversion efficiency for 9.6 μm wavelength yielded values between 62 to 75 $\mu\text{m}/\text{V}$ depending on the quality of crystals. GaSe samples could not be damaged with the 1.3 J/pulse, which corresponds to an energy density of 3.7 J/cm^2 . With these positive properties, GaSe was thought to be an exciting material for nonlinear optical applications.

Abdullaev et al. have investigated the efficiency of the GaSe single crystals for the second harmonic generation (SHG) of CO_2 laser pulses [25]. The efficiency of SHG in GaSe crystal of 0.65 cm thickness was up to 9%. SHG parameters of the GaSe and ZnGeP_2 crystals which are suitable materials for this SHG purpose were compared. The results indicated that GaSe can compete successfully with ZnGeP_2 for frequency doubling of CO_2 laser radiation.

Tunable SHG of pulsed CO_2 laser radiation in a GaSe crystal was presented in Ref. [26]. For tunable SHG, short pulsed CO_2 laser was used and SH radiation waveform at 4.8 μm was detected for incident laser beam with 9.6 μm . Fourier transform infrared (FTIR) spectroscopy measurements showed that 8 mm thick GaSe crystal is transparent in the 2.5-18 μm spectral region. The spectral dependence of SHG efficiency in the 4.6-5.3 μm range was studied to understand the performance of the crystal to be used as a frequency doubling converter.

GaSe and InSe crystals are attractive materials in the electronic device applications. As a one of these applications, Kyazym-zade et al. have developed GaSe and InSe detectors [27]. The photosensitivity of Pt-*n*-InSe and Pt-*p*-GaSe structures was investigated. The measurements and analysis revealed that these detectors show nearly same performance with silicon detectors under the same experimental conditions. However, GaSe and InSe detectors have additional advantages, such as simpler design and fabrication method, the absence of injection, a high sensitivity in a wide energy range and the presence of a fast recombination channel.

Taking into consideration the above-mentioned technological applications, $\text{Ga}_{0.75}\text{In}_{0.25}\text{Se}$ single crystals can be thought as an important candidate to be used in the relevant technological areas. After getting the characteristic properties of the $\text{Ga}_{0.75}\text{In}_{0.25}\text{Se}$ crystal and comparing with those of its constituents, the more detailed and accurate knowledge can be given about the adaptability of the crystal to the technological applications considering the advantageous and disadvantageous properties of the crystal. For that reason, the detailed characterization of the $\text{Ga}_{0.75}\text{In}_{0.25}\text{Se}$ crystal is given in the present study to guide the researchers/readers to give an opportunity to make interference about the possible usage areas. At this point, giving knowledge about the results of previous studies on the $\text{Ga}_x\text{In}_{1-x}\text{Se}$ compounds will be a worthwhile way.

1.1 Previous Studies on Ga_xIn_{1-x}Se

The most extended work on Ga_xIn_{1-x}Se compounds was done by Gousskov et al. [28]. The optical and electrical properties of Ga_xIn_{1-x}Se crystals were investigated in two extreme narrow ranges of $0 \leq x \leq 0.2$ and $0.9 \leq x \leq 1.0$. The composition dependence of energy band gap values was studied using three optical characterization techniques of absorption, Kelvin and photoconductivity measurements. It was observed that the band gap energy (E_g) varies almost linearly from 1.2 eV ($x = 0$) to 2.0 eV ($x = 1$). The linear fit of band gap energy versus composition graph estimated E_g value of Ga_{0.75}In_{0.25}Se ($x = 0.75$) as nearly 1.8 eV. Hall effect and resistivity measurements performed at room temperature deduced that conductivity of Ga_xIn_{1-x}Se crystals changes from n-type to p-type for values exceeding $x = 0.13$. The electrical resistivity of Ga_xIn_{1-x}Se varied from 4.9 Ωcm ($x = 0$) to 2.6×10^3 Ωcm ($x = 1$).

Belenkii et al. analyzed the absorption spectra of Ga_xIn_{1-x}Se crystals in the range of $0.8 < x < 1.0$ [29]. The variation of energy band gap with composition x was investigated in this work. The results indicated that E_g decreases linearly as x increases from 0 to 0.10, but deviates from linearity for values higher than $x = 0.10$.

Raman scattering measurements of Ga_xIn_{1-x}Se mixed crystals were carried out in the range of $0.8 \leq x \leq 1.0$ [30]. Measurements indicated that general appearance of observed spectra did not change with composition and the increase of x values shifted the Raman bands toward lower frequencies. Six Raman bands were observed in the measurements.

PL of Ga_xIn_{1-x}Se crystals at two photon optical excitation were studied by Tagirov et al. [31]. This research was carried out on the crystals with x from 0.80 to 1.0 values. The results of the analysis showed that PL spectra of the crystals had separate lines and the positions of these lines shift to long wavelength region with increasing x . The researchers also studied the photoconductivity in the crystals excited with Q-switched neodymium YAG laser.

The Ga_{0.90}In_{0.10}Se and Ga_{0.85}In_{0.15}Se crystals and their amorphous thin films were studied by Karatay et al. to reveal the nonlinear and saturable absorption characteristics [32]. The band gap energy values of the Ga_{0.90}In_{0.10}Se and Ga_{0.85}In_{0.15}Se crystals were found as 1.92 and 1.89 eV, respectively. However, it was observed that the band gap energies of the Ga_{0.90}In_{0.10}Se and Ga_{0.85}In_{0.15}Se thin films increases from 0.95 to 1.52 and 0.86 to 1.41 eV, respectively for 43, 48, 54 and 64 nm film thicknesses. The surface morphology of the thin films was analyzed from atomic force microscopy measurements.

1.2 Present Study

In the present thesis, the results of structural, optical and electrical characterizations of Ga_{0.75}In_{0.25}Se crystals were presented. Moreover, the trapping centers were investigated in the low temperature range using TSC and TL measurements. Obtained results of the applied all techniques were compared with those of the same and/or similar experimental methods performed on the constituent compounds GaSe and InSe crystals.

The structural characteristics of the samples were accomplished using x-ray diffraction and energy dispersive spectral analysis experiments. Lattice parameters of the crystal structure and atomic composition ratio of the crystals were determined.

The optical characterization of the studied samples was done using visible and IR reflectivity and transmittance, ellipsometry, Raman spectroscopy and PL measurements. As a result of analysis of visible reflectivity and transmittance measurements, the band gap energy, refractive index, oscillator and dispersion energies were found. The detailed information about the rate of change in the band gap energy with temperature and Debye temperature were obtained from the temperature dependence (10-300 K) of transmission measurements. The extensive knowledge about the spectral dependence of pseudorefractive index, pseudoextinction coefficient and pseudodielectric function was acquired from ellipsometry measurements. Moreover, the energies of interband transitions in electronic band structure of Ga_{0.75}In_{0.25}Se crystals were found using the critical point analysis method based on the theoretical fit of the second derivative spectra of the dielectric function. The vibrational spectra of the crystals were studied by IR reflectivity and transmittance and Raman spectra measurements in the frequency

ranges of 100–400, 400–4000 and 25–500 cm^{-1} , respectively. The optical constants, the frequencies of transverse and longitudinal optical modes, high- and low-frequency dielectric constants and oscillator strength were obtained from the analysis of the IR reflectivity measurements accomplished at room temperature. An attempt was made to interpret the bands observed in the IR transmittance spectrum in terms of two-phonon absorption processes. The characterization of radiative emission bands in $\text{Ga}_{0.75}\text{In}_{0.25}\text{Se}$ crystals were achieved using PL measurements. Experiments were carried out as a function of temperature (7-59 K) and excitation laser intensity (0.06-1.40 W cm^{-2}).

Dark resistivity, space charge limited current and photoconductivity measurements were carried out on the crystals for electrical characterization. The electrical measurements revealed the variation of the resistivity as a function of temperature in the range of 150-350 K. Resistivity activation energy has also been found from the analysis. Space charge limited current measurement analysis showed the presence of trapping centers in the crystal. Moreover, the dominant recombination mechanism in the crystal was determined from the photocurrent measurements.

In addition to above-mentioned characterization techniques, the trapping centers in the undoped samples were studied using TSC and TL measurements. The experimental data obtained from these techniques were analyzed using various methods to calculate the activation energies, capture cross sections, attempt to escape frequencies and concentration of the traps. The results of TSC and TL measurements carried out on the same crystal were compared. This comparison gave an important opportunity to relate these techniques.

In the light of these mentioned characterization processes, the theoretical background of the applied experimental techniques are given in chapter 2. The knowledge of used experimental systems and methods are mentioned in chapter 3. The results of the performed experiments on $\text{Ga}_{0.75}\text{In}_{0.25}\text{Se}$ single crystals are detailed in chapter 4. Finally, the physical interpretations and conclusions on the results of the characterization techniques are given in chapter 5.

CHAPTER 2

THEORETICAL APPROACH

2.1 Introduction

Materials between the metals and insulators in respect to band gap energy are called as semiconductors. Their resistivity values are in the range of 10^{-3} and 10^{+9} Ωcm . They behave as insulator at low temperatures. The most attractive property of the semiconductors in the technological areas is that they have controllable conductivities depending on the external effects. Transistors, diodes, solar cells, detectors and fiber-optic networks are some important application areas of semiconductors. Structural, optical and electrical properties of a semiconducting material have to be known to understand in which areas they are more effective and usable. For that purpose, in this chapter the theoretical background of the band structure of the semiconductors and techniques applied for characterizations are given in detail.

2.2 Electronic Properties of Semiconductors

2.2.1 Band Structure of Semiconductors

In the crystalline solids, atoms are positioned in a regularly three dimensional patterns. Therefore, the state of an electron inside a crystal lattice structure is described by the Schrödinger's wave equation for the case of periodic potential $V(r) = V(r + a)$ as

$$\psi(r) = u(r) \exp(ikr), \quad (2.1)$$

where $u(r) = u(r + a)$ is the Bloch function, k is the wave vector and r is the position vector. In order to analyze the state of an electron in a periodic crystal potential, some simplifications are used. Kronig-Penney is a simplification model in which the motion of electron is studied for a one-dimensional array of square potential barriers having a width of L and separated by V_0 potential (see Figure 2.1) [33].

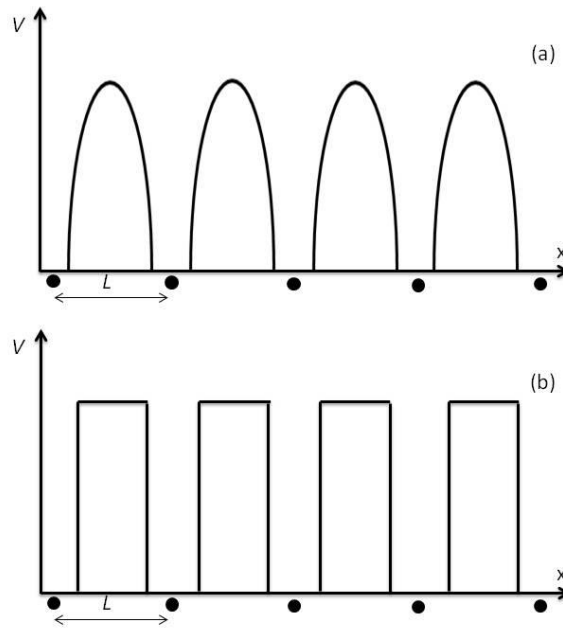


Figure 2.1. (a) Schematic representation of the dependence of potential energy of an electron in a one-dimensional crystal lattice. (b) Kronig-Penney model approximation to the realistic potential energy [34].

The Schrödinger's wave equation results with some important points;

- i. Allowed and forbidden energy bands exist for electrons moving in the crystal structure having periodic potential.
- ii. The forbidden bands become narrower as energy (E) increases.
- iii. The energy of an electron is found as

$$E = \frac{\hbar^2 k^2}{2m_e} \left(k = \frac{n\pi}{L} \quad n = \pm 1, \pm 2, \pm 3, \dots \right), \quad (2.2)$$

where m_e is the effective mass of the electron and \hbar is the reduced Planck's constant.

According to the result of the Schrödinger's equation, there exist discontinuities in energy at $k = n\pi/L$ which corresponds to the boundary of an allowed band. The dependency of the energy on k -values for the periodic lattice is nearly equal to that of free electron. The only difference is that there occurs a deviation from the parabolic $E(k)$ curve at the boundaries. Figure 2.2 indicates extended-zone representation of the dependence of energy on k -vector..

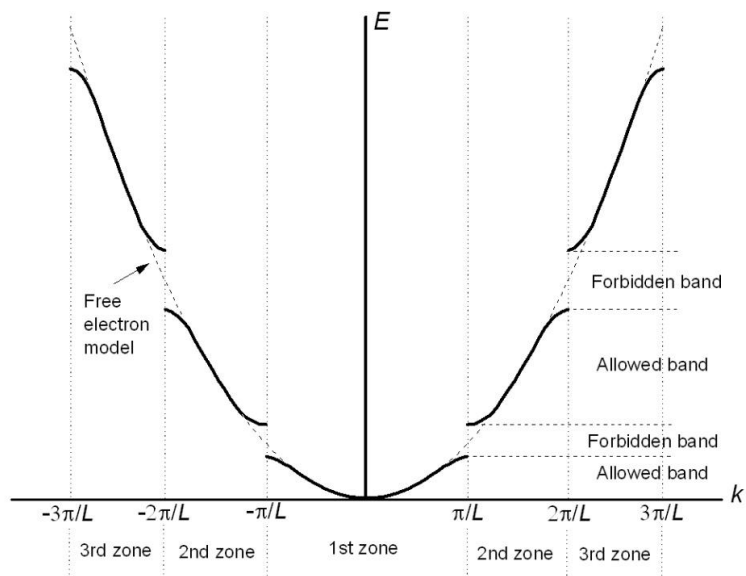


Figure 2.2. The extended-zone representation of the dependence of energy on k -vector [34].

As a more simple representation, the reduced-zone configuration and electronic energy bands are shown in figure 2.3.

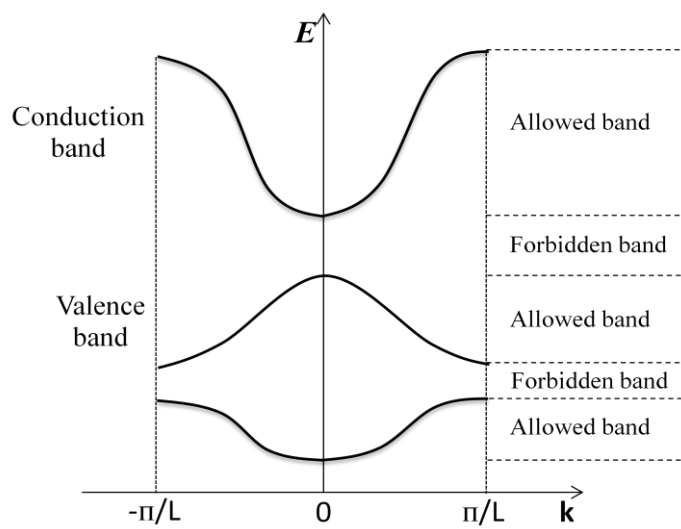


Figure 2.3. Simple diagram of the reduced-zone representation.

In the band structure of solids, the *valence band* is the highest energy band occupied by the electrons at $T = 0$ K. The lowermost allowed energy band is called as *conduction band*. In semiconductors, this band is not occupied by the electrons at absolute zero. The energy region between these bands is forbidden and called as *energy gap*. The location of the lowest conduction minima with respect to highest valence band maxima can be varied in different crystals. The materials, in which these minima and maxima positions are at the same point in k -space, are referred as *direct energy gap* materials. Otherwise, they are referred as *indirect energy gap* materials. Figure 2.4 shows simple configuration of the direct and indirect band gap structures.

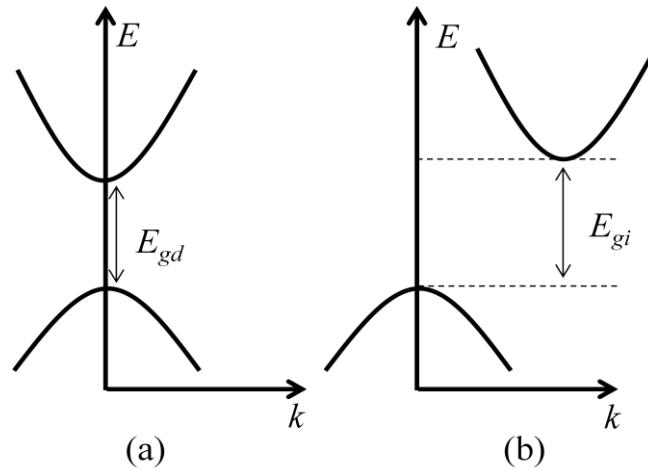


Figure 2.4. Schematic diagram of (a) direct and (b) indirect band structures.

The values of the band gap energy distinguish the metals, semiconductors and insulators from each other. In metals, energies of the filled and empty bands overlap. Therefore, there is no energy gap for the metals. In the insulators, the conduction and valence bands are separated by a large magnitude of band gap energy which is generally greater than 3 eV. Semiconductors have smaller band gap energy than insulators. In semiconductors, at $T = 0$ K, all the electrons occupy in the valence band and therefore they behave as insulators. For larger temperature values, electrons have probability to be excited to the conduction band. So, they can contribute to the carrier transport in the semiconductor.

2.2.2 Defects

Any irregularity in the ideal atomic arrangement is called as imperfection or defect. These defects can arise unintentionally during the crystal growth or be created intentionally for some purposes. Defects affect some properties of the crystals, such as strength, electrical conductivity. Defects are classified into four groups according to their dimensions. These are point defects (zero dimensional), line defects (1-dimensional), plane or surface defects (2-dimensional), volume defects (3-dimensional).

Point defects: This kind of defects is due to a missing atom or irregular location of an atom in the lattice structure. Point defects include mainly four types. All these types are represented in figure 2.5.

- i. *Self interstitial atoms*: These are the extra atoms, which are the same type with the bulk atoms, and locate in an interstitial position.
- ii. *Substitutional impurity atoms*: These are atoms different from the bulk atoms and replaces into the position of the bulk atoms.
- iii. *Interstitial impurity atoms*: These are same type of atoms with bulk atoms, but smaller than them. They locate in the open regions between bulk atoms.
- iv. *Vacancies*: A missing atom in the lattice structure creates an empty region. These empty regions are called as vacancies.

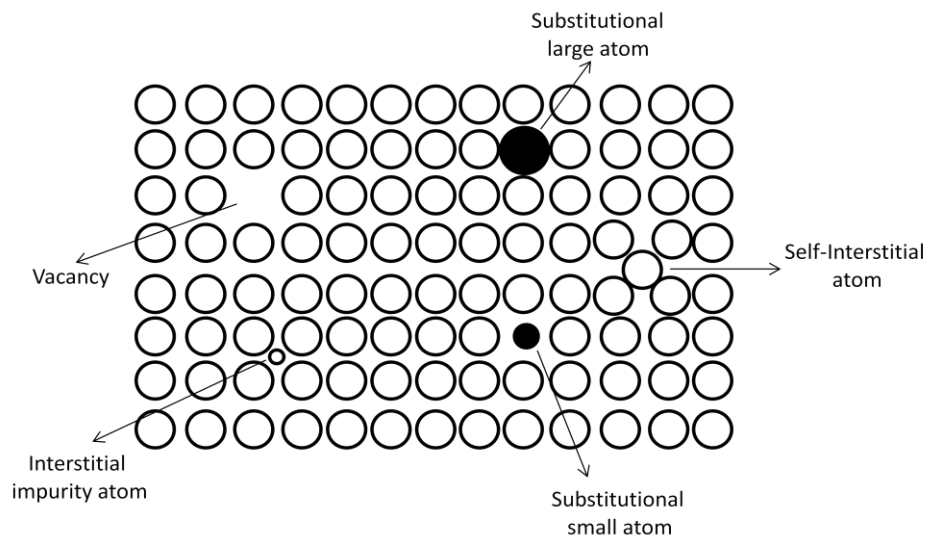


Figure 2.5. Representation of different point defect types in the semiconductors.

Line Defects: The atom groups in the lattice can be missing or found in wrong position. This type of disordering is referred to line defects which are generally called as dislocations. There exist two extreme types of dislocation in the crystal structure.

- i. *Edge Dislocations*: The replacement (removement) of a plane to (from) the crystal structure is described as edge dislocation.
- ii. *Screw dislocations*: A shear ripple stretching from side to side is called as screw dislocations.

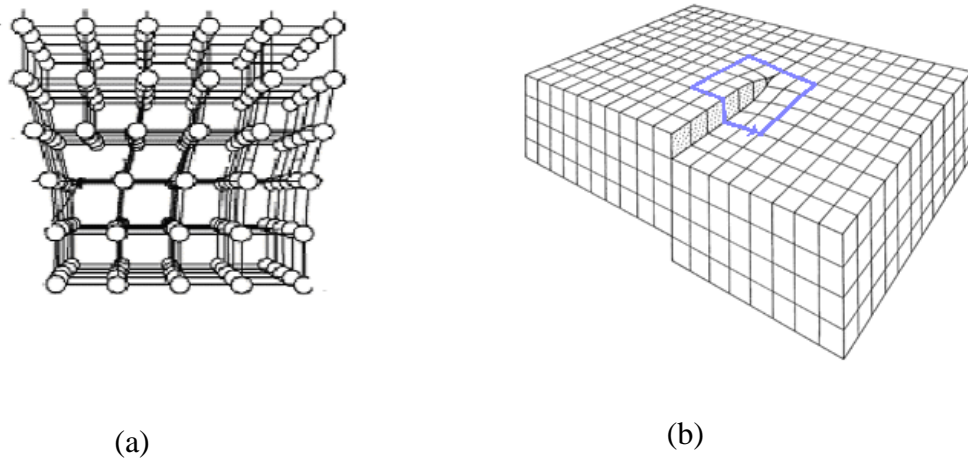


Figure 2.6. (a) Edge dislocation; (b) Screw dislocation [35].

Planar defects: These defects are the interfaces between the discrete parts of a crystal. *Stacking faults* and *grain boundaries* are two main important types of the planar defects. In the perfect crystal structure, atoms are positioned in a stacking sequence. Stacking fault is the defect coming out due to an error in the sequence for a few atomic spacing. If this error occurs for many atomic spacing, twin boundaries are created. For example, in the hexagonal close packed structures, the crystal arrangement continues as ABABABAB. If this regularity collapses by an addition of a different atom like C which results to a new arrangement of ABABABCAB, a stacking fault defect is formed. However, if the arrangement ABABABAB switches to ABCABCABC for a period of time and then switches to initial arrangement, a pair of twin boundaries is formed in the crystal structure.

Real materials generally consist of many small crystallites or grains. The different grains are separated by regions called as grain boundaries. The size of these grains varies from nanometers to millimeters. Crystals having grains are called as polycrystals.

Volume or Bulk Defects: These three dimensional defects are much larger than other type of defects. Voids are one of the common types of the bulk defects. They are small regions where a large amount of atoms are missing in the crystal structure. Voids can be described as clusters of vacancies. Precipitates are another type of bulk defects in which impurities can cluster together and form small areas of a different type.

2.2.3 Intrinsic and Extrinsic Semiconductors

One of the important factors affecting the conductivity in the semiconductors is existence of the impurities. Semiconductors are classified according to presence of impurities into two groups called as *intrinsic* and *extrinsic*. Intrinsic semiconductors are ideal perfect crystals which do not contain impurity or defect in their lattice. In the equilibrium state, there is no free charge carrier in the crystal. However, electrons in the valence band (VB) can be excited to conduction band (CB) when they get enough energy. In this case, a free electron is created in the conduction band. Correspondingly, an unoccupied state is created in the valence band in place of the excited electron. This state is called as *hole* which is regarded as a positive charge carrier. This process is called as “electron-hole pair creation”. In the intrinsic semiconductors, one hole is created in place of one electron. Therefore, the concentration of the electrons (n) in CB is equal to that of

holes (p) in the valence band. These concentrations are also related to intrinsic carrier concentration (n_i) as

$$n.p = n_i^2 \quad (2.3)$$

The extrinsic semiconductors are called as the crystals containing impurities. These impurities can be added into the lattice structure intentionally or unintentionally. The process of placing impurities in the crystal structure is called as *doping*. The main aim of doping is to increase the number of free charge carriers in the crystal structure. By this way, the conductivity of the semiconductor can be adjusted for the desired purpose. The type of the conductivity of the material is formed according to the added impurity atoms.

In the doping process, there are two types called as *n-type* and *p-type* doping. The most popular element used for doping is the Silicon (Si). Si is in the group IV and there are four valence electrons in the outer atomic shell of the each atom in the crystal. Each Si atom in the crystal bounds with the atoms of the neighboring atoms using its four valence electrons and a firm structure is formed.

n-type doping: If any element from the pentavalent group as phosphor (P) is added into Si-crystal, the four valence electrons of this element combine with the neighboring Si atoms. However, the fifth electron of the P-atom does not form any bound and can move freely in the crystal. Since there exists an excessive electron, the dopant phosphor is called as *donor* and negatively doped Si is called as *n-type semiconductor*. Figure 2.7(a) shows the added P-atom and excessive electron in the n-type doped silicon crystal. Moreover, this unbounded electron can be excited to CB by the help of relatively little energy. Therefore, in the band structure of the *n*-doped semiconductors, there is formed a donor level closer to the conduction band as shown in Figure 2.8(a).

p-type doping: If the Si-crystal is doped with a element from the group III as Boron (B), the three valence electrons of the boron atom form bounds with the three neighboring silicon atoms. In this way, a missing electron exists to create a firm structure and correspondingly a hole is produced in the place of missing electron. This added impurity is called as *acceptor* due to the existence of this hole and positively doped Si-crystal is called as *p-type semiconductor*. Figure 2.7(b) shows the added boron atom and created hole in the crystal structure. This hole can be occupied using low energy by an electron excited from the VB. Therefore, in the *p*-type semiconductor band structure, an acceptor level closer to VB is formed as shown in figure 2.8(b).

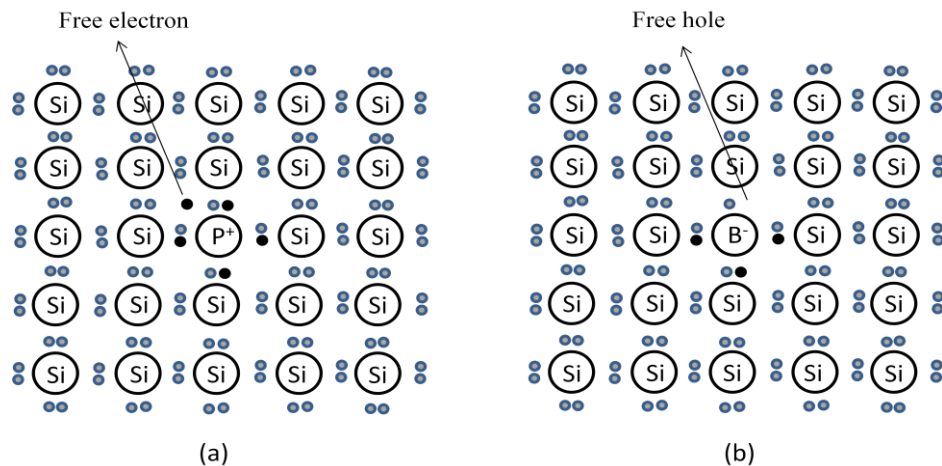


Figure 2.7. The doped Silicon crystals with (a) Phosphor atom (n-type doping), (b) Boron atom (p-type doping).

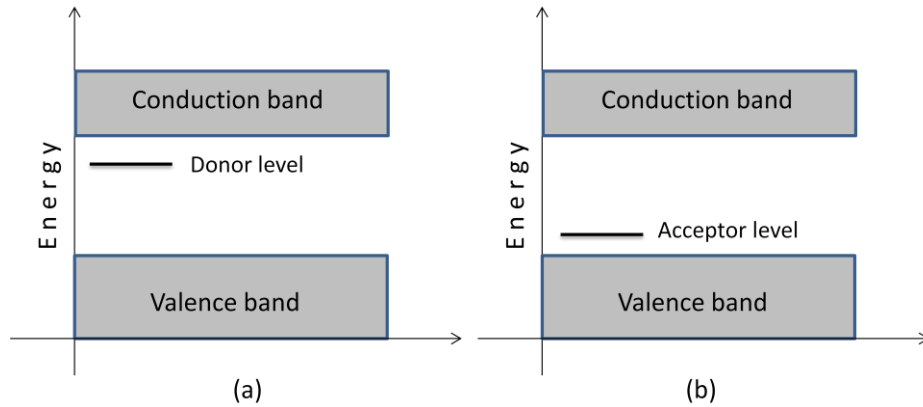


Figure 2.8. Representation of the (a) donor and (b) acceptor levels in the forbidden energy gap.

2.3 Theoretical Approach to Characterization Techniques

2.3.1 X-ray diffraction

One of the most important techniques used for the structural characterization of semiconductors is x-ray diffraction (XRD). The interatomic distance in the crystal lattice is in the range of 0.15-0.4 nm. The main reason of usage of x-rays in the structural characterization is the fact that x-rays have wavelengths in the same order of magnitude with the interplanar spacings of crystal structure. The wavelengths of the x-rays having energies of 120 eV to 120 keV are in the range of 0.01–10 nm.

The interaction of x-rays with the matter can be resulted in three different cases. As a first case, the electrons can be released from the bound atomic states after the interaction. This process is called as photoionization in which the energy and momentum of the x-rays are transferred to the electrons. Photoionization is in the group of inelastic scattering. The second case is another inelastic scattering called as Compton scattering. In this process, the energy is similarly transferred to the electrons. However, any releasing of the electrons from the atom comes true. The third case is Thomson scattering in which x-rays are scattered from the atoms elastically and wavelength of the incident x-rays is conserved. Structural characterization of the crystal makes use of this Thomson scattering case.

The diffracted x-rays from the different atoms as a result of elastic scattering form interference patterns. The constructive interference pattern gives us detailed information about the distribution of atoms in the crystal. Figure 2.9 shows the deflection of the incident x-rays from a crystal lattice having a interplanar spacing of d . If the diffracted x-rays from the darker atoms are considered, the path difference between them is given as

$$|AB| + |AC| = 2d \sin \theta . \quad (2.4)$$

If this path shift is equal to integer multiple of the wavelength (λ) of the x-rays, diffracted x-rays form a constructive interference. That means constructive interference occurs for the case of

$$2d_{hkl} \sin \theta = n\lambda \cdot \quad n = 0, 1, 2, 3, \dots \quad (2.5)$$

This expression called as Bragg law was formulated by W.L. Bragg [36]. The analysis of the obtained XRD data gives opportunity to find the interplanar spacing (d), lattice constants (a, b and c), Miller indices (h, k and l) and angles (α, β and γ) [37]. Table 2.1 gives detailed information about the seven different crystal classes.

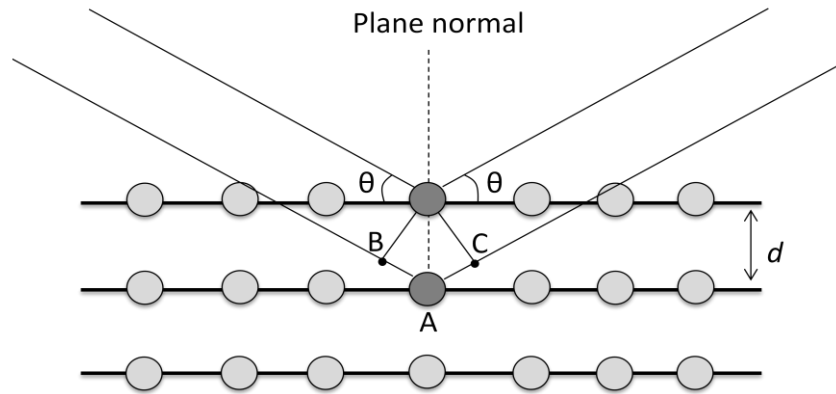


Figure 2.9. Representation of x-ray diffraction by a crystal lattice.

Table 2.1. Characteristics of the seven crystals classes.

Crystal System	a : b : c	Axial Angles	$\frac{1}{d_{hkl}^2}$
Cubic	1 : 1 : 1	$\alpha = \beta = \gamma = 90^\circ$	$\frac{h^2 + k^2 + l^2}{a^2}$
Tetragonal	1 : 1 : c	$\alpha = \beta = \gamma = 90^\circ$	$\frac{h^2 + k^2}{a^2} + \frac{l^2}{c^2}$
Orthorhombic	a : 1 : c	$\alpha = \beta = \gamma = 90^\circ$	$\frac{h^2}{a^2} + \frac{k^2}{b^2} + \frac{l^2}{c^2}$
Hexagonal	1 : 1 : c	$\alpha = \beta = 90^\circ$ $\gamma = 120^\circ$	$\frac{4}{3} \frac{h^2 + hk + k^2}{a^2} + \frac{l^2}{c^2}$
Rhombohedral	1 : 1 : 1	$\alpha = \beta = \gamma \neq 90^\circ$	$\frac{(h^2 + k^2 + l^2) \sin^2 \alpha + 2(hk + hl + kl)(\cos^2 \alpha - \cos \alpha)}{a^2(1 - 3 \cos^2 \alpha + 2 \cos^3 \alpha)}$
Monoclinic	a : 1 : c	$\alpha = \gamma = 90^\circ$ $\beta \neq 90^\circ$	$\frac{h^2}{a^2 \sin^2 \beta} + \frac{k^2}{b^2} + \frac{l^2}{c^2 \sin^2 \beta} - \frac{2hl \cos \beta}{ac \sin^2 \beta}$
Triclinic	a : 1 : c	$\alpha \neq \beta \neq \gamma \neq 90^\circ$	$\frac{1}{\left[1 + 2 \cos(\alpha) \cos(\beta) \cos(\gamma) - \cos^2(\alpha) - \cos^2(\beta) - \cos^2(\gamma) \right.}$ $\times \left[\frac{h^2 \sin^2(\alpha)}{a^2} + \frac{k^2 \sin^2(\beta)}{b^2} + \frac{l^2 \sin^2(\gamma)}{c^2} \right.}$ $\left. + \frac{2hk}{ab} (\cos(\alpha) \cos(\beta) - \cos(\gamma)) + \frac{2kl}{bc} (\cos(\beta) \cos(\gamma) - \cos(\alpha)) \right.}$ $\left. + \frac{2lh}{ac} (\cos(\gamma) \cos(\alpha) - \cos(\beta)) \right]}$

2.3.2 Energy Dispersive Spectral Analysis

Energy dispersive spectral analysis (EDSA) is a powerful technique to characterize the chemical composition of the samples. This spectroscopy method analyzes the data obtained as a result of the interaction of an excitation x-ray source and sample.

Rutherford-Bohr atom model reveals that electrons orbit around the nucleus in the different energy shells. The K-shell is the nearest shell to the nucleus. In turn, L and M shells follow this shell. The L and M shells split into three and five subshells, respectively. Each different transition between shells is called with a unique name. Since the atomic structure is a characteristic property of elements, energies of the transitions are like a fingerprint for different elements. EDSA takes advantage from this fingerprint atomic structure. Electrons in an atom occupy in the discrete energy levels at rest. When the sample is radiated with an excitation source, electrons in the inner shells are ejected from the shell and leave holes in their place. The electrons in the outer and higher energy shells fill these holes and energy equal to difference between final and initial shells is released as a form of x-ray. These emitted x-rays are measured as number and energy using an energy dispersive spectrometer. Since energy of emitted x-rays is the characteristic of the energy difference between shells, EDSA method gives us opportunity to determine the chemical composition of the samples.

2.3.3 Optical Absorption, Transmission and Reflection

Absorption, transmission and reflection measurements are non-destructive basic techniques used for the optical characterization of the semiconducting materials. In these techniques, a light beam is irradiated onto material surface and intensities of reflected and transmitted light comparative to the incident light are analyzed to get knowledge about the optical constants of the material.

2.3.3.1 Absorption

If a light source has energy bigger than band gap, some amount of the radiated light is absorbed and used to excite the electrons to higher energy levels. Therefore, the intensity of the incident light decreases due to this absorption process. If the light travels through the material as a distance of x , the ratio of the intensities of the incident (I_0) and propagating ($I(x)$) light is given as [38]

$$\frac{I(x)}{I_0} = \exp(-\alpha x) , \quad (2.6)$$

where α is the absorption coefficient defined in terms of the wavelength (λ) of the light beam and absorption index (k) of the material as

$$\alpha = \frac{4\pi k}{\lambda} . \quad (2.7)$$

Photon energy ($h\nu$) dependency of the absorption coefficient (α) is described as [39]

$$(\alpha h\nu) = A(h\nu - E_g)^p , \quad (2.8)$$

where E_g is band gap energy and A is a constant depending on the transition probability. The p is an index and equal to 2 and 1/2 for indirect and direct transitions, respectively.

2.3.3.2 Reflection

Reflection is described as the process in which a light is fallen on the surface of a material and some of this light is reemitted by the material into the medium from which the light propagates. The reflection coefficient (R) described as the intensity of the reflected light

comparative to the incident light is given in terms of the refractive index (n) and extinction coefficient (k) for normal incidence as [40]

$$R = \frac{(n-1)^2 + k^2}{(n+1)^2 + k^2} . \quad (2.9)$$

For the transparent range ($k = 0$), the reflection coefficient reduces to

$$R = \frac{(n-1)^2}{(n+1)^2} . \quad (2.10)$$

2.3.3.3 Transmission

When a light beam is fallen on a material surface, the light propagates through the material and after absorption of some amount of it, the light with reduced intensity leaves the material in the direction of initial propagation. Transmission spectroscopy deals with the photon energy dependence of this transmitted light. Transmission coefficient (T) defined as the intensity of the transmitted light comparative to the incident light is given by [40]

$$T = \frac{(1-R)^2 \exp(-ad)}{1-R^2 \exp(-2ad)} , \quad (2.11)$$

where d represents the thickness of the sample. For the large ad multiplication term, $\exp(-2ad)$ is nearly equal to zero and transmission coefficient reduces to

$$T \cong (1-R)^2 \exp(-ad) . \quad (2.12)$$

Equation 2.11 can be used to calculate the absorption coefficient if R and d are known. Moreover, there exist transmission interference fringes in the transmission spectra at wavelengths slightly longer than the absorption edge for thin samples. If the refractive index of the sample is known, sample thickness can be calculated using the expression

$$x = \frac{1}{2n} \left(\frac{\lambda_1 \lambda_2}{\lambda_1 - \lambda_2} \right) , \quad (2.13)$$

where λ_1 and λ_2 are the corresponding wavelengths of the maximum intensity positions of two neighboring peaks.

The photon energy dependence of n in the region of $h\nu < E_g$ can be analyzed using the single-effective-oscillator model in which n and $h\nu$ are related by [41,42]

$$n^2(h\nu) = 1 + \frac{E_{so} E_d}{E_{so}^2 - (h\nu)^2} , \quad (2.14)$$

where E_{so} and E_d represents the single oscillator energy and dispersion energy, respectively. The zero-frequency refractive index (n_0) can be calculated using equation 2.14 by replacing $h\nu = 0$;

$$n_0^2 = 1 + \frac{E_d}{E_{so}} . \quad (2.15)$$

The oscillator strength (S_{so}) and wavelength (λ_{so}) can be calculated from the analysis of the n . A single Sellmeier oscillator model gives refractive index in the low energy range as [43]

$$\frac{(n_0^2 - 1)}{(n^2 - 1)} = 1 - \left(\frac{\lambda_{so}}{\lambda^2} \right)^2 . \quad (2.16)$$

Rearranging equation 2.16 gives [44]

$$(n^2 - 1)^{-1} = \frac{1}{S_{so} \lambda_{so}^2} - \frac{1}{S_{so} \lambda^2} \quad , \quad (2.17)$$

where S_{so} can be described as

$$S_{so} = \frac{(n_0^2 - 1)}{\lambda_{so}^2} \quad . \quad (2.18)$$

The oscillator strength and oscillator wavelength can be calculated using these equations. Moreover, n and $h\nu$ are related in the low energy region in Cauchy model [45] as

$$n(\lambda) = A + \frac{B}{\lambda^2} + \frac{C}{\lambda^4} \quad , \quad (2.19)$$

where A , B and C are constants.

2.3.4 Ellipsometry

Ellipsometry is an optical measurement technique in which the change of an incident polarized light after reflected from the surface of a sample is measured and analyzed. Since the reflected light is generally “elliptical”, the name of “ellipsometry” is given to this measurement method. There are mainly two quantities named as ψ and Δ obtained as experimental data. ψ and Δ represent the amplitude ratio and phase shift of the parallel (p) and perpendicular (s) components of the reflected light.

2.3.4.1 p- and s-polarized light waves

Figure 2.10 represents a simple view of light reflection on the surface of a sample. The light are classified as p- and s-polarized light waves depending on the directions of the electric and magnetic fields of the incident and reflected light. The plane on which electric fields of incident and reflected waves lie is called as “*plane of incidence*”. The simple representation of directions of magnetic and electric fields in the p- and s-polarization is given in figure 2.11.

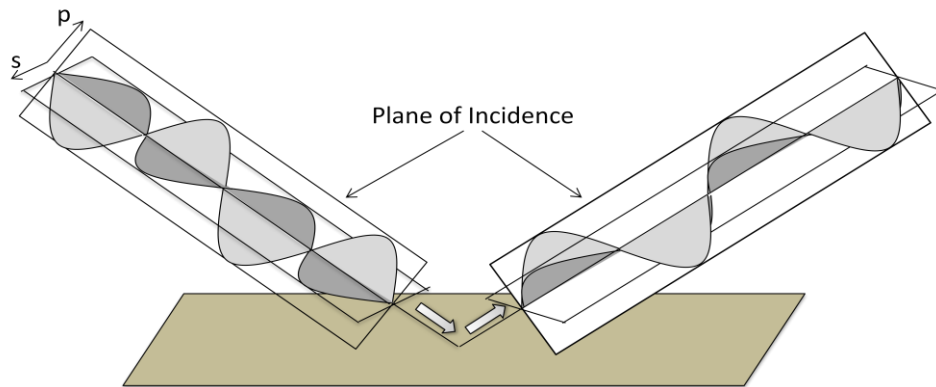


Figure 2.10. Reflection of p- and s- polarized light waves [46].

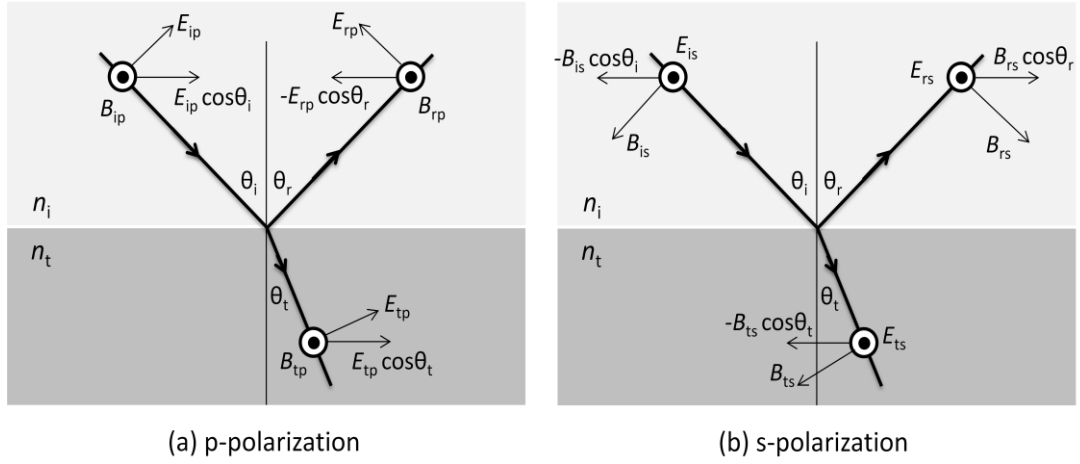


Figure 2.11. Representation of magnetic and electric fields in the p- and s-polarization

For the reflection, the electromagnetic waves must satisfy the boundary conditions which state the continuity of the components of the E - and B -fields parallel to the interface. This boundary condition carries us to the following relations for the p-polarized light [46,47];

$$E_{ip} \cos \theta_i - E_{rp} \cos \theta_r = E_{tp} \cos \theta_t \quad (2.20)$$

$$B_{ip} + B_{rp} = B_{tp} \quad , \quad (2.21)$$

where ip , rp and tp correspond to the incidence, reflection and transmission of p-polarized light, respectively. Using the basic electromagnetic relation, $E = sB$, where s is ratio of speed of light (c) to refractive index (n), equation 2.21 can be rewritten in terms of the electric field as;

$$n_i (E_{ip} + E_{rp}) = n_t E_{tp} \quad . \quad (2.22)$$

Using the Snell's law ($\theta_i = \theta_r$) and then combining equations 2.22 and 2.20, the amplitude reflection (r_p) and transmission (t_p) coefficients are found as

$$r_p = \frac{E_{rp}}{E_{ip}} = \frac{n_t \cos \theta_i - n_i \cos \theta_t}{n_t \cos \theta_i + n_i \cos \theta_t} \quad , \quad (2.23)$$

$$t_p = \frac{E_{tp}}{E_{ip}} = \frac{2n_i \cos \theta_i}{n_t \cos \theta_i + n_i \cos \theta_t} \quad . \quad (2.24)$$

Additionally, the boundary conditions for s-polarization are given as

$$E_{is} + E_{rs} = E_{ts} \quad , \quad (2.25)$$

$$-B_{is} \cos \theta_i + B_{rs} \cos \theta_r = -B_{ts} \cos \theta_t \quad , \quad (2.26)$$

where is , rs and ts correspond to the incidence, reflection and transmission of s-polarized light, respectively. Following the similar way used for p-polarization, the amplitude reflection and transmission coefficients are found as;

$$r_s \equiv \frac{E_{rs}}{E_{is}} = \frac{n_i \cos \theta_i - n_t \cos \theta_t}{n_i \cos \theta_i + n_t \cos \theta_t} \quad (2.27)$$

$$t_s \equiv \frac{E_{ts}}{E_{is}} = \frac{2n_i \cos \theta_i}{n_i \cos \theta_i + n_t \cos \theta_t} \quad (2.28)$$

Equations 2.23, 2.24, 2.27 and 2.28 are called as Fresnel equations. These expressions are correct if n is replaced with complex refractive index N given by [48]

$$N = n - ik \quad (2.29)$$

N is given from Maxwell's equations as

$$N^2 = \varepsilon \quad (2.30)$$

where ε is the complex dielectric constant and defined by its real and imaginary components as

$$\varepsilon = \varepsilon_1 + i\varepsilon_2 \quad (2.31)$$

Combining the equations 2.29, 2.30 and 2.31, n and k are related to components of dielectric constant by;

$$n = \left[(\varepsilon_1 + (\varepsilon_1^2 + \varepsilon_2^2)^{1/2}) / 2 \right]^{1/2} \quad (2.32)$$

$$k = \left[(-\varepsilon_1 + (\varepsilon_1^2 + \varepsilon_2^2)^{1/2}) / 2 \right]^{1/2} \quad (2.33)$$

Using the Snell's law ($N_i \sin \theta_i = N_t \sin \theta_t$) for the complex refractive index and equation 2.30, we get,

$$N_t \cos \theta_t = (N_i^2 - N_t^2 \sin^2 \theta_i)^{1/2} = (\varepsilon_t - \varepsilon_i \sin^2 \theta_i)^{1/2} \quad (2.34)$$

Fresnel equations for the reflection can be rewritten using the equation 2.34 as

$$r_p = \frac{N_{ii}^2 \cos \theta_i - (N_{ii}^2 - \sin^2 \theta_i)^{1/2}}{N_{ii}^2 \cos \theta_i + (N_{ii}^2 - \sin^2 \theta_i)^{1/2}} \quad (2.35)$$

$$r_s = \frac{\cos \theta_i - (N_{ii}^2 - \sin^2 \theta_i)^{1/2}}{\cos \theta_i + (N_{ii}^2 - \sin^2 \theta_i)^{1/2}} \quad (2.36)$$

2.3.4.2 Measured values in ellipsometry

In the ellipsometry measurements, p - and s -polarized light waves are sent on the sample surface at the Brewster angle. The amplitude and phase of these polarized light waves change after reflection. Experimental data obtained from the ellipsometry measurements are amplitude ratio (ψ) and phase difference (Δ) between the p - and s -polarizations. The amplitude reflection coefficients given in equations 2.35 and 2.36 are related to ψ and Δ by the expression [47]

$$\rho \equiv \tan(\psi) \exp(i\Delta) \equiv \frac{r_p}{r_s} \quad (2.37)$$

If the light transmission is measured instead of reflection,

$$\rho \equiv \tan(\psi) \exp(i\Delta) \equiv \frac{t_p}{t_s} \quad (2.38)$$

2.3.4.3 Pseudodielectric function

In the analysis of the ellipsometry measurement data, ψ and Δ are used in a optical theoretical model and then the refractive index and dielectric function of the sample are calculated. Since the dielectric function is calculated from the usage of ψ and Δ , it is called as pseudodielectric function represented by $\langle \varepsilon \rangle$. The optical models differ according to the type of the sample used in the measurements. In the crystals, the reflection occurs only at the air/sample interface. In the air/sample optical model, the amplitude ratio of the p- and s-polarized light given in equation 2.37 can be rewritten as

$$\begin{aligned} \rho &= r_p / r_s \\ &= \frac{\varepsilon_i \sin^2 \theta_i - N_{ii} N_{tt}}{\varepsilon_i \sin^2 \theta_i + N_{ii} N_{tt}} \\ &= \frac{\sin^2 \theta_i - \cos \theta_i \left[\varepsilon_t / \varepsilon_i - \sin^2 \theta_i \right]^{1/2}}{\sin^2 \theta_i + \cos \theta_i \left[\varepsilon_t / \varepsilon_i - \sin^2 \theta_i \right]^{1/2}} . \end{aligned} \quad (2.39)$$

By replacing the dielectric constant of the air ($\varepsilon_i = 1$) the pseudodielectric function ($\varepsilon_t = \langle \varepsilon \rangle$) is found as,

$$\langle \varepsilon \rangle = \varepsilon_t = \sin^2 \theta_i \left[1 + \tan^2 \theta_i \left(\frac{1 - \rho}{1 + \rho} \right)^2 \right] . \quad (2.40)$$

2.3.4.4 Critical Point Analysis

Different optical properties of the sample used in the ellipsometry can be obtained from different analysis methods of dielectric function obtained from the convenient optical model. One of these methods is the critical point (CP) analysis used to get knowledge on interband transitions in electronic band structure. The photon energy (E) dependence of the pseudodielectric function used for the CP analysis is given as

$$\langle \varepsilon(E) \rangle = C - A \exp(i\phi) (E - E_{cp} + i\Gamma)^{m-2} . \quad (2.41)$$

In the CP analysis method, the second derivative of the dielectric function is fitted using a fit program and CP energies (E_{cp}) are found as a result. The theoretical expressions used for the CP analysis are [46,48]

$$\frac{d^2 \varepsilon}{dE^2} = m(m-1) A \exp(i\phi) (E - E_{cp} + i\Gamma)^{m-2} \quad (m \neq 0) , \quad (2.42)$$

$$\frac{d^2 \varepsilon}{dE^2} = A \exp(i\phi) (E - E_{cp} + i\Gamma)^{-2} \quad (m = 0) . \quad (2.43)$$

where A , Γ and ϕ are amplitude, broadening parameter and phase angle, respectively. The parameter m is related to the dimensions of the wave vectors playing role in the optical transitions. The m values are equal to -1, -1/2, 0 and +1/2 for excitonic, one-, two- and three dimensional lineshapes, respectively.

2.3.5 Infrared Spectroscopy

Infrared (IR) spectroscopy covers several methods which are based on the absorption or reflection of electromagnetic radiation lying in the infrared region. This spectral range is classified into three groups called as near-, mid-, and far-infrared regions. The near-IR region

lies in the 14000-4000 cm^{-1} range. Harmonic vibrations can be excited by the light source in this region. The mid-IR region is in the 4000-400 cm^{-1} range and most accessible one for the characterizations of fundamental vibrations. The absorption bands consisting in this region generates a molecular fingerprint. Therefore, one can detect the compounds and deduct the structural details. The far-IR region lying in the 400-10 cm^{-1} has low energy and can be used for rotational spectroscopy.

Infrared spectra of the materials are obtained from the dispersive (scanning) and Fourier transform spectrometers. The spectrum gives the ratio of transmitted intensities with and without sample as a function of wavelength. This intensity ratio is defined as transmittance (T) and presented in the spectrum as percentage (% T) or absorbance $A = \log(1/T)$. In the infrared reflected spectra, reflectivity is used instead of transmittance. In the infrared spectroscopy measurements, the transmittance or reflectivity values are reported as a function of wavenumber (cm^{-1}). In the real crystals, atoms in the lattice are vibrating. When the crystals are radiated by an infrared source, incident radiation is absorbed at some specific energy values. In the infrared absorption spectra, some peaks can appear. These peaks correspond to the frequencies of a vibration of a part of a sample molecule.

2.3.5.1 Fourier Transform Infrared Measurements

Fourier transform infrared (FTIR) spectroscopy is an experimental method which is used to obtain infrared spectra of the materials. In the measurements, infrared light passes through an interferometer and then through material (or vice versa). A moving mirror is used to change the distribution of infrared light passing through the interferometer. The recorded signal (interferogram) presents light output as a function of mirror position. Then this data is turned into “light output as a function of wavelength (or wavenumber)” data using a data processing method called as Fourier transform. As described above, the sample’s spectrum is always compared with a reference and results of this comparison give the experimental data. Figure 2.12 shows processes up to obtaining a spectrum in the FTIR measurements.

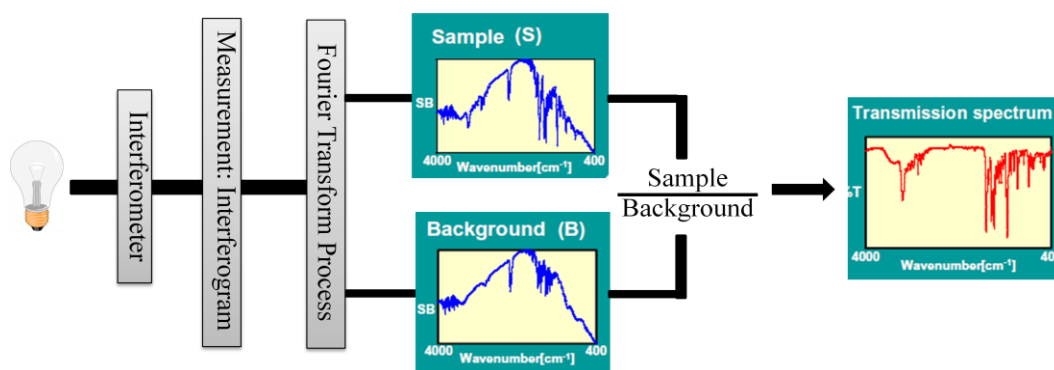


Figure 2.12. The processes in the FTIR measurements

2.3.5.2 Raman Spectroscopy

Raman spectroscopy is a powerful experimental method to obtain information about the vibrational modes in the crystals. It is based on the inelastic scattering (or Raman scattering) of monochromatic light produced by a laser source operating in the visible, near infrared or near ultraviolet range. When laser beam is radiated onto sample, it interacts with molecular

vibrations, phonons or other excitations. As a result of this interaction, laser photon energy shifts up or down. This shift gives knowledge about the vibrational modes in the crystal. If the final vibrational state of the molecule has more energy than the initial state, the emitted photon will have lower frequency to balance the total energy. This shift in frequency is called as Stokes shift. In the contrary case, the frequency will shift to higher frequency and this shift is called as Anti-Stokes.

Infrared and Raman spectroscopy techniques are used for the same purpose. They can be thought as complementary methods. In the Raman measurements, a sample is radiated with a laser source. Light from the illuminated region is collected using a lens and sent through a monochromator. In addition to Raman scattering, elastic Rayleigh scattering mechanism also occurs close to the laser line wavelength. These corresponding wavelengths are filtered out and the remaining part of the collected light is dispersed onto a detector.

2.3.5.3 Kramers-Kronig Dispersion Relations

The Kramers-Kronig dispersion relations connect the real and imaginary parts of a frequency dependent function $f(w)$ which is analytical in the upper half plane of the complex frequency plane [38]. These relations can be given for a frequency of w as

$$\text{Re } f(w) = \frac{2}{\pi} P \int_0^{\infty} \frac{w' \text{Im } f(w')}{w'^2 - w^2} dw' \quad (2.44)$$

$$\text{Im } f(w) = -\frac{2w}{\pi} P \int_0^{\infty} \frac{\text{Re } f(w')}{w'^2 - w^2} dw' \quad (2.45)$$

where the symbol P points out the principal value of the integral for $w' = w$.

In the infrared spectroscopy experiments, since reflectivity, $R(w)$, describes a linear relation between the amplitudes of the incident and reflected waves, these dispersion relations can be used to get the dispersion parameters.

2.3.6 Thermally Stimulated Current and Thermoluminescence

Thermally stimulated current (TSC) and thermoluminescence (TL) are two basic techniques used to determine the properties of the energy levels created due to the presence of defects in semiconductors and insulators. The theoretical approach and analysis methods of these experimental techniques are very close to each other. The main difference between these methods comes from the difference of obtained experimental data. In the TSC measurements, the charge carriers in the trap levels are excited by means of temperature and then subjected to an electric field. The temperature dependence of the current produced due to the motion of these excited charge carriers in the electric field is used as experimental data of TSC experiments. In the TL experiments, the charge carriers excited by means of temperature recombine with the opposite charge carriers. While this recombination takes place, an emission of photons is given outside. The temperature dependence of the count of these photon emissions is used as experimental data in TL experiments. The theoretical approach of the TSC and TL methods is mainly based on the transitions occurring in the energy band gap. Therefore, it will be a worthwhile way to give detailed information about these transitions.

2.3.6.1 Electronic Transitions in TSC and TL Methods

As mentioned before, conduction and valence bands (CB and VB) are separated from each other by energy difference of band gap energy and this separated energy region is forbidden. The defects and/or impurities in the semiconductors lead to an additional energy level(s) in this forbidden region. In a simple TSC/TL model, the existence of one electron trap

level below the conduction band and one hole trap level above the valence band is assumed as shown in figure 2.13. Trap level (T) below the conduction band is located above Fermi level (E_f) and empty before the excitation of electrons and holes. The other level called as R -level is the corresponding hole trap and can function as recombination centre. Under the light of this simple band structure and energy levels, figure 2.13 also shows the main possible electronic transitions occurring in the TSC-TL methods.

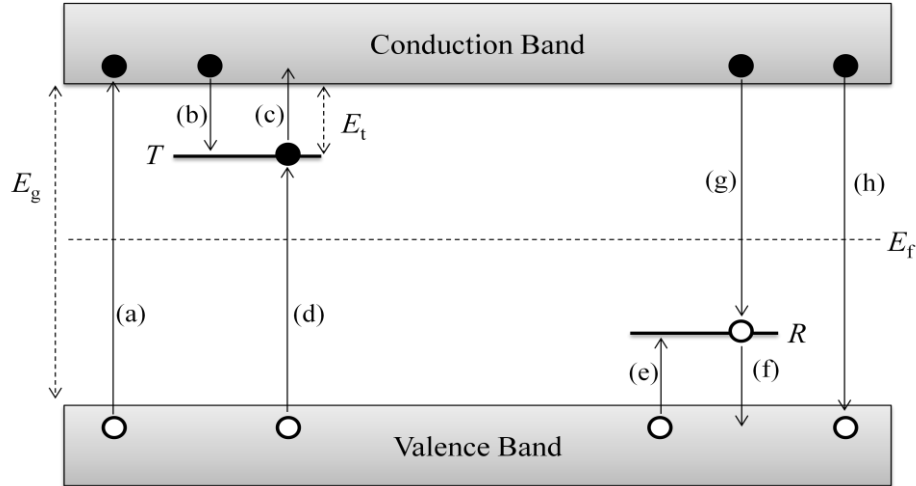


Figure 2.13. Possible electronic transitions in the TSC and TL techniques. (a) band-to-band excitation; (b) and (e) electron and hole trapping, respectively; (c) and (f) electron and hole releases; (d) and (g) indirect recombination; (h) direct recombination. Solid circles, open circles and arrows represent electrons, holes and transitions, respectively [49].

- (I) Transition (a): The electrons in the VB excite to the CB when they have energy larger than band gap energy ($h\nu > E_g$). As a result of this transition, free electrons and holes are created in the conduction and valence bands, respectively. Since this transition takes place between the delocalized conduction and valence bands, it is called as band-to-band transition.
- (II) Transitions (b) and (e): There are two ways for the excited charge carriers through the band-to-band transition. They either recombine with an opposite charge carrier or are trapped in the trap levels. Transitions (b) and (e) represent the corresponding transitions of electron and hole trapping, respectively.
- (III) Transition (h): The other choice for the free electrons and holes is the direct recombination. This transition represented by “h” is the consequence of the recombination of a free electron in CB with a free hole in VB.
- (IV) Transitions (c) and (f): Trapped charge carriers excite to conduction and/or valence bands from trap levels when they have enough energy. The excitations of trapped electrons and holes correspond to the transitions of (c) and (f), respectively. In the TSC and TL experiments, the energy needed for this transition is given by means of temperature.
- (V) Transitions (g) and (d): The charge carriers in the conduction and/or valence bands recombine with the opposite charge carriers in the trap levels. This transition called as indirect recombination is indicated by “g” and “d” transitions.

The possible transitions occurring in the TSC and TL experiments are given above. In this way, the simple physical events in these measurements are given as;

i) **TSC simple model:** In the low temperature, all charge carriers occupy in the VB. The sample to be used in the TSC experiments is subjected to a radiation satisfying the condition $h\nu > E_g$. In this manner, electrons are excited to conduction band (transition “a”). Most of the free electrons in the CB recombine with holes in the VB (transition h). However, some of these free carriers are trapped in trap levels (transition b). The corresponding holes are trapped in the hole traps (transition e). When the temperature of the sample is increased, the trapped charge carriers gain enough energy to be excited to the conduction and/or valence bands (transitions c and f). These excited charge carriers are subjected to an electric field and a current is produced on the sample. The temperature dependence of this current is obtained as experimental data to be analyzed. As a result of the analyses, properties of the trap levels, especially the energy level, can be found.

ii) **TL simple model:** All the physical events told in the TSC model up to applying an electric field process are same in the TL model. Excitation (transition a), trapping (transitions b and e), electron and hole releases (transitions c and f) events also come true in the TL measurements. After exciting the electrons and holes to the conduction and valence bands, respectively, by the help of temperature, any external effect is applied to the sample. In this case, excited charge carriers recombine with the opposite charge carriers (transition h). This recombination can be radiative or non-radiative. If it is radiative, the temperature dependence of the count of the photons emitted from the sample is used as experimental TL data. As a result of the analysis of this data, activation energies of trap levels can be found.

2.3.6.2 Theoretical Approach

The main factor affecting the magnitude of the TSC and TL intensity is the number and variation of the charge carriers in the trap levels, conduction and valence bands. The theoretical background of the TSC and TL techniques introduces the variation of the charge carriers in these levels through the appropriate transitions.

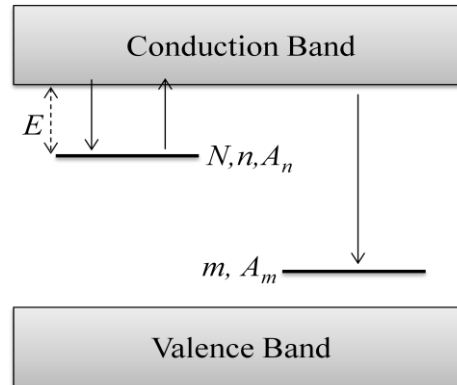


Figure 2.14. Simple diagram of the band structure consisting one electron and one hole trap.

At a temperature T , an electron can be released back into the conduction band from a trap depth of E with a probability (P) of

$$P = \nu \exp(-E/kT), \quad (2.46)$$

where ν is the attempt-to-escape frequency and k is the Boltzmann constant. In a semiconductor, ν is defined as

$$v = N_c A_n = N_c v_e S_t \quad , \quad (2.47)$$

where A_n is the retrapping probability, S_t is the capture cross section, N_c and v_e are the effective density of states in the conduction band and thermal velocity of the conduction electrons, respectively. N_c and v_e are given by

$$N_c(T) = 2 \left(\frac{kT m_e^*}{2\pi \hbar^2} \right)^{2/3} \quad (2.48)$$

and

$$v_e(T) = \sqrt{\frac{3kT}{m_e^*}} \quad , \quad (2.49)$$

where m_e^* is the electron effective mass.

Concentration (n) of filled traps is mainly based on the “traffic” of charge carriers among the trapping centers, conduction band, recombination center and valence band. The theoretical explanation of these transitions is [50];

I. *Stimulation*: The “traffic” of electrons between the trapping centers and conduction band is one of the physical events affecting the concentration of filled traps. Randall and Wilkins give the relation of change of the concentration of traps with time as [51]

$$\frac{dn}{dt} \propto -n v \exp(-E/kT) \quad . \quad (2.50)$$

II. *Retrapping*: There are two possible ways for the electrons (holes) excited to conduction (valence) band from trapping centers. One of these ways is the retrapping. The rate of retrapping is governed by the concentration of free electrons (n_c) in the conduction band and the concentration of unoccupied traps ($N - n$), where N is the total concentration of traps. The effect of retrapping event on the n is given by the relation

$$\frac{dn}{dt} \propto n_c (N - n) S_t v_e \quad . \quad (2.51)$$

Combining the relations 2.50 and 2.51, one gets

$$\frac{dn}{dt} = n_c (N - n) S_t v_e - n v \exp(-E/kT) \quad . \quad (2.52)$$

III. *Recombination*: Another choice for the electrons (holes) in the conduction (valence) band is to recombine with a hole (electron) in the recombination center. If the concentration of holes in the centre is represented by “ m ”, the rate of change of free electrons in conduction band is affected from recombination by the relation

$$\frac{dn_c}{dt} \propto \frac{dm}{dt} = -n_c m A_m \quad , \quad (2.53)$$

where A_m is the recombination probability. The right part of the equation 2.53 can be written in terms of lifetime (τ) for recombination of free electrons as

$$\frac{dn_c}{dt} \propto -n_c m A_m = \frac{n_c}{\tau} \quad . \quad (2.54)$$

Considering these three transitions affecting the free electron concentration in the conduction band and charge neutrality, one can write

$$n_c = m - n \Rightarrow \frac{dn_c}{dt} = \frac{dm}{dt} - \frac{dn}{dt} \Rightarrow \frac{dn_c}{dt} = -\frac{n_c}{\tau} - \frac{dn}{dt} \quad (2.55)$$

$$\frac{dn_c}{dt} = -\frac{n_c}{\tau} - n_c(N-n)S_t\nu_e - n\nu \exp(-E/kT) \quad .$$

Solution of the equation 2.52 is obtained using two fundamental assumptions.

i) **Slow retrapping (First order kinetics)**

In the case of slow retrapping, the electrons excited to conduction band have much more probability of recombining with a hole compared to retrapping. The governing transitions in the slow (or negligible) retrapping is the release of electrons from the trapping centers and recombination with a hole in the recombination center. In relation, this case means that [51]

$$\frac{n_c}{\tau} \gg n_c(N-n)S_t\nu_e \quad (2.56)$$

and

$$\left| \frac{dn_c}{dt} \right| \ll \left| \frac{dn}{dt} \right|, \left| \frac{dm}{dt} \right| \quad (2.57)$$

Using equations 2.56 and 2.57, equation 2.52 becomes

$$\frac{dn}{dt} \approx -n\nu \exp(-E/kT) \quad , \quad (2.58)$$

and

$$\frac{dn_c}{dt} \approx -\frac{n_c}{\tau} \quad (2.59)$$

The integration of equation 2.58 for the case of linear heating function $T = T_0 + \beta t$ gives

$$n = n_0 \exp \left\{ - \int_{T_0}^T \frac{\nu}{\beta} \exp(-E/kT) dT \right\} \quad (2.60)$$

As mentioned before, TSC and TL experiments deal with different measured data. TSC uses the current produced due to the motion of free electrons in conduction band. Therefore, concentration of these free electrons affects magnitude of the current measured in the TSC experiments. By this way, substituting the equations 2.59 and 2.60 into 2.58, we obtain

$$n_c = n_0 \tau \nu \exp \left\{ - \frac{E}{kT} - \int_{T_0}^T \frac{\nu}{\beta} \exp(-E/kT) dT \right\} \quad , \quad (2.61)$$

and thermally stimulated conductivity σ is obtained from the relation

$$\sigma = n_c e \mu = n_0 \tau \nu e \mu \exp \left\{ - \frac{E}{kT} - \int_{T_0}^T \frac{\nu}{\beta} \exp(-E/kT) dT \right\} \quad , \quad (2.62)$$

where μ is the mobility. Using the Ohm's law, the thermally stimulated current is found as

$$I_{TSC} = n_0 \tau v e \mu \left(\frac{V}{L} \right) A \exp \left\{ -\frac{E}{kT} - \int_{T_0}^T \frac{v}{\beta} \exp(-E/kT) dT \right\}, \quad (2.63)$$

where V is applied voltage, A and L are cross sectional area and length of the sample.

In TL measurements, intensity is proportional to the count of photons emitted from the sample during the process of recombination of free electrons in the conduction band and holes in recombination centers. Therefore, the variation of trapped electrons with time is the main starting point of the expression giving the TL intensity. This intensity under the assumption of slow retrapping is [49]

$$I_{TL} = -\frac{dn}{dt}. \quad (2.64)$$

Combining equations 2.58 and 2.60, TL intensity is given as

$$I_{TL} = n_0 v \exp \left\{ -\frac{E}{kT} - \int_{T_0}^T \frac{v}{\beta} \exp(-E/kT) dT \right\}. \quad (2.65)$$

ii) Fast retrapping (Second order kinetics)

Garlick and Gibson studied the case of dominant retrapping. In this case, the time required for thermal equilibrium between the conduction electrons and trapped electrons is much shorter than the recombination lifetime [52-53]. Therefore the concentration relations for fast retrapping process are given as,

$$N \gg n \quad \text{and} \quad n = m$$

Then the rate of change of total electrons is

$$\frac{dm}{dt} \approx \frac{dn}{dt} = -\frac{n_c}{\tau} = -n_c m A_m = -n_c m v_e S_t. \quad (2.66)$$

Combining expressions 2.52 and 2.66,

$$\frac{dn}{dt} = -\frac{1}{N} n^2 v_e \exp \left[-\frac{E_t}{kT} \right]. \quad (2.67)$$

Integration of the equation 2.67 gives

$$I_{TL} = -\frac{dn}{dt} = \left(\frac{n_0^2}{N} \right) v \exp \left[-\frac{E}{kT} \right] \left[1 + \frac{n_0 v}{\beta N} \int_{T_0}^T \exp(-E/kT) dT \right]^{-2} \quad (2.68)$$

and TSC is

$$I_{TSC} = \sigma \left(\frac{V}{L} \right) A = -\tau \frac{dn}{dt} e \mu \left(\frac{V}{L} \right) A \quad (2.69)$$

$$I_{TSC} = \left(\frac{V}{L} \right) A \frac{n_0^2 \tau \mu e v}{N} \exp \left[-\frac{E}{kT} \right] \left[1 + \frac{n_0 v}{\beta N} \int_{T_0}^T \exp(-E/kT) dT \right]^{-2}. \quad (2.70)$$

2.3.6.3 Curve Fitting

(i) **Slow Retrapping:** TSC and TL curves for the slow retrapping are described by equations 2.63 and 2.65, respectively. If it is assumed that ν is independent of temperature T and the variation of μ and τ is ignorable with temperature in the studied range, equations can be rewritten as [54]

$$I = A_0 \exp \left\{ -t + B' \int_{t_0}^t \exp(-t) t^{-2} dt \right\}, \quad (2.71)$$

where $t = \frac{E}{kT}$ and, A_0 and B' are constants:

$$A_0 = n_0 \tau e \mu \nu \frac{V}{L} A \quad (\text{for TSC}), \quad A_0 = n_0 \nu \quad (\text{for TL}), \quad \text{and} \quad B' = \frac{\nu E_t}{\beta k}. \quad (2.72)$$

If repeated integration by parts of integral in equation 2.71 is taken, we get a convergent infinite series expression;

$$I = A_0 \exp \left[-t - B' \left\{ \exp(-t) t^{-2} - 2 \exp(-t) t^{-3} + 3 \times 2 \exp(-t) t^{-4} \dots \right\}_{t_0}^t \right]. \quad (2.73)$$

Because t is large in practice, by making approximation, infinite series can be written as

$$I \approx A_0 \exp \left[-t - B' \exp(-t) t^{-2} \right], \quad (2.74)$$

$$I \approx I_0 + A_0 \exp \left[-t - B' \exp(-t) t^{-2} \right]. \quad (2.75)$$

If equation 2.75 is differentiated and equated to zero to find the maximum of the curve, which occurs at

$$t = t_m = \frac{E_t}{kT_m}, \quad (2.76)$$

then

$$B' = \exp(t_m) \frac{t_m^3}{t_m + 2}. \quad (2.77)$$

(ii) **Fast Retrapping:** In the equations 2.68 and 2.70 for second order kinetics, if we insert $t = \frac{E}{kT}$, it becomes [55]

$$I = \frac{A_0 \exp(-t)}{\left[1 - B' \int_{t_0}^t \exp(-t) t^{-2} dt \right]^2}, \quad (2.78)$$

where

$$A_0 = \frac{n_0^2 \tau e \mu \nu V}{N L} A \quad (\text{for TSC}) \quad \text{and} \quad A_0 = \frac{n_0^2}{N} \nu \quad (\text{for TL}) \quad (2.79)$$

$$\text{and} \quad B' = \frac{n_0 \nu E_t}{N \beta k}. \quad (2.80)$$

If repeated integration by parts of integral in equation 2.78 is taken, we get a convergent infinite series expression;

$$I = \frac{A_0 \exp(-t)}{\left[1 + B' \left\{ \exp(-t)t^{-2} - 2 \exp(-t)t^{-3} + 3 \times 2 \exp(-t)t^{-4} \dots \right\}_{t_0}^t \right]^2} . \quad (2.81)$$

Because t is large in practice, the infinite series can be approximated as

$$I \approx I_0 + \frac{A_0 \exp(-t)}{\left[1 + B' \exp(-t)t^{-2}\right]^2} . \quad (2.82)$$

If equation 2.82 is differentiated and equated to zero to find the maximum of the curve, which occurs at

$$t = t_m = \frac{E_t}{kT_m} , \quad (2.83)$$

then

$$B' = \exp(t_m) \frac{t_m^3}{t_m + 4} . \quad (2.84)$$

More than one peak or overlapped peaks can be analyzed simultaneously using the fitting function given by the sum

$$I(T) = \sum_{i=1}^n I_i(T) , \quad (2.85)$$

where $I_i(T)$ is the current contribution of each peak calculated by means of equations 2.75 or 2.82 for slow and fast retrapping, respectively, and n denotes the number of traps involved in the calculation.

Once the TSC and TL curves have been fitted and the values E_t and T_m for peaks determined, equations 2.77 and 2.84 can be used to calculate B' for slow and fast retrapping processes, respectively. Also for the first order kinetics, ν can be calculated using equation 2.72. Then, cross sections of the traps can be calculated using the ν and expression

$$S_i = \frac{\nu}{N_c v_{th}} , \quad (2.86)$$

where v_{th} is thermal velocity of a free electron.

The concentration of the traps was estimated using the expression [56]

$$N_t = \frac{Q}{ALeG} . \quad (2.87)$$

Here, Q is the quantity of charge released during a TSC measurement and can be obtained from the area under TSC peaks; e is electronic charge and G is photoconductivity gain. G is equal to number of electrons passing through the crystal for each absorbed photon. G is calculated using relation [57]

$$G = \frac{\tau}{t_{tr}} = \frac{\tau \mu V}{L^2} , \quad (2.88)$$

where τ is carrier lifetime and t_{tr} is carrier transit time between electrodes.

2.3.6.4 Initial Rise Method

Initial rise method is one of the main analysis method to determine the activation energies of the trap levels [53]. The main point of this method is based on the fact that integrals in the first and second order equations 2.63, 2.70 (for TSC) and 2.65, 2.68 (for TL) are very small when the charge carriers started to exciting from trap levels. Therefore, exponential terms in the integrals

in abovementioned equations are very close to unity for this initial temperature region. So TSC/TL intensities are written as

$$I = C \exp(-E_t / kT) , \quad (2.89)$$

where C is constant. If logarithm of both sides is taken, one obtains

$$\ln(I) = C - \frac{E_t}{kT} .$$

Plot of $\ln(I)$ versus $1/T$ gives a straight line with a slope of $(-E_t/k)$ in initial part of the glow curve. This method cannot be applied for the overlapped peaks. One of the attractive properties of this method is the usability in both of order of kinetics.

2.3.6.5 Peak Shape Method

The other analysis method in the thermally stimulated processes is the peak shape method in which E_t is associated using three parameters: $\tau = T_m - T_l$, $\delta = T_h - T_m$ and $w = T_h - T_l$, where T_m is the temperature corresponding to maximum current, T_l and T_h are the low and high half-intensity temperatures, respectively [50]. E_t is obtained from the average of three energies given below.

$$E_\tau = [1.51 + 3.0(\mu_g - 0.42)]kT_m^2 / \tau - [1.58 + 4.2(\mu_g - 0.42)]2kT_m \quad (2.90)$$

$$E_\delta = [0.976 + 7.3(\mu_g - 0.42)]kT_m^2 / \delta \quad (2.91)$$

$$E_w = [2.52 + 10.2(\mu_g - 0.42)]kT_m^2 / w - 2kT_m , \quad (2.92)$$

where $\mu_g = \delta/w$. Halperin and Braner proposed to use μ_g to learn order of kinetics. The values of μ_g were predicted as 0.42 and 0.52 for first and second-order kinetics, respectively [50]. Overlapped peaks can be separated for the application of this method. If such a curve occurs in the experimental data, analyzed peak can be cleaned from the other satellite peaks.

2.3.6.6 Differential Analysis Method

The derivative of the natural logarithm of the TSC and TL intensity for slow retrapping case (equations 2.63 and 2.65), under the assumption of that ν is independent of T , is obtained as [58],

$$\frac{d(\ln I)}{dT} = \frac{E_t}{kT^2} - \frac{\nu_t}{\beta} \exp(-E_t / kT). \quad (2.93)$$

Since intensity is maximum at $T = T_m$, the equation 2.93 yields

$$\frac{E_t}{kT_m^2} = \frac{\nu_t}{\beta} \exp(-E_t / kT_m). \quad (2.94)$$

Using the equation 2.94, the second derivative of the $\ln(I)$ can be written at $T = T_m$ as

$$\left[\frac{d^2(\ln I)}{dT^2} \right]_m = -\frac{E_t}{kT_m^3} \left(2 + \frac{E_t}{kT_m} \right) = \alpha_m. \quad (2.95)$$

E_t value is obtained from slope of the tangent (α_m) at $T = T_m$ of the first derivative of the glow curve.

2.3.6.7 Various Heating Rate Method

The heating rate of the TSC/TL experiments is expressed in terms of peak temperature and E_t as [49]

$$\beta = v \frac{kT_m^2}{E_t} \exp\left(-\frac{E_t}{kT_m}\right). \quad (2.96)$$

If the temperature dependence of v is assumed as $v \propto T^\alpha$, then

$$\frac{1}{\beta} = C \frac{E_t}{k} \left(\frac{1}{T_m}\right)^{2+\alpha} \exp\left(\frac{E_t}{kT_m}\right), \quad (2.97)$$

where C is a constant. If TSC/TL measurements are performed for different heating rates and T_m values are determined, E_t value can be found using the expression 2.97. If v is assumed to be independent of temperature ($\alpha = 0$), then slope of $\ln(T_m^2/\beta)$ vs. $1/T$ graph gives the activation energy E .

2.3.7 Photoluminescence Experiments

Photoluminescence (PL) spectroscopy is a basic, non-destructive and contactless method to characterize some properties of the semiconductors, especially to get information about the band gap energy and electronic levels. PL measurements are based on the excitation of the sample with a source having energy greater than band gap and then analysis of the emitted light from the sample due to the transitions occurring in the band structure. As mentioned in the theory of TSC and TL measurements, when a sample is exposed to radiation having energy greater than the band gap, electrons are excited to higher energy levels. As a result, electron-hole pairs are created. After a short time, the electrons recombine with holes in such a way that excess energy of this recombination is given out as emission of light (radiative recombination) or not (non-radiative recombination). This energy is equal to difference of the energies of electronic levels taking part in the recombination process. As a result of the analysis of PL spectroscopy measurements, detailed information about these levels is obtained.

Three main steps take important attention in the PL measurements [59].

- i. *Excitation*: This is the process in which electrons are excited to higher energy levels after absorbing energy from an excitation source. Electron-hole pairs are created as a result of excitation process. The excitation is presented in the figure 2.15 (a).
- ii. *Thermalization*: In this step, excited electron and hole pairs relax towards quasi-thermal equilibrium distributions (figure 2.15 (b)).
- iii. *Recombination*: This is the step in which thermalized pairs recombine by emitting light (figure 2.15 (c)).

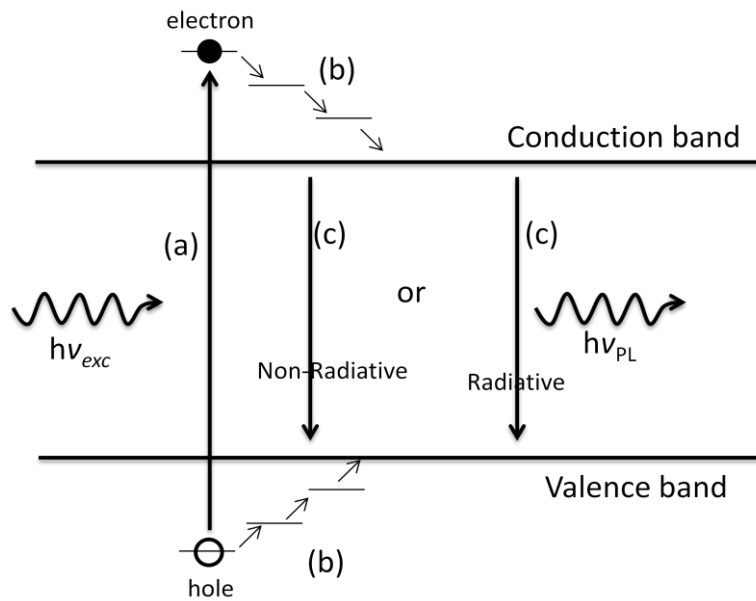


Figure 2.15. Representation of the (a) excitation, (b) thermalization and (c) recombination mechanisms in the energy band gap structure.

The excitation and thermalization steps are straightforward in the PL measurements. However, recombination step is the most important one and has different forms.

2.3.7.1 Recombination Mechanisms

The electron-hole recombination can occur mainly in three ways called as band-to-band, free-to-bound and donor-acceptor pair transitions. Figure 2.16 shows the possible recombination ways in the band structure [59].

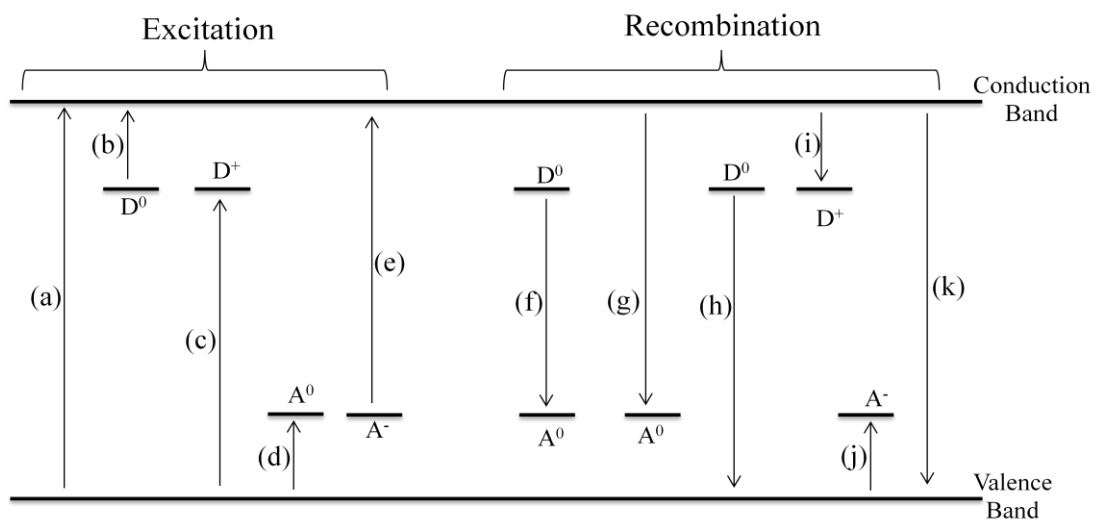


Figure 2.16. Possible transitions in the band structure.

i. *Band-to-band transitions*

The excited carriers occupy at the conduction and valence maxima, respectively, after thermalization process. These electron-hole pairs recombine and emit light after a short time. Since this transition occurs as a result of recombination of free electrons and holes in the conduction and valence bands, respectively, it is called as band-to-band or free-to-free transition. The emission rate (R) depends on the initial (n_i) and final (n_f) densities of states and probability (P_{if}) for the transition from the initial state to final state by the expression [40]

$$R = n_i n_f P_{if} . \quad (2.98)$$

The transition probability depends on the type of the band gap. In the direct band gap transition, the momentum is conserved since the transition occurs between direct valleys as shown in figure 2.17 (a). Therefore, the transition probability P_{if} does not depend on photon energy. The energy conservation relates the photon energy ($h\nu$) to initial (E_i) and final (E_f) energies by

$$h\nu = E_f - E_i . \quad (2.99)$$

However, in the indirect transitions, the energy and momentum of the excited electrons change. Conservation of momentum is provided via phonon interactions (Figure 2.17 (b)). The transition from E_i to E_f takes place after a phonon is either emitted or absorbed. The corresponding relation of equation 2.99 for indirect transition is given by

$$h\nu = E_f - E_i \pm E_p , \quad (2.100)$$

where E_p is the energy of phonon.

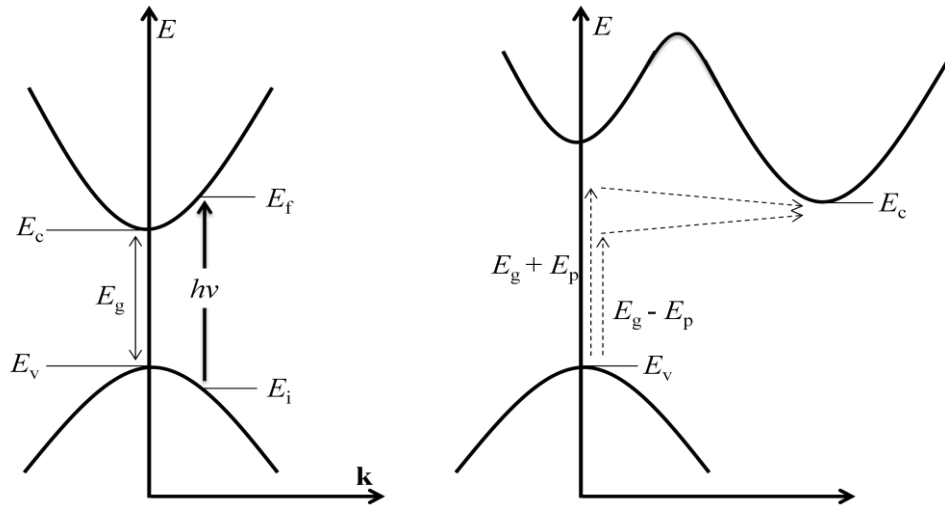


Figure 2.17. Schematic diagram of the absorption transitions in (a) direct band gap semiconductors and (b) indirect band gap semiconductors [34].

ii. *Free-to Bound transition:*

In the semiconductors, donor and acceptor levels can come out due to the defects or doped atoms as mentioned before. After excitation of a sample, these levels can be occupied by electrons and holes. Free to bound transitions occur when an electron (hole) in the donor

(acceptor) level recombines with a free hole (electron) in the valence (conduction) band. In these transitions, the emitted photon energy is given by

$$h\nu = E_g - E_{A,D} \quad \text{for direct transition} \quad (2.101)$$

$$h\nu = E_g - E_{A,D} - E_p \quad \text{for indirect transition} \quad (2.102)$$

where E_g , $E_{A,D}$ and E_p are the band gap, acceptor/donor and photon energies, respectively.

iii. Donor-Acceptor Transition

Most of the semiconductors have both of donor and acceptor levels. In these materials, acceptor levels are at least partly filled by electrons and donor levels are at least partly empty. Therefore, one of the possible transitions in the semiconductor is the transition between these levels. In this case, the coulomb interaction between donor and acceptor levels affects energy of emitted photon. If the energies of donor and acceptor levels are defined by E_d and E_a , respectively, the emitted photon has energy

$$h\nu = E_g - E_A - E_d + \frac{q^2}{\epsilon r} \quad \text{for indirect transition} \quad (2.103)$$

where q is the charge, ϵ is static dielectric constant and r is distance between the ionized donor and acceptor levels.

2.3.7.2 Laser Excitation Power Dependence of Photoluminescence Peak Energy

Information about type of recombination mechanisms in the PL experiments can be obtained from the laser excitation power dependence of the PL intensity. PL intensity (I) and laser excitation power (L) are related to each other as [60-63]

$$I \propto L^\delta, \quad (2.104)$$

where δ is a constant giving information about the recombination mechanisms. The constant δ is generally between 1 and 2 for the free and bound exciton emission and between 0 and 1 for free to bound and donor-acceptor pair recombination [64,65].

In addition to the PL intensity, laser excitation power also affects the peak energy. The dependency of the peak energy on laser excitation power was considered in the theoretical study given by E. Zacks and A. Halperin in Ref. 66. Their work was based on a crystal with donor and acceptor concentrations N_d and N_a , respectively. Assumptions in their study were that one of the impurities is in minority ($N_d \ll N_a$) and temperature of the crystal is low enough so that thermal ionization of donors or acceptors is ignorable. Under these assumptions the excitation intensity (J) is revealed as [66-69]

$$J = D \frac{(h\nu_m - h\nu_\infty)_m^3}{h\nu_B + h\nu_\infty - 2h\nu_m} \exp\left(-\frac{2(h\nu_B - h\nu_\infty)}{h\nu_m - h\nu_\infty}\right), \quad (2.105)$$

where D is a proportionality constant, $h\nu_B$ is emitted photon energy of a closer donor-acceptor pair, $h\nu_\infty$ is emitted photon energy of an infinitely distant donor-acceptor pair, $h\nu_m$ is emission energy of band maxima.

2.3.7.3 Temperature Dependence of Photoluminescence

Photoluminescence measurements can also be used to obtain information about the nature of the emission processes and electronic energy levels in the semiconductor band structure. For this purpose, temperature dependence of the observed bands is studied and variation of the peak intensity with temperature analyzed to find the activation energies of the energy levels. When the probability for a radiative transition (P_r) is assumed as temperature-independent, efficiency of emission (η) is described by the relation [40]

$$\eta = \frac{P_r}{P_r + P_{nr}} \quad , \quad (2.106)$$

where P_{nr} is probability for a non-radiative relation. The temperature dependence of the non-radiative transition is given by

$$P_{nr} = P_{nro} \exp(-E_t / kT) \quad , \quad (2.107)$$

where E_t is some activation energy and P_{nro} is a temperature independent coefficient. Combining equations 2.106 and 2.107, the luminescence efficiency is obtained as

$$\eta = \frac{1}{1 + C \exp(-E_t / kT)} \quad , \quad (2.108)$$

where $C = P_{nro} / P_r$ is a constant. Moreover, the temperature dependence of the PL peak intensity, $I(T)$, can be expressed under the light of same theoretical approach given above and described by the relation

$$I = \frac{I_0}{1 + \alpha \exp(-E_t / kT)} \quad , \quad (2.109)$$

where I_0 is proportionality constant and α is rate parameter. The equation 2.109 gives the $I(T)$ dependence for one activation energy. But, in some semiconductors there can be more than one electronic energy level taking role in the PL measurements. The generalized relation of equation 2.109 for n number of thermal quenching processes is given as

$$I = \frac{I_0}{1 + \sum_n \alpha_n \exp(-E_n / kT)} \quad , \quad (2.110)$$

where E_n are activation energies of the energy levels.

In addition to the PL intensity, temperature variation also affects the peak maximum position on temperature and thereby the energy of the emitted photon. In the semiconductors, lattice expands with increasing temperature. This expansion increases the oscillations of the atoms about their equilibrium lattice positions. Consequently, the energy levels expand and band gap energy of the semiconductors decreases [70]. Band gap energy (E_g) depends on the temperature by the following equation [71]

$$E_g(T) = E_g(0) + \frac{\gamma T^2}{T + \beta} \quad , \quad (2.111)$$

where $E_g(0)$ is band gap energy at $T = 0$ K, γ is rate of change of band gap with temperature ($\gamma = dE_g / dT$) and β is Debye temperature. Since E_g decreases with temperature, activation energies of the electronic levels are also expected to be decreasing. This decrease is observed in the PL experimental data as a shift of the peak maximum temperature to higher values (that is to lower energies).

2.3.8 Electrical Measurements

2.3.8.1 Electrical Conductivity

Conductivity is one of the most important properties of the materials to be known in the electrical characterization. Electrical conductivity is a measure of material's ability to conduct electricity and directly proportional to electron (n) and hole (p) concentrations in conduction and valence bands, respectively. Conductivity (σ) of a semiconducting material is given as [72]

$$\sigma = e(\mu_e n + \mu_p p) \quad (2.112)$$

where e is the elementary charge, μ_e and μ_p are electron and hole mobilities, respectively. In the intrinsic semiconductors, n and p values are equal. However, the hole (electron) contribution to the conductivity of an n -type (p -type) is negligible, since hole (electron) concentration is negligible compared to electron (hole) concentration. Considering an n -type semiconducting material, the conductivity is expressed as,

$$\sigma = N_c e \mu e^{-(E_c - E_i)/kT} \quad (2.113)$$

where E_c and E_i are valence band and intrinsic level energies, respectively. N_c is defined as,

$$N_c = 2 \left(\frac{2\pi m_e^* kT}{h^2} \right)^{3/2} \quad (2.114)$$

where m_e^* is the electron effective mass. As seen from the equation 2.114 N_c is proportional to $T^{3/2}$. At the same time in the high temperature range, mobility decreases with temperature according to relation of $\mu \sim T^{-3/2}$. Therefore, the conductivity in equation 2.113 for sufficiently high temperatures can be given as,

$$\sigma = \sigma_0 e^{-(E_c - E_i)/kT} \quad (2.115)$$

where σ_0 is a constant. The conductivity activation energy of the material is obtained from slope of the $\ln(\sigma) - 1/T$ graph [34].

2.3.8.2 Space Charge Limited Currents

Space charge limited current (SCLC), used to get information about the impurity level depends on the analysis of the current-voltage characteristic of the material. In this technique, the current flowing through the ohmic contact is measured as a function of applied voltage. If the used sample has trap level, a large number of space charges is located in the trap center. If the applied voltage is sufficiently increased, traps are saturated and electrons are injected into the bulk of the material and contribute to flowing current [73]. In the case of a single shallow trap level, the behavior of the I - V characteristics can be divided into three main branches [74-78]:

i. *Ohmic Region*; The current density (J) depends linearly on the applied voltage (V) by the relation,

$$J = e\mu \frac{V}{L} \quad (2.116)$$

ii. *Space Charge Region*; Injected charges dominate the current and current density-voltage are related by the relation,

$$J = \frac{9}{8} \varepsilon \mu \theta \frac{V^2}{L^3} \quad (2.117)$$

iii. *Trap filled region*: In this region, shallow trap level is filled by the excess injected charges and current increases towards the ideal trap free characteristic ($\theta = 1$). In this case, the trap filled voltage limit is given by

$$V_{TFL} = \frac{2N_t e L^2}{3\epsilon} \quad (2.118)$$

In the above expressions, L is the distance between electrodes and N_t is the density of the trap levels. The quantity θ is the fraction of injected charge which is available for conduction band and given by

$$\theta = \frac{gN_c}{N_t} \exp(-E_t / kT) \quad (2.119)$$

where g is the degeneracy factor and E_t is the energy of the trap level.

2.3.8.3 Photoconductivity

One of the factors affecting the conductivity is the illumination of the sample. When the materials are exposed to light having energy greater than band gap, free electrons and holes are created in the conduction and valence bands, respectively. These free charge carriers increase the conductivity of the material. Change in the conductivity due to the illumination is defined as photoconductivity. If a homogeneous material in which there is only one carrier transport (assume n -type) is illuminated, the carrier density (n) and carrier mobility (μ) changes due to this photoexcitation. Therefore, the conductivity can be defined as

$$\sigma = \sigma_0 + \Delta\sigma = e(n_0 + \Delta n)(\mu_0 + \Delta\mu) \quad (2.120)$$

where Δn and Δp are increases of the free electron and hole concentrations, respectively, and σ_0 is the dark conductivity [57]. Since $\sigma_0 = n_0 e \mu_0$, the increase in the conductivity is

$$\Delta\sigma = e\mu_0\Delta n + (n_0 + \Delta n)e\Delta\mu \quad (2.121)$$

The increase of the carrier density can be written in terms of the photo-excitation rate (ϕ) and electron lifetime (τ_n) as $\Delta n = \phi\tau_n$. Then equation 2.122 can be re-written as

$$\Delta\sigma = e\mu_0\tau_n\phi + n_0e\Delta\mu \quad (2.122)$$

Assuming that mobility and lifetime is independent of illumination, photoconductivity change in equation 2.122 is

$$\Delta\sigma = e\mu_0\tau_n\phi \quad (2.123)$$

However, if the lifetime varies as ϕ^{n-1} then $\Delta\sigma$ varies with ϕ^n . In that case, photocurrent defined as the change of the current under illumination will be proportional to ϕ^n . The value of n gives us opportunity to understand the behavior of photoconductivity [57].

- If $n < 1$, lifetime decreases with increasing light intensity. The behavior is called as “sublinear”.
- If $n > 1$, lifetime increases with increasing light intensity and consequently material becomes more photosensitive. The behavior is called as “supralinear”.
- If $0 < n < 1$, the recombination is dominated by a single type of imperfection level.
- If $n = 0.5$ and $n = 1$, there exist recombination at the surface (bimolecular) and in the bulk (bimolecular), respectively.

CHAPTER 3

EXPERIMENTAL TECHNIQUES

3.1 Introduction

Structural, optical, electrical and defect characterizations of the $\text{Ga}_{0.75}\text{In}_{0.25}\text{Se}$ single crystals were studied using x-ray diffraction (XRD) analysis, energy dispersive spectral analysis (EDSA), visible and infrared reflectivity and transmittance, ellipsometry, Raman spectroscopy, photoluminescence (PL), dark electrical resistivity, space-charge-limited current (SCLC), photoconductivity, thermally stimulated current (TSC) and thermoluminescence (TL) experiments. $\text{Ga}_{0.75}\text{In}_{0.25}\text{Se}$ polycrystals were synthesized from particular high purity elements taken in stoichiometric proportions. Growth of single crystals was accomplished using Bridgman method.

3.2 Energy Dispersive Spectral Analysis

The determination of the chemical composition of $\text{Ga}_{0.75}\text{In}_{0.25}\text{Se}$ single crystals was performed using the EDSA experiments. The experiments were performed using JSM-6400 scanning electron microscope. The used microscope has two equipments called as “Noran System6 X-ray microanalysis system” and “Semafore Digitizer” which take part in the analysis of experimental data. Figure 3.1 shows simple schematic configuration of used experimental system.

3.3 X-ray Diffraction Experiments

The crystal structure properties of the $\text{Ga}_{0.75}\text{In}_{0.25}\text{Se}$ were identified using XRD experiments. Measurements were performed using “Rigaku miniflex” diffractometer with $\text{CuK}\alpha$ radiation ($\lambda = 0.154049 \text{ nm}$). The scanning speed of the diffractometer was $0.02^\circ/\text{s}$. Figure 3.2 shows simple schematic representation of XRD measurement system. Least-squares computer program “TREOR 90” was used for analysis. Crystal system, Miller indices of the diffraction peaks and lattice parameters were obtained from the analysis. Experiments were accomplished in the diffraction angle (2θ) range of $10\text{-}80^\circ$.

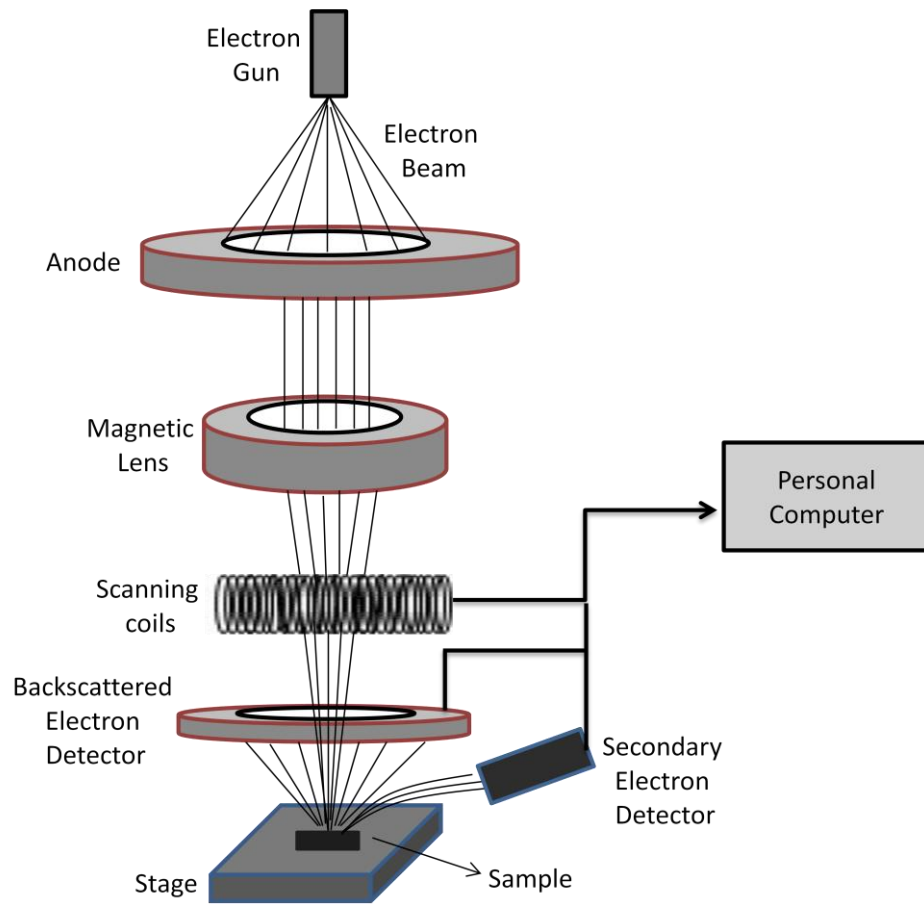


Figure 3.1. Schematic representation of scanning electron microscope

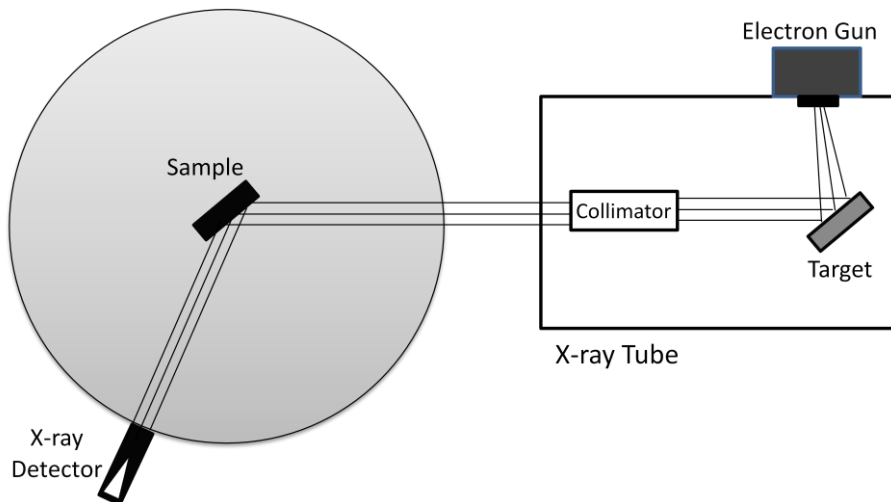


Figure 3.2. Simple schematic representation of XRD experiment.

3.4 Transmission-Reflection Experiments

Transmission and reflection measurements are basic experimental techniques used for the optical characterization of $\text{Ga}_{0.75}\text{In}_{0.25}\text{Se}$ semiconductor crystals.

Experiments were accomplished at room temperature in the 380-1100 nm spectral range. Shimadzu UV 1201 model spectrophotometer with resolution of 5 nm, which consisted of a 20 W halogen lamp, a holographic grating and a silicon photodiode, was used for the experiments. Transmission measurements were carried out under normal incidence of light with a polarization direction along the (001) plane. This plane is perpendicular to the c-axis of the crystal. For the reflection experiments, a specular reflectance measurement attachment with a 5° incident angle was used. Transmission measurements were made in the 10-300 K temperature range. Advanced Research Systems, Model CSW-202 closed cycle helium cryostat was used to cool the sample. Accuracy of the cooling system was 0.5 K. Technical reasons did not allow us to perform the reflection measurements at low temperatures. Figure 3.3 shows the schematic representation of the experimental systems used for transmission and reflection measurements.

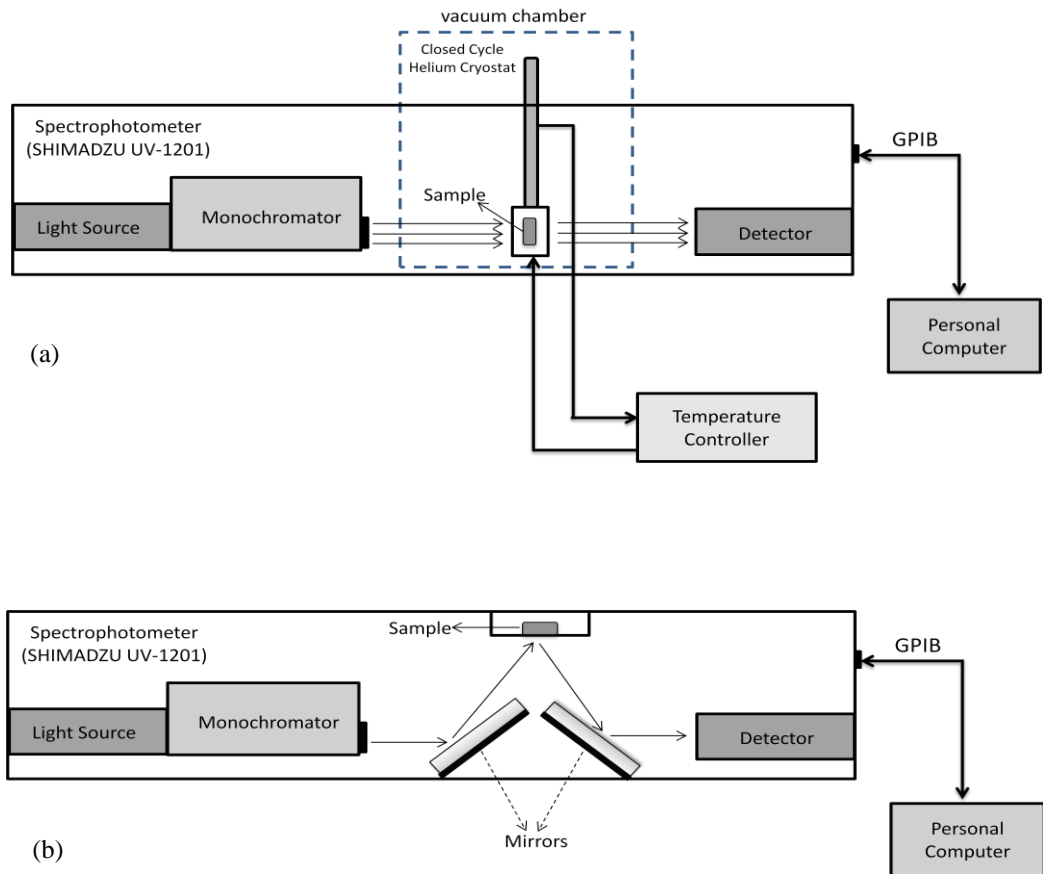


Figure 3.3. Simple schematic representation of (a) transmission and (b) reflection experimental set-up.

3.5 Ellipsometry Experiments

The optical characterization of the $\text{Ga}_{0.75}\text{In}_{0.25}\text{Se}$ single crystals was expanded by carrying out ellipsometry measurements. Analysis of the experimental data gave important knowledge about the spectral dependence of real and imaginary parts of the pseudodielectric function, pseudorefractive index and pseudoextinction coefficient of the used sample. Moreover, the interband transition (critical point) energies were found from the analysis of the second derivative spectra of the pseudodielectric function.

The ellipsometric measurements on $\text{Ga}_{0.75}\text{In}_{0.25}\text{Se}$ were taken at room temperature in the 1.2-6.0 eV spectral range with 0.01 eV increments using SOPRA GES-5E rotating-polarizer ellipsometer. The angle of incidence of the light beam was 70° . The measurements were performed on the layer-plane (001) crystal surface which is perpendicular to the optic axis c . Since the crystals have layered structures, it is very difficult to perform measurements on any other surfaces than the sample natural layer-plane surfaces. The samples were prepared by easy cleavage an ingot parallel to the crystal layer. The freshly cleaved surfaces are mirror-like.

3.6 Infrared and Raman Spectroscopy Measurements

The vibrational spectra of $\text{Ga}_{0.75}\text{In}_{0.25}\text{Se}$ layered crystals were studied using infrared reflectivity and transmittance and Raman scattering. IR reflection measurements were performed on the layer-plane (001) crystal surfaces with light polarization $E \perp c$. IR reflection spectra were recorded at room temperature with FIS-21 IR spectrometer in the frequency range from 100 to 400 cm^{-1} . The spectral resolution was 1 cm^{-1} . Infrared transmittance spectra were recorded with a Nicolet 6700 FTIR spectrometer (Thermo Scientific, USA) equipped with a He/Ne laser source (632.8 nm), KBr beamsplitter, DTGS-KBr detector. The spectral range was between 400 and 4000 cm^{-1} (middle-IR). IR beam was focused onto a 6 mm diameter area in the center of the holder. Scanning of sample and processing of spectra were performed with OMNIC software. Raman scattering spectra were excited by the 532 nm line of YAG:Nd³⁺ laser. The spectra were registered at room temperature in the frequency range 25–400 cm^{-1} with “Horiba Jobin Yvon RMS-550” Raman spectrometer at a resolution of 1 cm^{-1} .

3.7 Photoluminescence Experiments

As a further optical method, photoluminescence measurements have been carried out on $\text{Ga}_{0.75}\text{In}_{0.25}\text{Se}$ layered single crystals to get detailed information about the radiative transition in the crystal. Figure 3.4 shows schematic representation of the used PL experimental set-up. The sample with dimensions of $6 \times 4 \times 1 \text{ mm}^3$ was irradiated along the c -axis using an argon-ion laser operating at wavelength of 488.0 nm. The PL emission was collected from the laser-illuminated surface of the sample in a direction close to the normal of the (001) plane. The crystals were cooled from room temperature to 7 K using a CTI-Cryogenics M-22 closed cycle He cryostat. The accuracy of the temperature measurements was within $\pm 0.5 \text{ K}$. U-1000 Jobin Yvon double grating spectrometer and a cooled GaAs photomultiplier endowed with the necessary photon counting electronics were used to analyze the PL spectra in the wavelength range of 580-670 nm. The excitation intensity dependence of the PL spectra measurements have been performed using neutral-density filters placed in front of the laser. The laser beam intensity was varied from 0.06 to 1.40 W cm^{-2} .

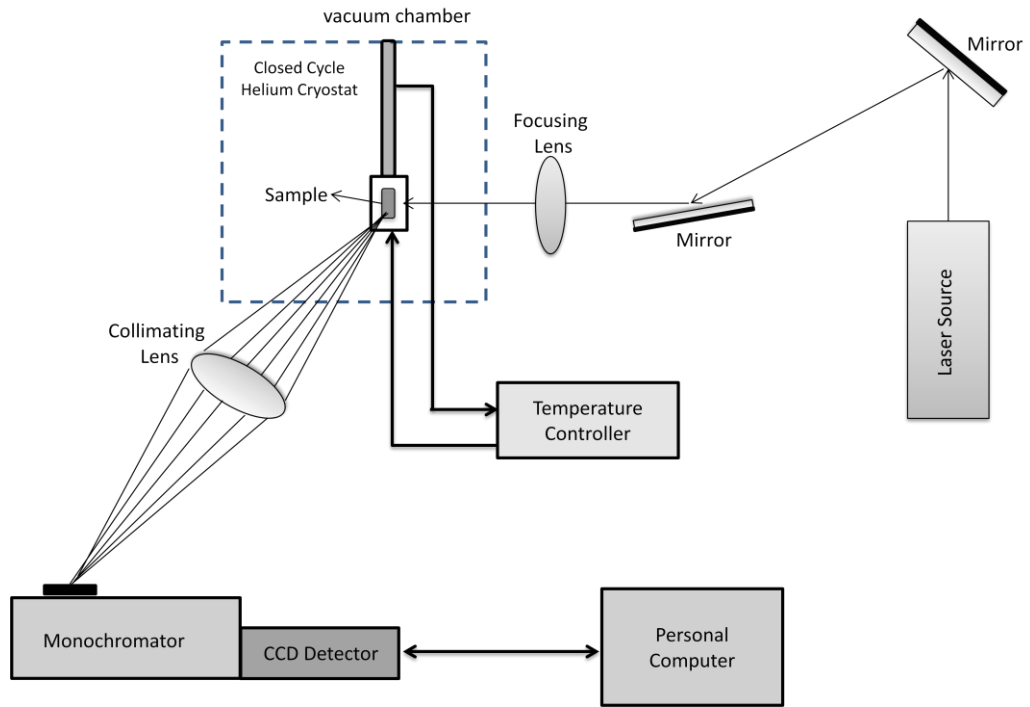


Figure 3.4. Simplified block diagram of the PL measurement set-up.

3.8 Electrical Measurements

In the electrical characterization studies, the temperature and illumination dependence of the resistivity/conductivity of $\text{Ga}_{0.75}\text{In}_{0.25}\text{Se}$ crystals were investigated. In the measurements, four contacts were placed on the circumference of the sample having arbitrary shape classified in the van der Pauw geometry (Figure 3.5). Ohmic sufficiently small contacts were made using electrodes connected to crystal with high purity silver paste. The contacts showed ohmic behavior which was verified from linearity of the current-voltage characteristics. The temperature-dependent resistivity, SCLC and photoconductivity measurements were accomplished in an automated closed-cycle Lakeshore cryogenic system. The current was supplied by a Keithley 220 programmable current source. Keithley 2182 Nanovoltmeter was used for the measurement of voltage across the contacts.

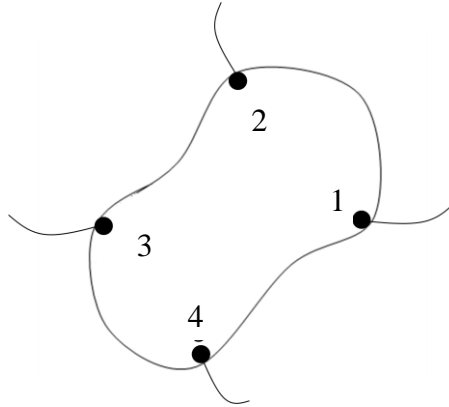


Figure 3.5. Representation of the contacts on arbitrary shaped van der Pauw geometry.

The resistivity measurements were conducted by applying a constant current through the neighboring two contacts and measuring voltage across the other two contacts. By this way, there exist four different measurement forms. The corresponding values for each measurement are calculated using Ohm's law. Table 3.1 shows the possible measurement ways and corresponding resistance values.

Table 3.1 The applied currents between contact pairs, measured potential differences between neighboring contacts and corresponding resistances

Current	Voltage	Resistance	
I_{12}	V_{34}	$R_a = V_{34}/I_{12}$	$R_1 = R_a + R_b$
I_{23}	V_{41}	$R_b = V_{41}/I_{23}$	
I_{34}	V_{12}	$R_c = V_{12}/I_{34}$	$R_2 = R_c + R_d$
I_{41}	V_{23}	$R_d = V_{23}/I_{41}$	

The resistivity of the material with thickness d is calculated from the relation [79]:

$$\rho = \frac{\pi d}{\ln(2)} \frac{R_1 + R_2}{2} f\left(\frac{R_1}{R_2}\right)$$

where f is a correction factor. If the R_1 and R_2 values agree within $\pm 10\%$, f is taken as 1 [72]. The thickness of the used sample was 1 mm.

3.9 Thermally Stimulated Current Experiments

The main point which the TSC experiments based on is to provide a transition of carriers from trapping centers located in the forbidden energy region to conduction and/or valence bands and to obtain a current by moving the carriers under the effect of an electric field. For this purpose, firstly the trapping centers are filled with charge carriers at low temperatures (T_0). Then, the sample is excited at temperature T_0 using a suitable light source and so the transition of electrons from valence band to conduction band is achieved by making a band-to-band transition. The electrons (holes) in the conduction (valence) band pass back to valence (conduction) band after spending their lifetimes. But some of them are trapped in the trapping centers when they are making transitions. The trapped charge carriers must have enough energy to be excited to the conduction and/or valence bands. In the thermally stimulated current measurements, the needed energy is provided by heating the sample. Since the analysis methods mainly depend on the constant heating rate assumption, the sample is heated using a constant rate. The charge carriers excited to conduction and/or valence bands from the trapping centers by the help of thermal energy are exposed to a constant electric field. The temperature dependence of the current flowing on the sample due to this electric field is obtained as experimental data in the TSC experiments. The current-temperature curve is called as “glow curve”. The properties of the trapping center(s) are found as a result of the analysis of the glow curve.

The dimensions of used $\text{Ga}_{0.75}\text{In}_{0.25}\text{Se}$ in the TSC experiments were $7 \times 6.5 \times 1 \text{ mm}^3$. We have prepared the sample connections using sandwich geometry configuration. In this type of configuration, one of the electrodes is connected to front surface of the sample. This connection was done using a small droplet of silver paste. The circuit connection was completed by connecting the second electrode to the cryostat. This type of connection lets the electrons and/or holes to flow through the crystal in the direction of parallel to the c -axis. The simple representation of the sandwich geometry is shown in the figure 3.6. Hot probe application showed that the electrical conductivity of $\text{Ga}_{0.75}\text{In}_{0.25}\text{Se}$ crystal was p-type.

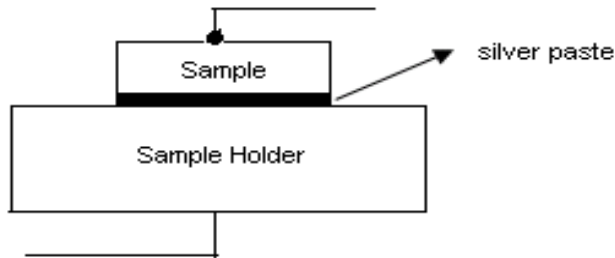


Figure 3.6. The simple representation of the sample with sandwich configuration.

In our TSC experiments, the excitation of the sample at low temperature was done using a LED generating the light at a maximum peak of 2.6 eV. The trap level(s) was filled at temperature of $T_0 = 10 \text{ K}$ under the effect of excitation for 600 sec and bias voltage of $V_1 = 1 \text{ V}$. Then, excitation was turned off and an elapsed expectation time of 300 sec was waited in the dark. After this time interval, the sample was heated at constant rate under a bias voltage of $V_2 = 50 \text{ V}$. TSC experiments were done in the temperature range of 10-300 K using an Advanced Research systems closed-cycle helium cryostat. Constant heating rate was achieved thanks to Lake-Shore 331 temperature controller. A Keithley 228A voltage/current source and a Keithley 6485 picoammeter were used in the experiments. The temperature and current sensitivities of the

system were about 10 mK and 2 pA, respectively. The simplified block diagram of the TSC system is shown in the figure 3.7.

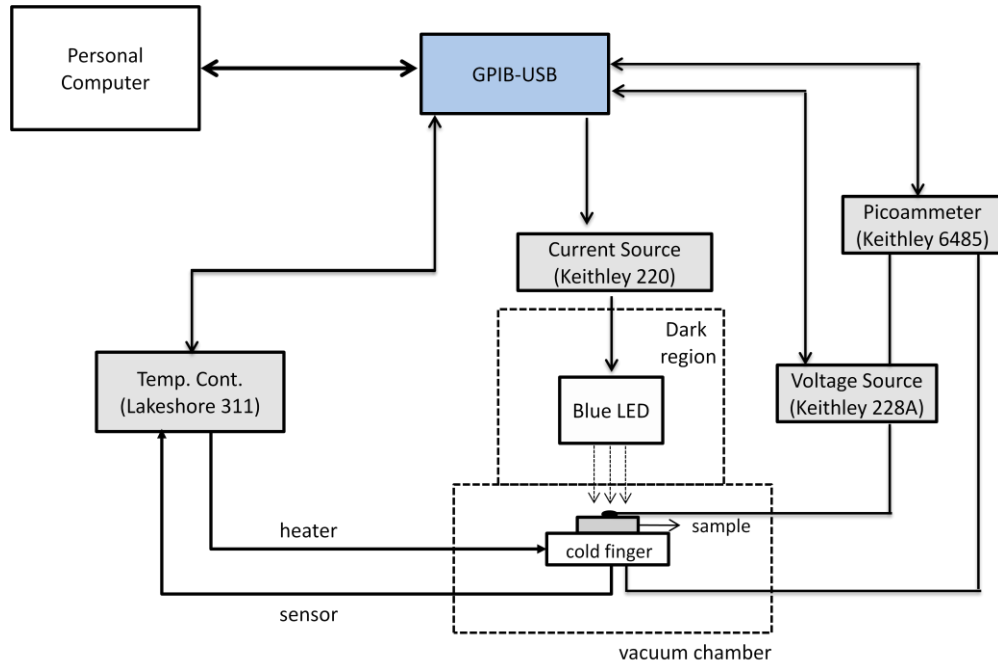


Figure 3.7. Simplified block diagram for TSC experimental set-up.

3.10 Thermoluminescence Experiments

The experimental procedure of the thermoluminescence measurements shows very big similarities with that of TSC experiments. In the TL experiments, the trapping centers are also filled using a suitable light source. Then, the sample is heated with constant heating rate after expectation time has elapsed. As distinct from the TSC experiments, in the TL measurements no contact is used on the surface of the sample and the sample is not exposed to a potential throughout the TL experiments. In the TL experiments, electrons (holes) excited to the conduction (valence) band from the trapping centers by the help of thermal energy de-excites to the valence (conduction) band after a very short time (lifetime). In the process of this transition, photons are released out from the sample. The data proportional to the count of these photons are received using suitable experimental devices. Although the current flowing over the sample is taken as experimental data in the TSC experiments, a measurement directly proportional to the number of photon counts are received as experimental data in the TL experiments. The curve of the temperature dependence of the TL intensity was called as the “glow curve” of the TL experiments. This glow curve is analyzed using the analytical methods mentioned in the chapter 2 and properties of the trapping centers are found. As experimental procedure, TL experiments have some advantages compared with TSC. Not dealing with background current and not encountering with contact problems can be considered as two important advantages. However, the need of large enough number of photon counts for the application of the analysis methods can be thought as the disadvantage side of the TL experiments.

TL measurements were carried out using a home-made set-up which was constructed by modifying the existing TSC measurement system (see figure 3.8). The system is built around a closed cycle helium gas cryostat (Advanced Research Systems, Model CSW-202). Sample temperature was controlled using a LakeShore Model 331 temperature controller which is connected to a personal computer via the GPIB bus. Temperature was measured using a semiconductor diode detector. The temperature controller is able to control the sample temperature between 10 and 300 K and can ramp the temperature linearly at a maximum rate of 1.0 K/s.

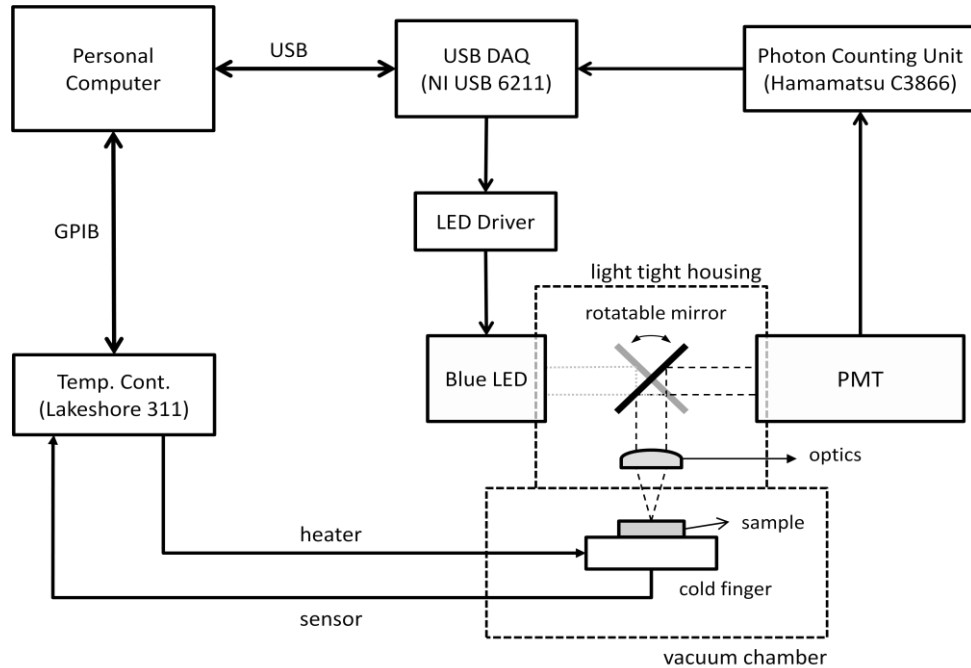


Figure 3.8. Simplified block diagram of the TL experimental set-up.

A light tight measurement chamber which carries the detector (a photomultiplier tube, PMT), light source (Light Emitting Diode, LED) and the optics was connected to the optical access port of the cryostat (quartz window) where the sample lies on the focal plane of the optics for both measurement and illumination. To focus the illumination light on to the sample or to direct the luminescence onto the detector window, a rotatable front surface mirror was installed into the light tight housing. Luminescence emitted from the sample was measured using a photomultiplier tube (Hamamatsu R928; spectral response: 185 to 900 nm) working in photon counting regime. Pulses from the photomultiplier were converted into TTL pulses using a fast amplifier/discriminator (Hamamatsu Photon Counting Unit C3866) and counted by the counter of a data acquisition module (National Instruments, NI-USB 6211). The DAQ unit was connected to a PC using the standard USB interface. A high power blue LED emitting at ~ 470 nm (2.6 eV) was used for illuminating the sample. For this purpose the mirror position was changed to the LED side. The flux at the sample position was about a few mW/cm^2 . The LED was driven by a computer controlled constant current source via the DAQ interface. Whole measurement system was controlled by a computer using software written in LabViewTM graphical development environment.

For a TL measurement, the sample was irradiated for 300 seconds using the blue light at 10 K, after 120 seconds of waiting (to allow the unstable components to decay), the sample was warmed up linearly at a predetermined heating rate and the emitted luminescence is recorded as a function of temperature.

3.11 Photoconductivity Decay Experiments

Photoconductivity decay experiments were performed to determine the carrier lifetime. In the experiments, two electrodes were connected to the opposite surfaces of crystal using silver paste droplets. Then, one of the contacts was illuminated by a high efficiency short-pulsed LED controlled by “NI USB-6211 high-performance USB data acquisition device”. The determination of the decay time of the photocurrent was done using data obtained by means of a signal transmitted to the computer during the experiment. The schematic representation of the used experimental set-up is shown in figure 3.9.

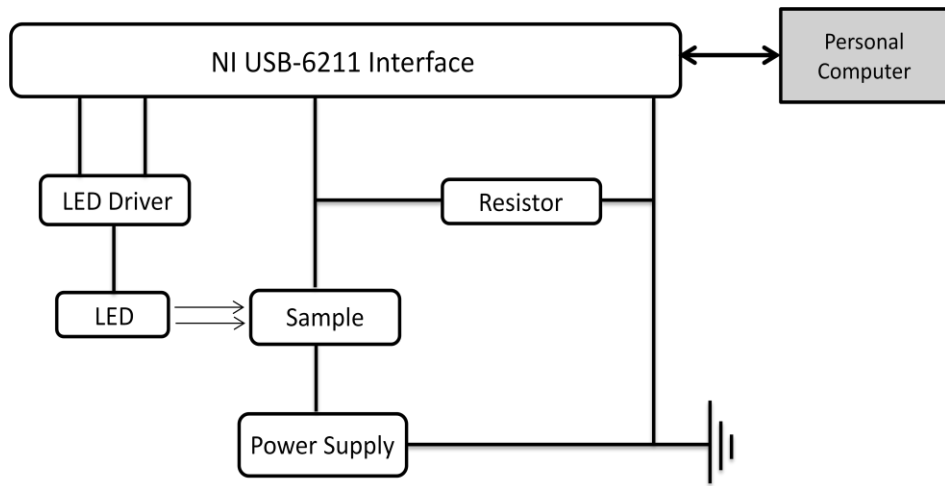


Figure 3.9. Simplified block diagram of photoconductivity decay experimental set-up.

CHAPTER 4

RESULTS AND DISCUSSION

4.1 Introduction

In this chapter, the results of the applied experimental techniques for the structural, optical, electrical and defect characterization of $\text{Ga}_{0.75}\text{In}_{0.25}\text{Se}$ single layered crystals will be given in detail. The obtained results will be compared with the results of the studies on GaSe crystal which is the main constituent compound of $\text{Ga}_{0.75}\text{In}_{0.25}\text{Se}$. The variation of the characteristic properties of GaSe as a result of addition of the indium atoms will be revealed.

4.2 X-ray Diffraction and Energy Dispersive Spectral Analysis

Structural properties of $\text{Ga}_{0.75}\text{In}_{0.25}\text{Se}$ single layered crystals were determined using energy dispersive spectroscopy and x-ray diffraction (XRD) experiments. The chemical composition of $\text{Ga}_{0.75}\text{In}_{0.25}\text{Se}$ crystals was identified using energy dispersive spectroscopy experiments. Figure 4.1 shows the resulting spectroscopy obtained from the measurements carried out in 0-9 keV energy range. The atomic composition ratio of constituent elements (Ga : In : Se) in the crystal was found out as 39.8 : 11.3 : 48.9, respectively [80].

The crystal structure was obtained by means of XRD experiments. Figure 4.2 shows x-ray diffractogram of $\text{Ga}_{0.75}\text{In}_{0.25}\text{Se}$ crystal. The crystal system, Miller indices of the diffraction peaks and lattice parameters were acquired from the outputs of the least-squares computer program "TREOR 90". Miller indices ($h k l$), observed and calculated interplanar spacings (d) and relative intensities (I/I_0) of the diffraction lines evaluated from the program are given in table 4.1. It is seen from the table that calculated and observed interplanar spacings were in good agreement with each other. Moreover, the lattice parameters of the orthorhombic unit cell were found to be $a = 0.62365$, $b = 0.52206$ and $c = 1.59194$ nm [80]. The effect of addition of In atoms to GaSe compound on the crystal structure can be revealed by comparing the obtained results with those of GaSe studied in Ref. [9]. In this study, the structural analysis showed that GaSe has hexagonal crystal structure with lattice parameters of $a = 0.3755$ and $c = 1.5946$ nm. It is seen that addition of In atoms to GaSe compound transforms the structure of the mixed crystal $\text{Ga}_{0.75}\text{In}_{0.25}\text{Se}$ from hexagonal to orthorhombic with above given lattice parameters. This transformation can probably be due to the difference between the atomic radii of indium and gallium atoms (about 14 %) leading to the local distortions of the crystal structure [81].

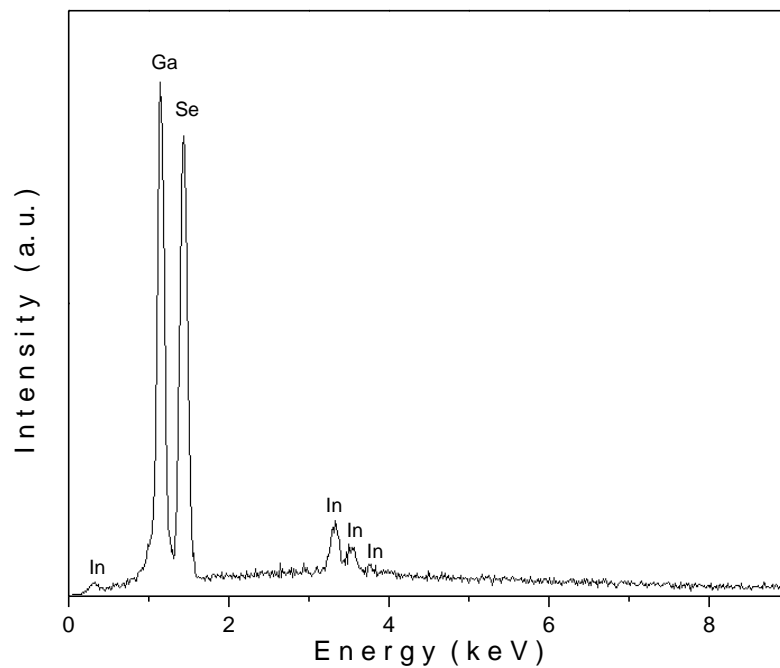


Figure 4.1. Energy dispersive spectroscopic analysis of Ga_{0.75}In_{0.25}Se crystal.

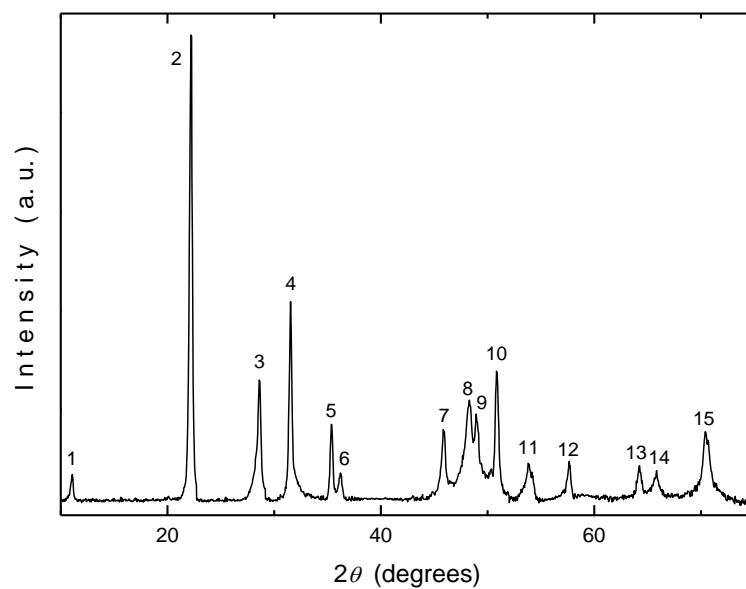


Figure 4.2. X-ray powder diffraction pattern of Ga_{0.75}In_{0.25}Se crystal.

Table 4.1. X-ray powder diffraction data for Ga_{0.75}In_{0.25}Se crystal

No.	<i>h k l</i>	<i>d</i> _{obs} (nm)	<i>d</i> _{calc} (nm)	<i>I</i> / <i>I</i> ₀
1	2 0 0	0.79647	0.79597	7.1
2	0 2 1	0.40011	0.40032	100
3	0 4 0	0.31186	0.31182	27.0
4	5 2 0	0.28344	0.28357	43.7
5	2 4 1	0.25371	0.25374	17.7
6	2 0 2	0.24794	0.24804	7.4
7	7 2 1	0.19775	0.19774	16.5
8	6 4 1	0.18828	0.18845	22.8
9	8 0 1	0.18593	0.18594	19.8
10	8 3 0	0.17942	0.17949	28.9
11	9 2 0	0.17026	0.17017	9.4
12	6 4 2	0.15977	0.15979	9.8
13	5 6 2	0.14486	0.14482	8.9
14	6 2 3	0.14172	0.14171	7.8
15	8 5 2	0.13363	0.13363	16.1

4.3 Transmission and Reflection Experiments

Figure 4.3 shows temperature dependence of the transmittance (*T*) spectra of Ga_{0.75}In_{0.25}Se crystals in the wavelength (λ) range of 380-1100 nm and temperature range of 10-300 K [82]. The room temperature reflection measurements were accomplished using the samples with natural cleavage planes and the thickness such that $ad \gg l$ (inset of figure 4.3). Absorption coefficient (α) and refractive index (*n*) were calculated from the transmittance (*T*) and reflectance (*R*) spectra using expressions

$$\alpha = \frac{1}{d} \ln \left\{ \frac{(1-R)^2}{2T} + \left[\frac{(1-R)^4}{4T^2} + R^2 \right]^{1/2} \right\} \quad (4.1)$$

$$n = \frac{1+R}{1-R} + \left[\frac{4R}{(1-R^2)} - \left(\frac{\alpha\lambda}{4\pi} \right)^2 \right]^{1/2} . \quad (4.2)$$

which are derived from the equations 2.7, 2.9 and 2.11 [40].

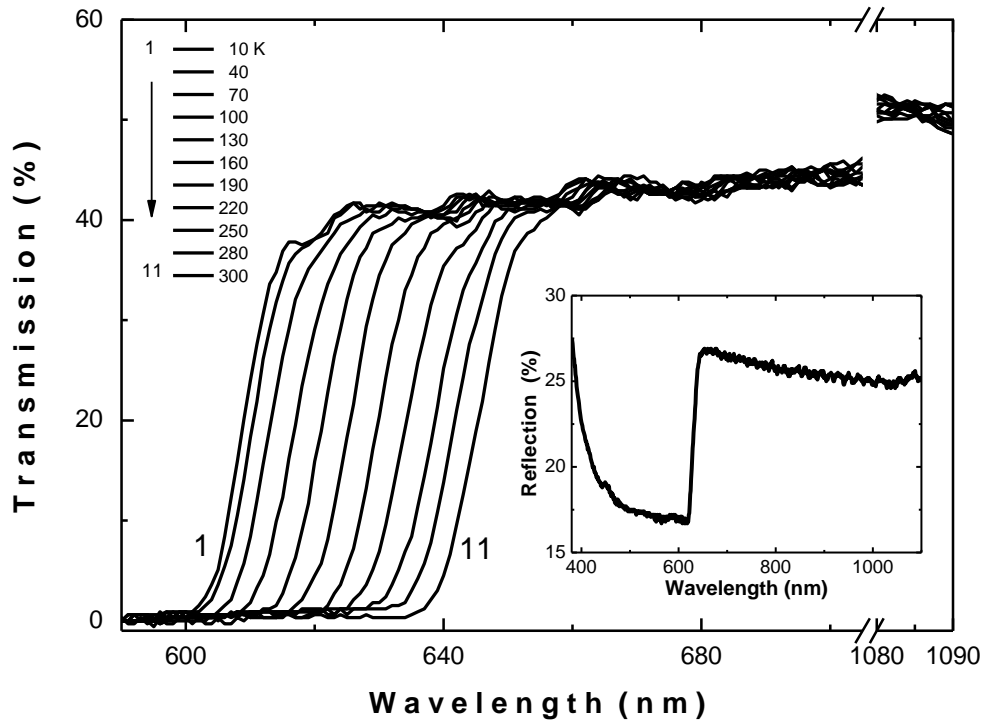


Figure 4.3. The spectral dependence of transmission for $\text{Ga}_{0.75}\text{In}_{0.25}\text{Se}$ crystal in the temperature range of 10–300 K. Inset: The spectral dependence of reflectivity at room temperature.

Thickness of the used crystal was measured as 100 μm . In order to get more information about the energy band gaps of the crystal, dependence of α on photon energy ($h\nu$) was used in the high absorption region. Figure 4.4 shows the corresponding dependence for each temperature. It was observed that room temperature absorption coefficient (α) for $\text{Ga}_{0.75}\text{In}_{0.25}\text{Se}$ crystal changes from 27 to 457 cm^{-1} with increasing photon energy from 1.82 to 1.95 eV. Analysis of the experimental data revealed that $(\alpha h\nu)$ and $(h\nu - E_g)$ relation gives a good coherence for $p = 2$ corresponding to indirect band gap transitions (see equation 2.8). The indirect band gap energies (E_{gi}) at studied temperatures were found from intersection point of fitted line with photon energy axis. Temperature dependence reflection measurements could not be performed in our experimental set-up. Therefore, spectral dependence of room temperature reflectivity was uniformly shifted in energy according to the blue shift of the absorption edge for calculation of α . E_{gi} values increases from 1.89 to 2.01 eV as the temperature decreases from 300 to 10 K (Figure 4.5). The linear fit of band gap energy versus composition graph, accomplished on $\text{Ga}_x\text{In}_{1-x}\text{Se}$ compounds in the two extreme narrow ranges of $0 \leq x \leq 0.2$ and $0.9 \leq x \leq 1.0$ estimated E_g value of $\text{Ga}_{0.75}\text{In}_{0.25}\text{Se}$ ($x = 0.75$) as nearly 1.8 eV [24]. The obtained energy band gap at the room temperature from our measurements conforms to this estimated value.

At this point, it will be worthwhile to make an inference about the usage application of $\text{Ga}_{0.75}\text{In}_{0.25}\text{Se}$ crystal. Iwamura et al. showed that band gap energy of GaSe shifts from 1.990 to 1.927 eV (nearly 63 meV shift) by applying 20 V voltage to the sample [23]. Since the absorption edge energy takes value smaller than 1.959 eV (He-Ne laser emission energy), the authors proposed a light modulator for the He-Ne laser on the base of GaSe crystal. If it is

assumed that under application of voltage, $\text{Ga}_{0.75}\text{In}_{0.25}\text{Se}$ will show similar behavior as GaSe, the band gap energy will decrease from 1.89 eV to 1.827 eV. Since band gap energy moves to lower value than 1.833 eV (Krypton laser emission energy), $\text{Ga}_{0.75}\text{In}_{0.25}\text{Se}$ crystal may be used as a light modulator for this Krypton laser line.

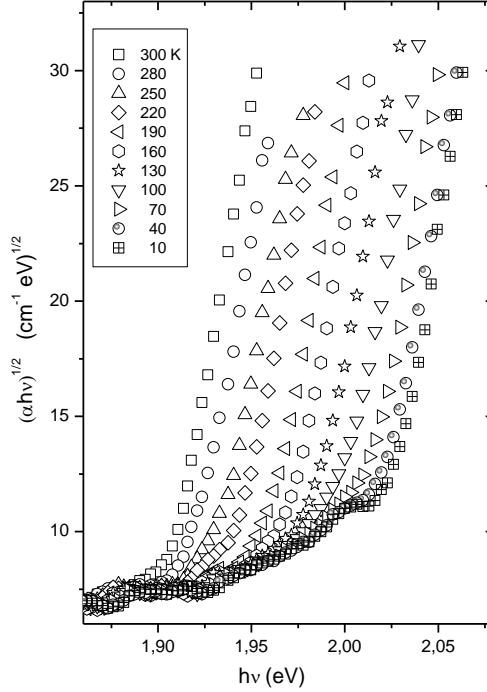


Figure 4.4. The dependence of $(\alpha h\nu)^{1/2}$ on photon energy in the temperature range of 10–300 K.

Temperature dependence of the band gap energy (E_{gi}) was analyzed using the equation [71]

$$E_g(T) = E_g(0) + \frac{\gamma T^2}{T + \beta} \quad (2.111)$$

Figure 4.5 represents fit (solid line) of experimental data (open circles) according to equation 2.111. The fit of the experimental data results with $E_{\text{gi}}(0) = 2.01$ eV, $\gamma = -6.2 \times 10^{-4}$ eV/K and $\beta = 177$ K. The Lindemann's melting rule [70] using x-ray results and melting temperature $T_m = 1033$ K gives Debye temperature for $\text{Ga}_{0.75}\text{In}_{0.25}\text{Se}$ crystal as $\beta = 160$ K which is consistent with our result.

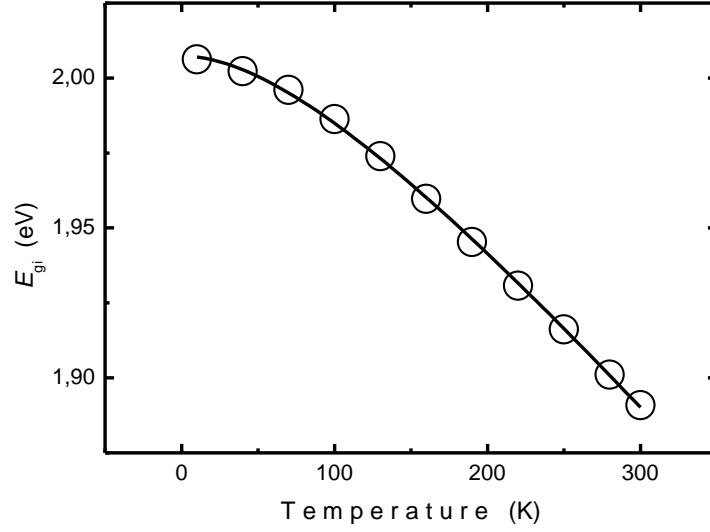


Figure 4.5. The indirect band gap energy as a function of temperature. The circles are experimental data and the solid line represents the fit according to equation 2.111

Figure 4.6 presents the variation of the refractive index (n) obtained from equation 4.2 as a function of wavelength (λ). Refractive index of $\text{Ga}_{0.75}\text{In}_{0.25}\text{Se}$ decreases from 3.15 for $\lambda = 650$ nm to 3.03 for $\lambda = 1100$ nm in the $h\nu < E_g$ region. The long wavelength refractive index 3.03 calculated for $\text{Ga}_{0.75}\text{In}_{0.25}\text{Se}$ crystals shows is in good agreement with values of $n = 3$ for InSe [83] and $n = 2.92$ for GaSe [84]. Refractive index spectrum was fitted using the Cauchy model which relates n and λ in the low energy region as [45]

$$n(\lambda) = A + \frac{B}{\lambda^2} + \frac{C}{\lambda^4} \quad (2.19)$$

Inset of the figure 4.6 indicates theoretical fit of equation 2.19 to experimental data. A , B and C parameters were obtained to be 2.88, $1.18 \times 10^5 \text{ nm}^2$ and $-7.5 \times 10^8 \text{ nm}^4$, respectively.

Moreover, the wavelength dependence of the dispersive refractive index in $h\nu < E_g$ range can be analyzed to determine the energy of the single effective dispersion oscillator energy (E_{so}), dispersion energy (E_d), zero-frequency refractive index (n_0) and dielectric constant (ϵ_0) using single-effective-oscillator model in which n is related to $h\nu$ by [41-43]

$$n^2(h\nu) = 1 + \frac{E_{so}E_d}{E_{so}^2 - (h\nu)^2} \quad (2.14)$$

The linear fit of the experimental data under the light of equation 2.14 is shown in figure 4.7. The result of fitting process gives oscillator parameters as $E_{so} = 4.60$ eV, $E_d = 34.21$ eV, $\epsilon_0 = n_0^2 = 8.43$ and $n_0 = 2.9$.

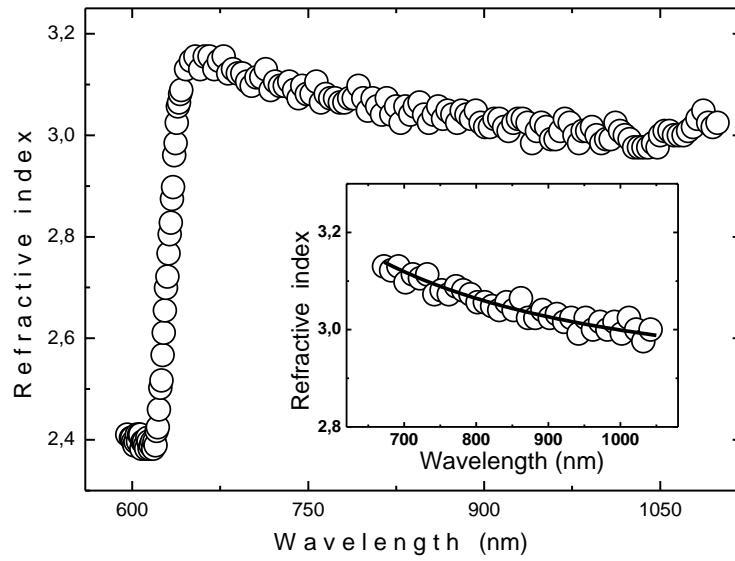


Figure 4.6. The variation of refractive index as a function of wavelength at room temperature. Inset: The circles show experimental data. The solid line represents the fit according to equation 2.19 in the low energy region.

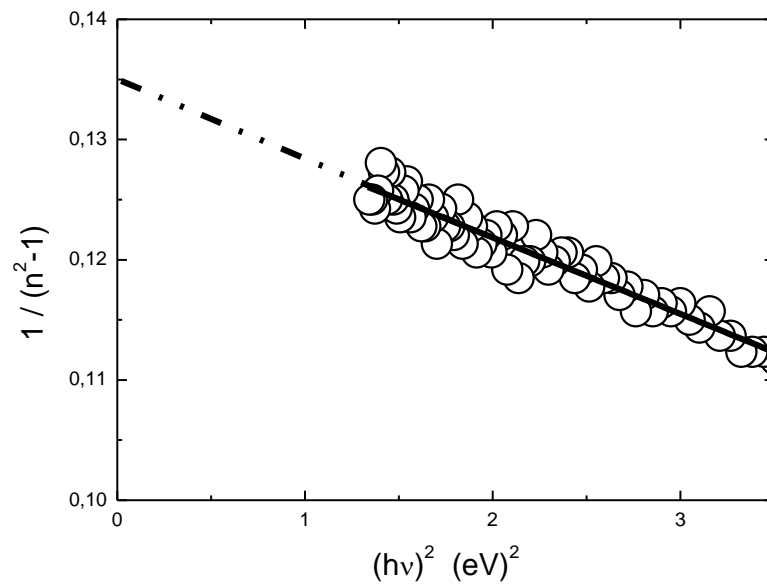


Figure 4.7. Plot of $(n^2-1)^{-1}$ vs. $(h\nu)^2$ in the $h\nu < E_g$ range at room temperature. Open circles are experimental data and the solid line represents the fit using equation 2.14.

The oscillator strength (S_{so}) and wavelength (λ_{so}) for $\text{Ga}_{0.75}\text{In}_{0.25}\text{Se}$ were calculated using analysis of the refractive index in the low energy range from single Sellmeier oscillator model. The refractive index is given in this model as [44]

$$(n^2 - 1)^{-1} = \frac{1}{S_{so}\lambda_{so}^2} - \frac{1}{S_{so}\lambda^2} \quad (2.17)$$

S_{so} and λ_{so} values were obtained from the $(n^2 - 1)^{-1}$ versus λ^{-2} curve as $1.01 \times 10^{14} \text{ m}^{-2}$ and $2.71 \times 10^{-7} \text{ m}$, respectively.

Once the n and k values are known, the real (ε_1) and imaginary (ε_2) parts of the dielectric constant can be calculated from the relations [48]

$$\varepsilon_1 = n^2 - k^2 \quad \text{and} \quad \varepsilon_2 = 2nk$$

which are derived from the equations 2.32 and 2.33. Figure 4.8 and its inset show the spectra of the ε_1 and ε_2 in the 600-1100 nm wavelength range, respectively. The spectrum of ε_2 is similar to that of refractive index due to ignorable extinction coefficients in low energy region. Sellmeier and Cauchy model analysis applied to our measurements corresponds to region where $\varepsilon_2 \approx 0$ [46]. The small values of ε_2 indicate that these models are applicable for $\text{Ga}_{0.75}\text{In}_{0.25}\text{Se}$ single crystals.

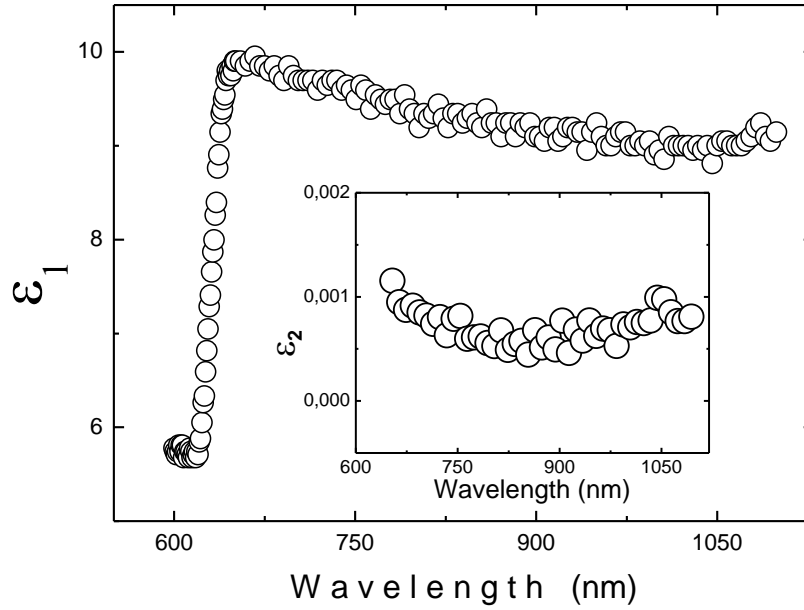


Figure 4.8. The spectrum of the ε_1 in the 600–1100 nm wavelength range at room temperature. The inset represents the spectrum of the ε_2 in the same range.

4.4 Ellipsometry Measurements

Detailed information about the optical constants, real and imaginary components of pseudodielectric function, pseudorefractive index and pseudoextinction coefficient of $\text{Ga}_{0.75}\text{In}_{0.25}\text{Se}$ crystal was obtained from analysis of ellipsometric data [85]. Figure 4.9a shows the spectra of components of pseudodielectric function in the range of 1.2–6.0 eV. The ε_2 values

vary between 1 and 8.5 values in the studied region and two peaks were observed in its spectra, their maximum positions were shifted towards to lower energy values nearly by amount of 0.3-0.7 eV as compared with those of GaSe [12, 86-89]. This can be due to the fact that the replacing of Se atoms by In atoms in GaSe crystal leads to the modification of band structure. The pseudorefractive index ($\langle n \rangle$) and pseudoextinction coefficient ($\langle k \rangle$) of the studied $\text{Ga}_{0.75}\text{In}_{0.25}\text{Se}$ crystal can be calculated using the expressions

$$\langle n \rangle = \left[\left(\langle \varepsilon_1 \rangle + (\langle \varepsilon_1 \rangle^2 + \langle \varepsilon_2 \rangle^2)^{1/2} \right) / 2 \right]^{1/2}, \quad (2.32)$$

$$\langle k \rangle = \left[\left(-\langle \varepsilon_1 \rangle + (\langle \varepsilon_1 \rangle^2 + \langle \varepsilon_2 \rangle^2)^{1/2} \right) / 2 \right]^{1/2}, \quad (2.33)$$

relating the pseudodielectric constants to $\langle n \rangle$ and $\langle k \rangle$ values. The pseudorefractive index and pseudoextinction coefficient spectra of $\text{Ga}_{0.75}\text{In}_{0.25}\text{Se}$ crystal obtained from the above-mentioned expressions are presented in figure 4.9b. Two peaks in the pseudoextinction coefficient spectra were observed at peak energies of 3.6 and 4.7 eV. These peaks can be attributed to strong absorption of photon energy at the corresponding critical points (interband transitions).

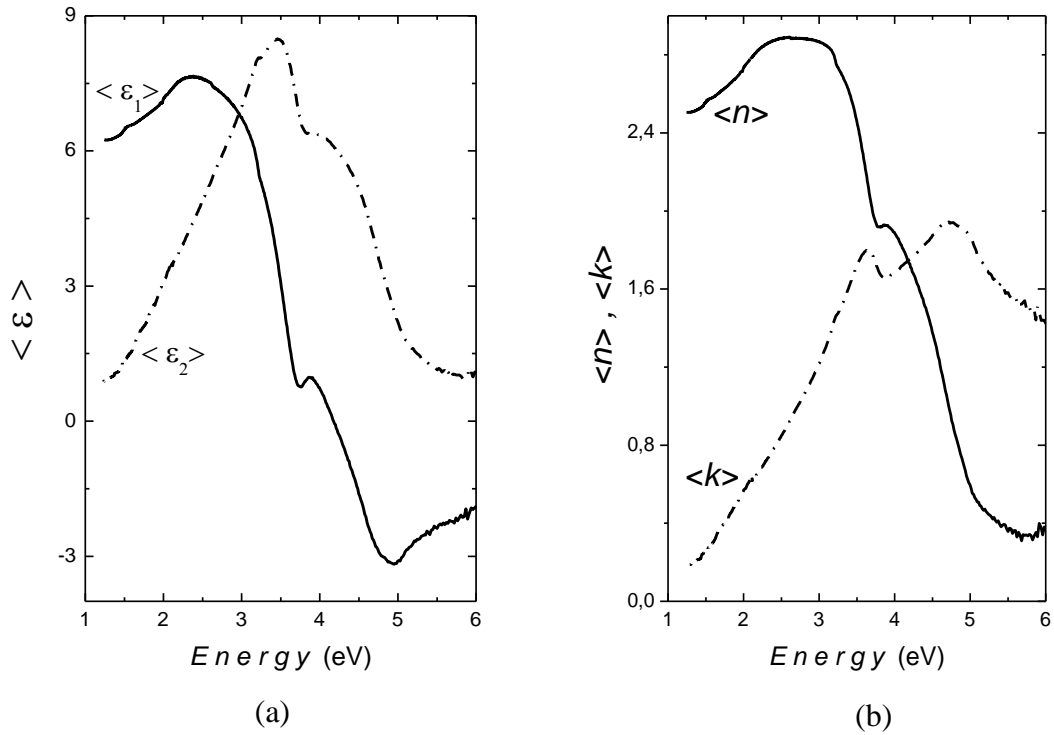


Figure 4.9. (a) The spectra of the pseudodielectric function of $\text{Ga}_{0.75}\text{In}_{0.25}\text{Se}$. Solid and dot-dashed curves represent the real and imaginary part spectra, respectively. (b) The spectra of the refractive index and extinction coefficient. Solid and dot-dashed curves represent the refractive index and extinction coefficient spectra, respectively.

The reflectivity R of the crystal was determined using the following relation

$$R = \frac{(n-1)^2 + \kappa^2}{(n+1)^2 + \kappa^2} . \quad (2.9)$$

The spectral dependence of reflectivity is shown in figure 4.10.

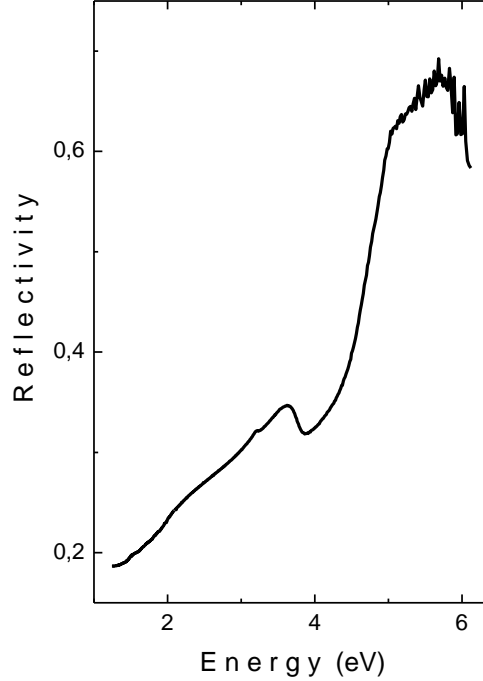


Figure 4.10. The spectral dependence of reflectivity of $\text{Ga}_{0.75}\text{In}_{0.25}\text{Se}$ crystal.

Ellipsometric data giving the dielectric constants as a function of energy can also be used to get comprehensive information about the interband transitions in the electronic band structure of $\text{Ga}_{0.75}\text{In}_{0.25}\text{Se}$ crystal. To this end, the critical point (CP) analysis method was performed on the second derivative spectra of real ($d^2 \langle \varepsilon_1 \rangle / dE^2$) and imaginary ($d^2 \langle \varepsilon_2 \rangle / dE^2$) parts of the pseudodielectric constant calculated from the spectra given in figure 4.11. The second derivative spectra were fitted under the light of theoretical expressions 2.42 and 2.43 for each case of m values. As $m = -1$ case gives the lowest mean-square deviations, obtained spectra were fitted for the case corresponding to excitonic optical transitions [12]. The second derivative spectra were obtained after smoothing the graph using low level binomial filtering. CP analysis were accomplished above the band gap energy $E_g = 1.89$ eV [46]. Because the second derivative values are very sensitive to small changes of the main data, the smoothing process should be done without giving any damage/variation to the data. Therefore, since smoothing process strongly distorts the main experimental data in the 2.0-3.0 eV range, we accomplished fitting process only for the region above 3.0 eV. In the energy range from 3 to 6 eV, four CP lineshapes of 3.16, 3.53, 4.05 and 4.53 eV were appeared as a result of least-square fitting program. These points are indicated by arrows in figure 4.11. We listed in table 4.2 the results of the CP analysis of $\text{Ga}_{0.75}\text{In}_{0.25}\text{Se}$ and also previously reported results of GaSe which is the main constituent of the studied crystal.

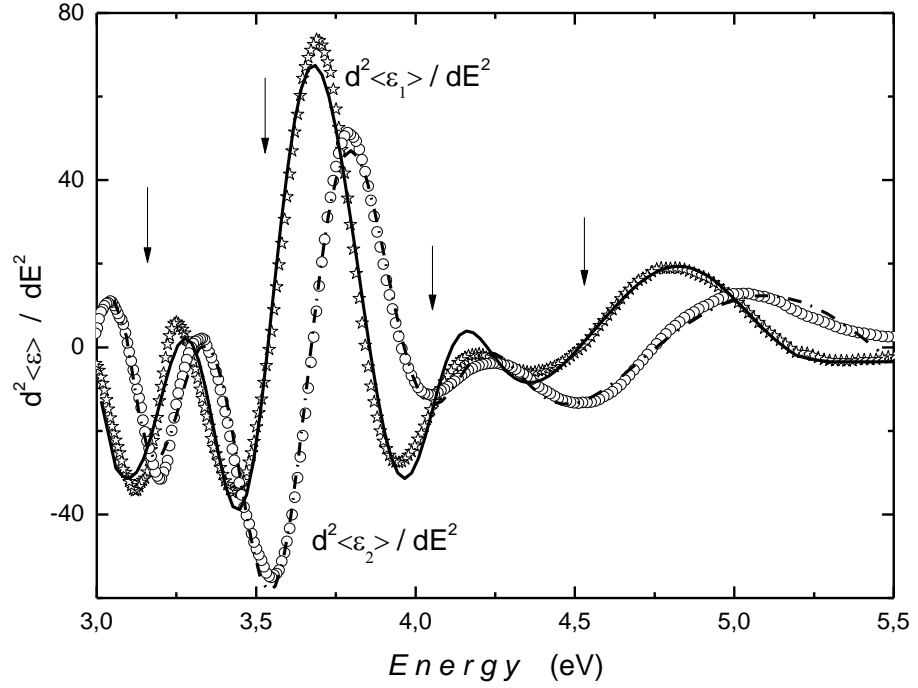


Figure 4.11. Second-energy derivative of the dielectric function of $\text{Ga}_{0.75}\text{In}_{0.25}\text{Se}$. Stars and open circles represent the second-energy derivative spectra of the real and imaginary part of the dielectric function, respectively. The solid and dot-dashed curves show the fit to the experimental data.

Table 4.2. Critical point energies for $\text{Ga}_{0.75}\text{In}_{0.25}\text{Se}$ and GaSe single crystals.

Ref.	Crystal	E_A	E_B	E_C	E_D
This work	$\text{Ga}_{0.75}\text{In}_{0.25}\text{Se}$	3.16	3.53	4.05	4.53
Ref. [12]	GaSe	3.23	3.75	4.03	4.69
Ref. [90]	GaSe:Te	3.35	3.67	4.10	4.57

At this point, it is worthwhile to make some interpretations on the critical point energies of 3.16 and 3.53 eV. In accordance with Ref. [91], a theoretical study about the electronic energy band structure of GaSe and InSe, we supposed two deeper valence bands with Se p_x , p_y symmetry at 1.27 and 1.64 eV below the uppermost valence band with Se p_z symmetry for $\text{Ga}_{0.75}\text{In}_{0.25}\text{Se}$ crystal. Figure 4.12 shows the diagram of the electronic energy band structure of

the crystal plotted according to this suggested model. Following the assignments made in Refs. [12, 18], we attributed tentatively the *CP* structures in the higher energy region to the excitations of Se p_x, p_y electrons to either the second or the third group of conduction bands.

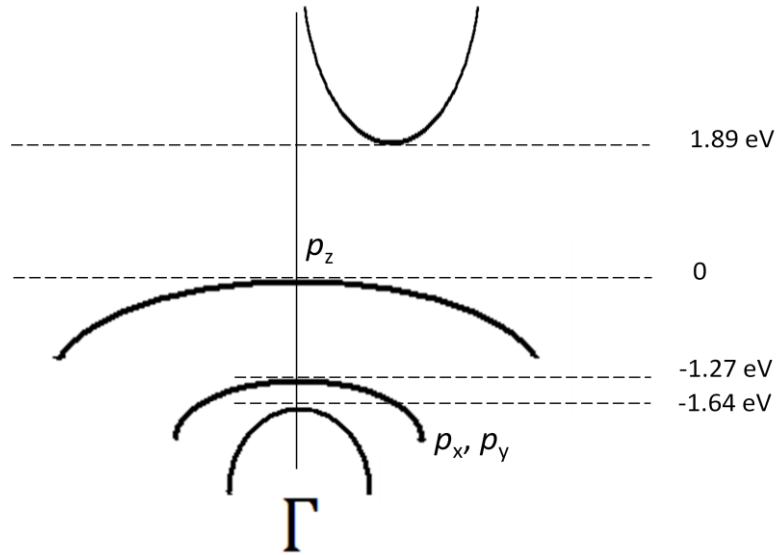


Figure 4.12. Sketch of the electronic energy band structure of $\text{Ga}_{0.75}\text{In}_{0.25}\text{Se}$ crystal near the bandgap at the Brillouin zone center.

4.5 Infrared and Raman Spectroscopy Measurements

Figure 4.13a shows IR reflectivity spectrum of $\text{Ga}_{0.75}\text{In}_{0.25}\text{Se}$ crystals in the frequency range of $100\text{--}400\text{ cm}^{-1}$. Kramers-Kronig analysis has been performed to get the dispersion parameters. The frequencies of transverse (ν_T) and longitudinal (ν_L) optical phonons were determined from the maxima of the function of ϵ_2 and function of energy losses $\text{Im}(1/\epsilon)$, respectively. The spectral dependencies of ϵ_2 and $\text{Im}(1/\epsilon)$ are presented in figure 4.13b. The values of ν_T and ν_L were determined as 209 and 243 cm^{-1} , respectively. Moreover, the dependencies of optical constants n and k on the frequency were calculated from reflectivity spectra (figure 4.13c). The high- and low-frequency refractive indices were determined as 2.42 ($\nu = 400\text{ cm}^{-1}$) and 3.09 ($\nu = 100\text{ cm}^{-1}$), respectively, with maximum value of $n = 5.95$ corresponding to the frequency $\nu = 206\text{ cm}^{-1}$. The oscillator strength was determined from

$$S = \frac{\gamma}{\nu_T} \epsilon_2(\text{max}) \quad (4.3)$$

where $\epsilon_2(\text{max})$ is the value of the imaginary part of the dielectric constant in the reflection band maximum and γ is full-width at half maximum of ϵ_2 peak (damping constant). Using the obtained values of $\epsilon_2(\text{max}) = 45.9$ and $\gamma = 10\text{ cm}^{-1}$ (see figure 4.13b), the magnitude of oscillator strength was found to be $S = 2.2$. The high-frequency dielectric constant $\epsilon_\infty = 6.7$ was established from the high-frequency reflection coefficient R_∞ ($\nu = 400\text{ cm}^{-1}$) in accordance with formula

$$\epsilon_{\infty} = \left(\frac{1 + \sqrt{R_{\infty}}}{1 - \sqrt{R_{\infty}}} \right)^2 \quad (4.4)$$

The low-frequency dielectric constant ϵ_0 , determined from relation $\epsilon_0 = \epsilon_{\infty} + S$, was found to be 8.9.

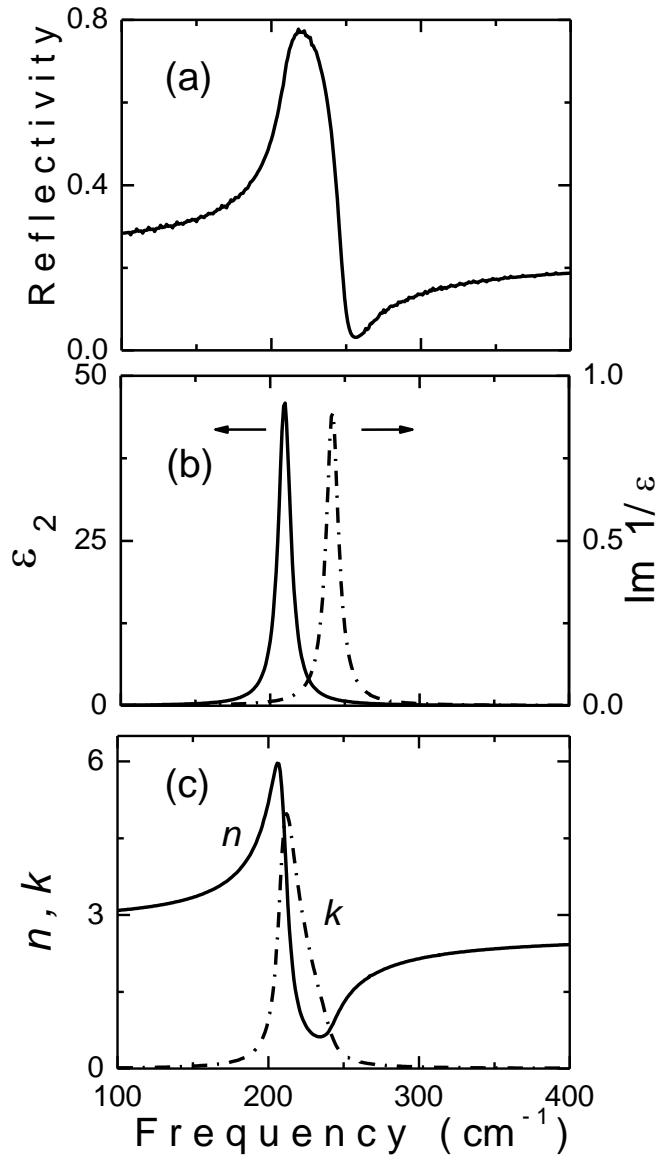


Figure 4.13. The spectral dependencies for Ga_{0.75}In_{0.25}Se crystal: (a) Infrared reflectivity; (b) ϵ_2 and $\text{Im}(1/\epsilon)$; (c) Optical constants n and k .

Figure 4.14 shows the Raman scattering spectrum of $\text{Ga}_{0.75}\text{In}_{0.25}\text{Se}$ crystals registered in the frequency range $25\text{--}500\text{ cm}^{-1}$ in back scattering geometry. In this configuration parasitically scattering light from exciting line gets into the spectrometer. Therefore, we were unable to measure the Raman spectra in the range lower than 25 cm^{-1} . Unpolarized excitation and detection, allowing all the lines to be visible, have been used for this spectrum.

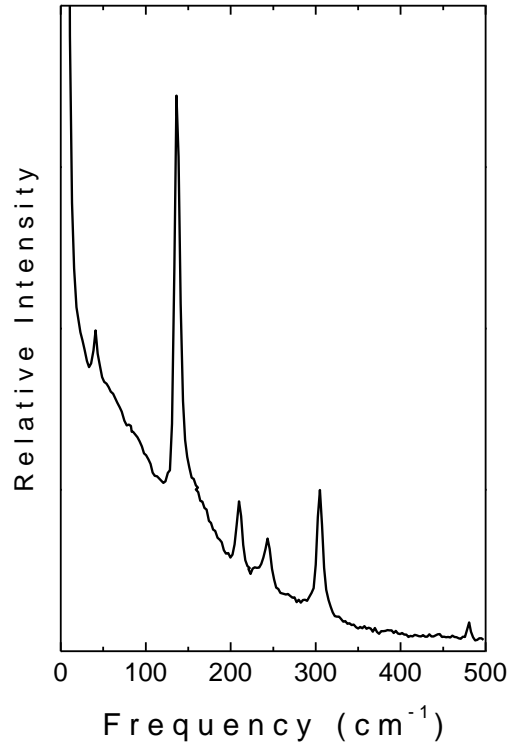


Figure 4.14. Unpolarized Raman scattering spectrum of $\text{Ga}_{0.75}\text{In}_{0.25}\text{Se}$ crystal.

Six lines with frequencies of $41, 136, 210, 242, 305$ and 480 cm^{-1} were observed in the spectrum. The latter line with frequency of 480 cm^{-1} may be assigned to the overtone of mode with frequency of 242 cm^{-1} . We attribute the two lines with frequencies of 210 and 247 cm^{-1} , revealed in the Raman spectrum, to the TO and LO branches of the polar mode, respectively. These frequencies are in good agreement with those determined by infrared reflection measurements (209 and 243 cm^{-1}). Earlier, the similar interpretation of the lines observed in the Raman spectra of GaSe layered crystals was made by authors of Refs. [92-95]. The coincidence of the Raman and infrared reflection mode frequencies shows that the investigated $\text{Ga}_{0.75}\text{In}_{0.25}\text{Se}$ single crystal has non-centric space symmetry group. In other words, the lack of inversion in crystal symmetry implies the simultaneous Raman and infrared activity of vibrational modes.

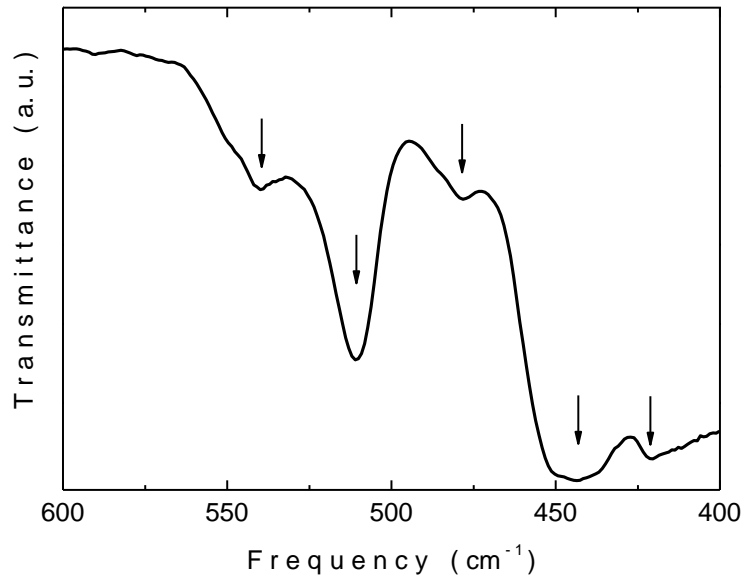


Figure 4.15. Infrared transmittance spectrum of $\text{Ga}_{0.75}\text{In}_{0.25}\text{Se}$ crystal.

Figure 4.15 presents the infrared transmittance spectrum of $\text{Ga}_{0.75}\text{In}_{0.25}\text{Se}$ crystal in the frequency range of $400\text{--}600\text{ cm}^{-1}$. The minima at 421 , 443 , 480 , 511 and 540 cm^{-1} are considered as caused by the two-phonon absorption. In analogy to the situation in GaSe [96] and InSe [97] layered crystals, it can be expected that the phonon combination modes are due to zone-centered phonons. The bands observed in the transmittance spectrum of $\text{Ga}_{0.75}\text{In}_{0.25}\text{Se}$ fit closely with the possible combinations among the frequencies found from Raman spectrum in figure 4.14. The proposed assignments of these bands are presented in table 4.3. The bands in IR spectrum with frequencies of 421 and 480 cm^{-1} were attributed to the overtones of modes with frequency of 210 and 242 cm^{-1} observed in the Raman spectrum of $\text{Ga}_{0.75}\text{In}_{0.25}\text{Se}$ crystal. In Table 4.3, we also present the known frequencies of IR and Raman-active modes of binary compounds GaSe and InSe, which are the constituents of $\text{Ga}_{0.75}\text{In}_{0.25}\text{Se}$ crystal. It is seen from the table, that obtained frequencies of IR and Raman-active modes of $\text{Ga}_{0.75}\text{In}_{0.25}\text{Se}$ are slightly lower than those of GaSe crystal. Since the frequencies of modes for InSe are lower than those for GaSe, it is an expected result to reveal the slight decrease of frequency values for $\text{Ga}_{0.75}\text{In}_{0.25}\text{Se}$ crystal.

Table 4.3. The frequencies of IR and Raman modes (cm^{-1}) of GaSe, InSe and $\text{Ga}_{0.75}\text{In}_{0.25}\text{Se}$ crystals, and attributions of IR transmittance minima due to two-phonon absorption processes in $\text{Ga}_{0.75}\text{In}_{0.25}\text{Se}$ crystal

IR Reflection			Raman Scattering			IR Transmittance			Proposed Assigment
GaSe [96]	InSe [97]	$\text{Ga}_{0.75}\text{In}_{0.25}\text{Se}$ this work	GaSe [92]	InSe [97]	$\text{Ga}_{0.75}\text{In}_{0.25}\text{Se}$ this work	GaSe [96]	InSe [97]	$\text{Ga}_{0.75}\text{In}_{0.25}\text{Se}$ this work	$\text{Ga}_{0.75}\text{In}_{0.25}\text{Se}$ this work
–	–	–	–	41	41	409	409	–	–
–	–	–	59	–	–	422	420	421	$210 \times 2 = 420$
–	–	–	–	115	–	446	–	443	$136 + 305 = 441$
–	–	–	134	–	136	478	–	480	$242 \times 2 = 484$
–	178	–	–	176	–	511	–	511	$210 + 305 = 515$
214	212	209	213	–	210	540	–	541	$242 + 305 = 547$
–	–	–	–	225	–	–	–	–	–
255	–	243	253	–	242	–	–	–	–
–	–	–	308	–	305	–	–	–	–

4.6 Photoluminescence Measurements

Figure 4.16 shows temperature dependence of PL spectra of $\text{Ga}_{0.75}\text{In}_{0.25}\text{Se}$ crystals in the 580-670 nm range at laser excitation intensity of 1.40 W cm^{-2} [98]. There exist two peaks in the PL spectra in the temperature range of 7-59 K. Since the low intensity values of first peak centered at nearly 595 nm do not let us to achieve the temperature and laser excitation intensity dependence analysis, we left this peak out of work in the present study.

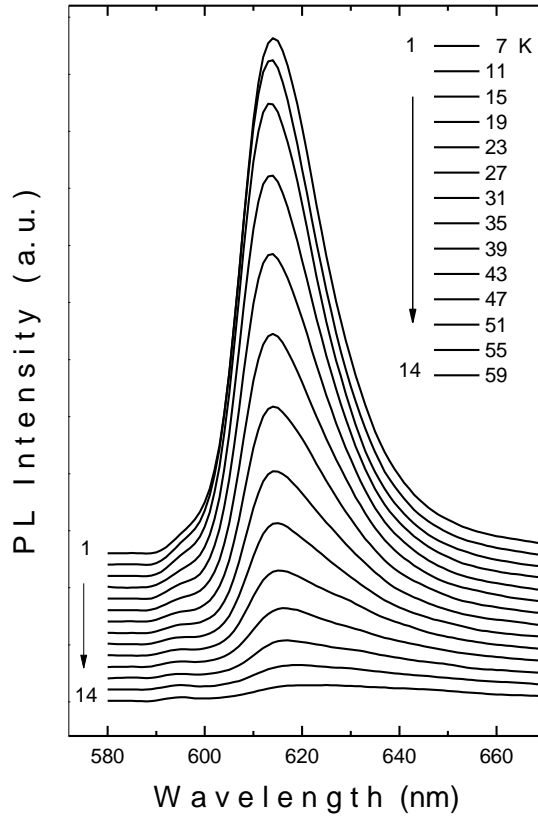


Figure 4.16. PL spectra of $\text{Ga}_{0.75}\text{In}_{0.25}\text{Se}$ crystal in the 7–59 K temperature range and 580–670 nm wavelength region with excitation laser intensity of $L = 1.40 \text{ W cm}^{-2}$.

The observed strong peak at nearly 613 nm was fitted using least square fitting method under the consideration of Gaussian distribution. When the PL spectrum at $T = 7 \text{ K}$ was fitted by the composition of two peaks (A and B), we obtained a good fit as shown in figure 4.17. As a result the corresponding peak positions were determined as $E_A = 613 \text{ nm}$ (2.02 eV) and $E_B = 623 \text{ nm}$ (1.99 eV). In the present work, each PL spectra obtained in the temperature and laser excitation dependence measurements were decomposed to two peaks and then analysis were carried out with the corresponding values of fit results.

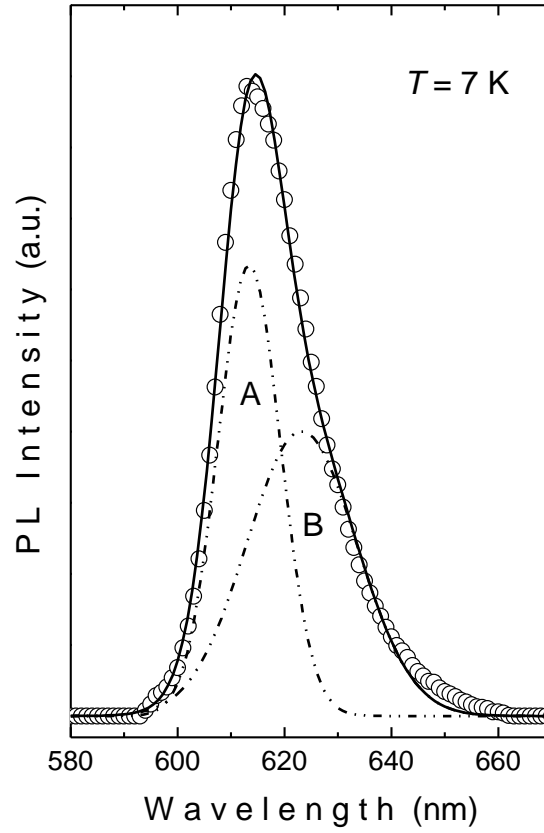


Figure 4.17. Deconvolution of the PL spectrum into Gaussian lineshapes at $T = 7$ K.

Figure 4.16 also indicates that increase of temperature results with a decrease in the peak intensity and a shift of its energy to lower values (red shift). With increasing temperature half-widths of the decomposed peaks rises from 0.046 to 0.057 eV and from 0.076 to 0.106 eV for A- and B- peaks, respectively. Inset in figure 4.18 illustrates shift of the peak energy to lower energies with increasing temperature. It is known that energy of the donor-acceptor pair transition decreases along with the band gap energy as the temperature is increased [59].

Temperature dependence of the intensities of decomposed PL spectra was analyzed to get essential knowledge about the electronic energy levels in the forbidden energy gap. For this purpose, the curve of maximum intensities of each peaks versus $1000/T$ was plotted (figure 4.18) and fitted using the expression [39]

$$I(T) = \frac{I_0}{1 + \alpha \exp(-E_t / kT)} \quad (2.109)$$

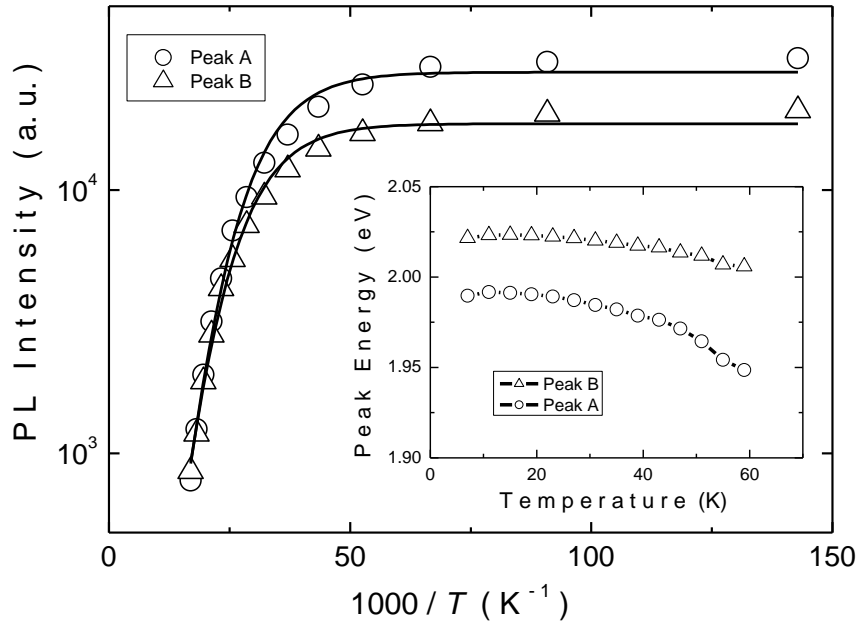


Figure 4.18. Temperature dependencies of observed A- and B-band intensities for $\text{Ga}_{0.75}\text{In}_{0.25}\text{Se}$ crystal. Circles and triangles are experimental data. Solid curves show the theoretical fits using equation 2.109. Inset: Temperature dependence of emission band energies.

The activation energies of quenching process were found as 0.01 eV for both bands as a result of analysis. Since $\text{Ga}_{0.75}\text{In}_{0.25}\text{Se}$ is a p-type material, as determined by the hot probe technique, we believe that this calculated energy belongs to a shallow acceptor located at 0.01 eV above the top of the valence band. This shallow level can be thought as arising from defects, created during the growth of crystals, and/or unintentional impurities.

In addition to temperature dependence of the PL spectra, we have also studied the laser excitation intensity dependency of the observed emission bands to get additional valuable information about the recombination mechanism responsible for the observed luminescence. Figure 4.19 illustrates the PL spectra of $\text{Ga}_{0.75}\text{In}_{0.25}\text{Se}$ single crystals at different laser intensities at $T = 7$ K. Measured PL spectra reveal that the increase of excitation intensity results an increase on the peak energies (blue shift). The behavior of the emission band is in agreement with the idea of inhomogeneously distributed donor-acceptor pairs for which increasing laser excitation intensity leads to blue shift of the band by exciting more pairs that are closely spaced [40].

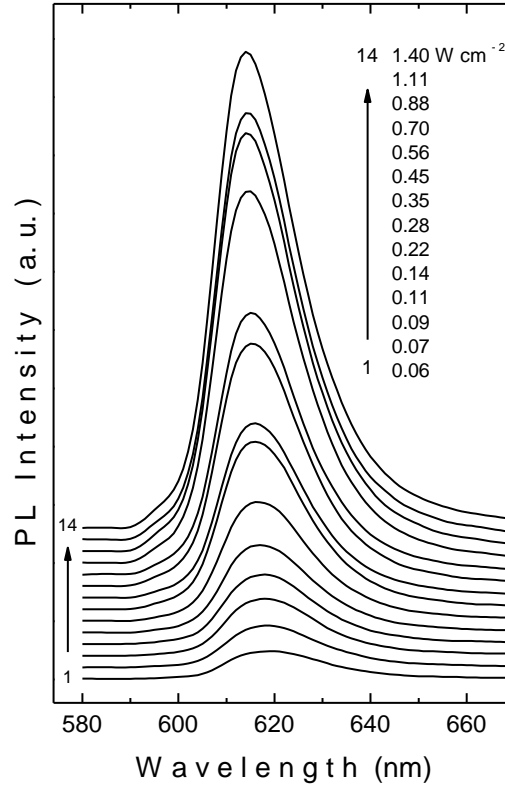


Figure 4.19. PL spectra of $\text{Ga}_{0.75}\text{In}_{0.25}\text{Se}$ crystal for different excitation laser intensities at $T = 7$ K.

At low excitation laser intensities, carriers are trapped by only a small portion of the donor and acceptor levels. This results in recombination from distant pairs only. When sufficient high excitation laser intensities were used, all donors and acceptors are excited. In this manner, contribution to recombination from closer pairs is also provided. The energy of the emitted photon during a donor–acceptor pair transition has a positive contribution from a Coulomb interaction between ionized impurities. The decrease of the separation between pairs increases this contribution [59]. Furthermore, radiative transition probabilities which are different for distinct pair separations decrease exponentially as a function of the distance between pairs [59]. Distant pair recombination saturates at high excitation laser intensities; whereas close pairs have larger transition probability and can trap more carriers. Therefore, a shift of the peak energy of the emission band to higher energy is observed as the excitation laser intensity increases.

Figure 4.20 shows the dependence of the emission band peak energies (E_p) at $T = 7$ K as a function of excitation laser intensity (L). The experimental data are fitted by the expression [66]

$$L(E_p) = L_0 \frac{(E_p - E_\infty)^3}{E_B + E_\infty - 2E_p} \exp\left[-\frac{2(E_B - E_\infty)}{E_p - E_\infty}\right]. \quad (2.105)$$

From a nonlinear least square fit to the experimental data, the photon energy values for an infinitely distant donor–acceptor pair and a close donor–acceptor pair are found to be $E_\infty = 1.96$ eV, $E_B = 2.07$ eV for A-band and $E_\infty = 1.92$ eV, $E_B = 2.04$ eV for B-band, respectively. These limiting photon energy values are in good agreement with the band gap energy ($E_g = 2.08$ eV [81]) and the observed values of the peak energy positions for A- and B-peaks ($E_\infty < 2.01$ eV $< E_P < 2.02$ eV $< E_B < E_g$) and ($E_\infty < 1.98$ eV $< E_P < 1.99$ eV $< E_B < E_g$), respectively.

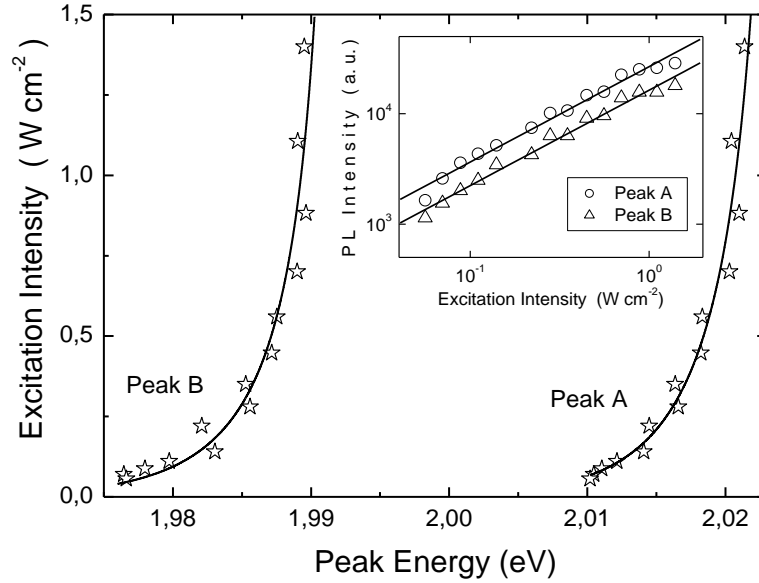


Figure 4.20. Dependence of emission band band energies on excitation laser intensity at $T = 7$ K. Stars are experimental data. Solid curves represent the theoretical fit using equation 2.105. Inset: Dependence of PL intensities at the emission band maximums versus excitation laser intensity at $T = 7$ K. The solid lines show the theoretical fit using equation 2.104.

In PL spectra of $\text{Ga}_{0.75}\text{In}_{0.25}\text{Se}$ crystal, the increase in the peak intensities of emission band with increase in the laser excitation intensity was also observed. The logarithmic plot of PL intensity versus laser excitation intensity is given in inset of figure 4.20. Experimental data can be fitted by a simple power law of the form [60-63]

$$I \propto L^\delta, \quad (2.104)$$

where I corresponds to the PL intensity, L corresponds to excitation laser intensity and γ is a dimensionless constant. The linear fits for both A- and B-bands give the equal value of δ as 0.86. This result confirms the above-mentioned supposition that A- and B-bands are related to the same acceptor level with activation energy of 0.01 eV. The exponent δ for excitation laser photon energy exceeding the band gap energy E_g is generally $1 < \delta < 2$ for free- and bound-exciton emission, whereas $0 < \delta \leq 1$ is typical for free-to-bound and donor–acceptor pair recombination [64].

Under the light of the results of the analysis of the PL spectra studied as a function of temperature and excitation laser intensity, we may construct a simple possible scheme for the states located in the forbidden energy gap of $\text{Ga}_{0.75}\text{In}_{0.25}\text{Se}$ crystal. It should be noted that the top of valence band is formed prevalingly by p -state of Se and the bottom of conduction band is originated from the s - d cationic states [99]. In the proposed scheme shown in figure 4.21, shallow acceptor level (a) is located at 0.01 eV above the top of the valence band. The sum of the activation energies of the donor (E_d) and acceptor (E_a) levels, involved in the emission band, is given by the general relation for the emission energy of donor–acceptor pair [59]

$$E_a + E_d = E_g - E_\infty . \quad (4.5)$$

Considering that the acceptor level (a) is located at 0.01 eV above the top of the valence band and taking into consideration the $E_g = 2.08$ eV [81] and $E_\infty = 1.96$ eV (for A-band) and 1.92 eV (for B-band), the donor levels (d_1 and d_2) involved in the emission A- and B-bands are located at 0.11 eV and 0.15 eV below the bottom of the conduction band, respectively. Taking into account the above considerations, the observed emission bands in the PL spectra have been attributed to the radiative transitions from the donor levels to the acceptor level.

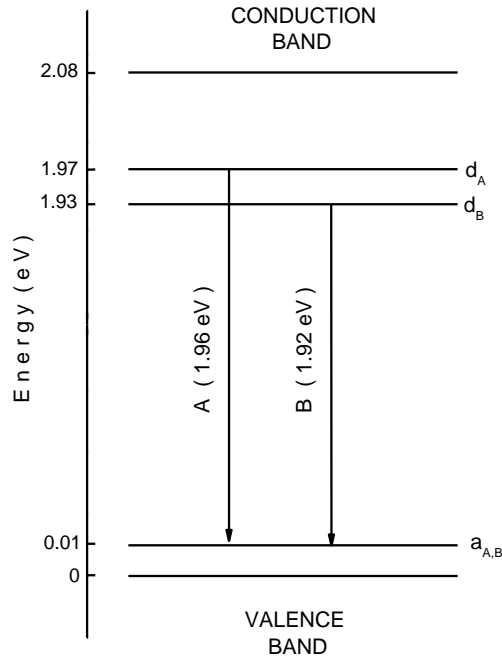


Figure 4.21. Proposed energy band diagram for $\text{Ga}_{0.75}\text{In}_{0.25}\text{Se}$ crystal.

4.7 Temperature Dependence of Dark Electrical Resistivity

The dark electrical resistivity measurements were carried out on $\text{Ga}_{0.75}\text{In}_{0.25}\text{Se}$ crystals in the temperature range of 150-350 K. Figure 4.22 shows temperature dependence of the resistivity. The room temperature resistivity (ρ_{room}) was found as $2.2 \times 10^3 \Omega\text{cm}$. In Ref. 28, the

resistivities of GaSe and InSe crystals were reported as 2.6×10^3 and $4.9 \Omega\text{cm}$, respectively. The closeness between the values obtained for $\text{Ga}_{0.75}\text{In}_{0.25}\text{Se}$ and GaSe crystals can be interpreted as that major constituent, GaSe, dominates the electrical properties of the mixed crystal $\text{Ga}_{0.75}\text{In}_{0.25}\text{Se}$. In the studied temperature range, it was observed that the resistivity of $\text{Ga}_{0.75}\text{In}_{0.25}\text{Se}$ sample decreases from 8.5×10^4 to $1.1 \times 10^3 \Omega\text{cm}$ as temperature increases from 150 K to 350 K.

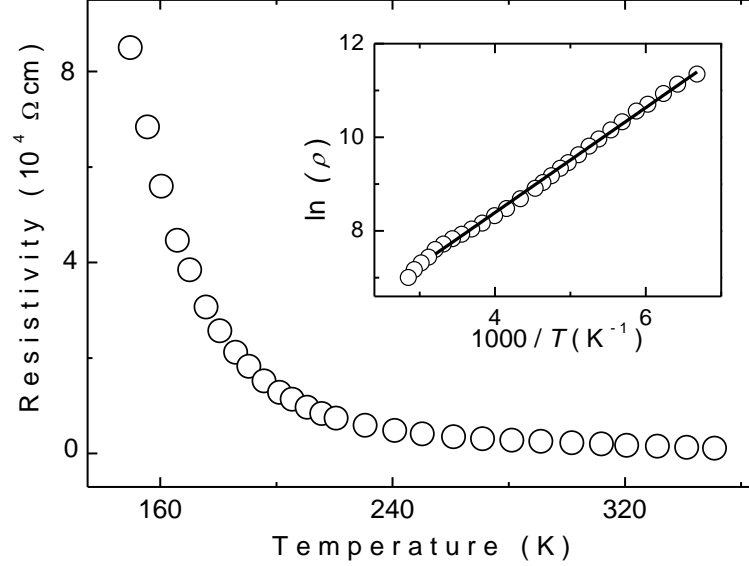


Figure 4.22. Temperature dependence of resistivity of $\text{Ga}_{0.75}\text{In}_{0.25}\text{Se}$ crystal. The inset shows the linear fit (solid line) of the experimental data (circles) according to equation 4.6.

The experimental data of resistivity-temperature dependence was found to follow the relation

$$\rho = \rho_0 \exp\left(\frac{E_\rho}{kT}\right) \quad (4.6)$$

where ρ_0 is the pre-exponential factor and E_ρ is the resistivity activation energy. E_ρ value was found from the linear fit of the $\ln \rho - 1000/T$ graph. In the studied temperature range, there exists only one linear region representing the E_ρ value as 0.10 eV. Moreover, this energy level was found to be same for all applied illumination intensities in that region. It will be worthwhile to compare this energy value with those found from the previous experimental techniques. In the photoluminescence measurements, two donor levels with activation energies of 0.11 and 0.15 eV were revealed. Taking into account the errors, the energies 0.10 and 0.11 eV obtained from dark resistivity and PL measurements, respectively, may possibly assign to the same level.

4.8 Space Charge Limited Current Analysis

The current-voltage characteristics of $\text{Ga}_{0.75}\text{In}_{0.25}\text{Se}$ single crystal have been investigated as a function of temperature. The I - V measurements revealed that both ohmic and space-charge-limited (SCL) characters exhibit in the 180-300 K range. The ohmic behavior prevails in the low applied voltage up to 1 Volt. After that value current becomes SCL and increases as a function of square of the applied voltage. Figure 4.23 shows the applied voltage (V) dependence of the

current density (J). Figure 4.24 represents the plot of $\ln(J)$ versus $\ln(V)$ which is used to get ratio of the free carrier density to the trapped carrier density (θ). The θ values were calculated using the slope of the graph and equation 2.117 taking into account the electron mobility as $210 \text{ cm}^2\text{V}^{-1}\text{s}^{-1}$ [100], distance between the electrodes as 1.8 cm and the dielectric constant as 9.2 [82]. Then the graph of $\ln(\theta)-1000/T$ was plotted to find the energy of the trap. The linear fit of the graph resulted with an activation energy of 0.11 eV (inset of figure 4.23). This value shows a good agreement with the values found from the dark resistivity and photoluminescence measurements.

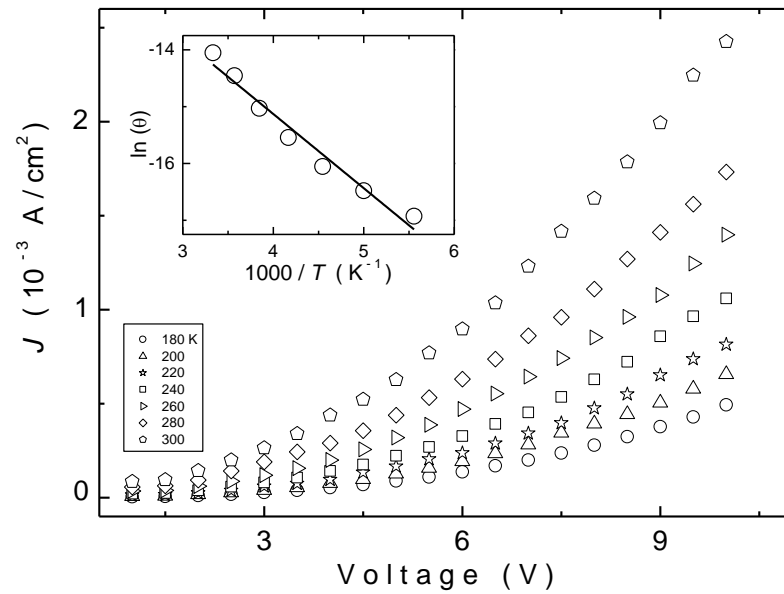


Figure 4.23. The variation of current density as a function of applied voltage. Inset shows the $\ln(\theta) - T^{-1}$ variation. Circles are experimental data and solid line is the linear fit.

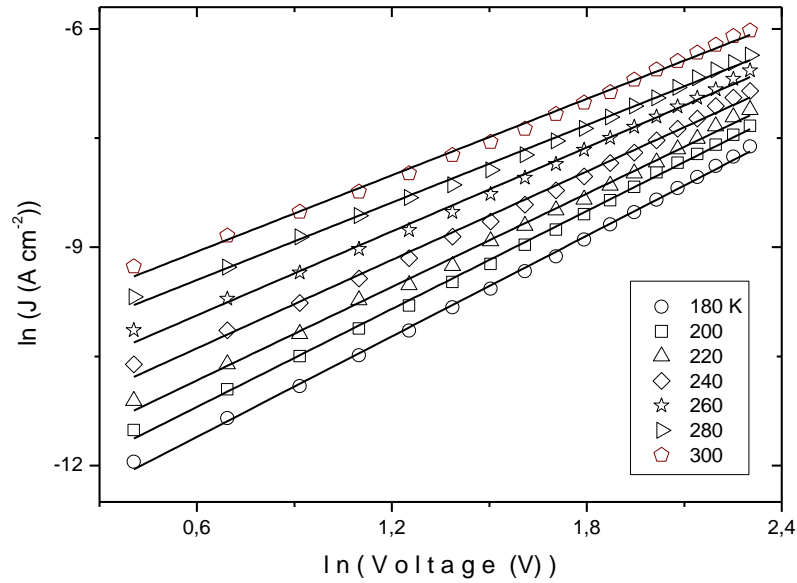


Figure 4.24. The $\ln(J) - \ln(V)$ characteristics in the SCL region.

4.9 Temperature Dependence of Photocurrent Measurements

Photoconductivity measurements were performed at different light intensities (F) in the range of $9.8\text{--}81.1 \text{ mWcm}^{-2}$ and in the temperature range of $150\text{--}300 \text{ K}$. The electric field was 6 V/cm (ohmic region). The photocurrent was measured along the layer, while the incident light was perpendicular to the layer. Figure 4.25 shows some of the dependence of the photocurrent (I_{ph}) on illumination intensity (F) at different temperatures. The photocurrent-illumination intensity relation follows the $I_{ph} \propto F^n$ expression, where the power exponent (n) indicates the behavior of the recombination mechanism. In all measured data, it was found that n values were nearly equal to 0.5 which indicates that there exists recombination (sublinear recombination) at the surface.

Figure 4.26 shows the dependence of photocurrent on temperature at different illumination intensities. It was seen that the photocurrent decreases exponentially with decreasing temperature and plots of $\ln(I_{ph}) - 1000/T$ consist of one distinct region. In the studied temperature range, the exponential increase in photocurrent with temperature in accordance with the relation $I_{ph} \propto \exp(-E_{ph}/kT)$ gives the photocurrent energy (E_{ph}) as 12 meV . Taking into account the possible errors, this energy value shows a good agreement with 10 meV energy found from photoluminescence measurements.

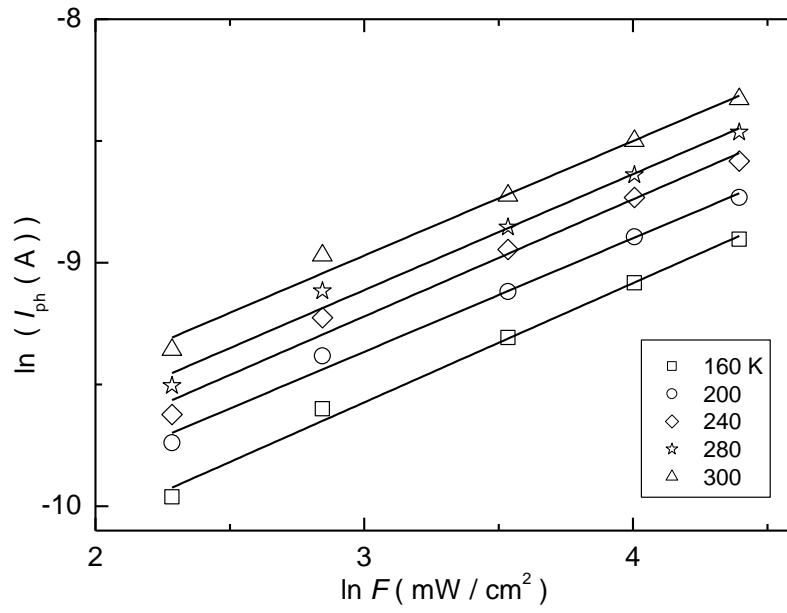


Figure 4.25. Variation of I_{ph} with F at different temperatures for $Ga_{0.75}In_{0.25}Se$ crystals.

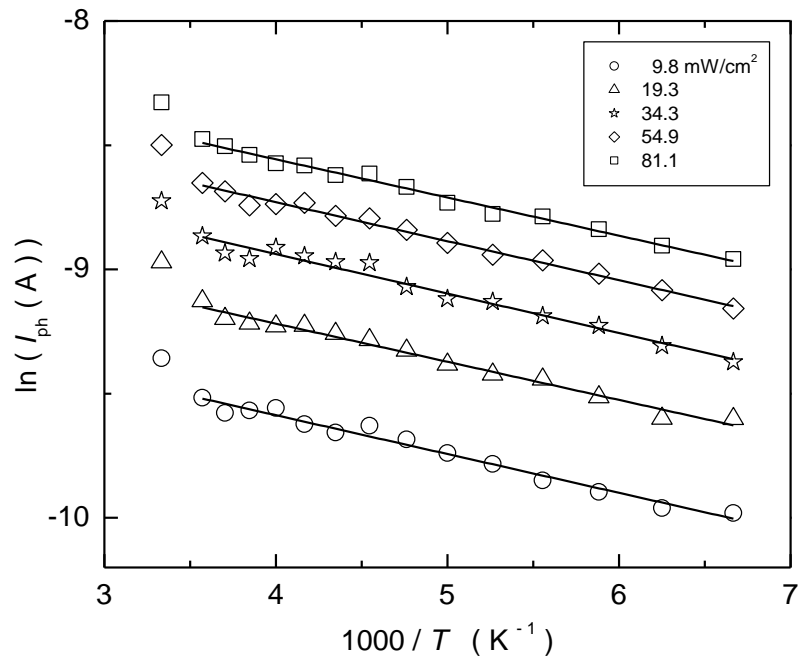


Figure 4.26. The temperature dependence of photocurrent at various illumination intensities.

4.10 Thermally Stimulated Current Measurements

i. Determination of the type of the charge carriers and minimum excitation time

TSC measurements performed on $\text{Ga}_{0.75}\text{In}_{0.25}\text{Se}$ crystals were carried out in the temperature range of 10–300 K with constant heating rate of $\beta = 0.8$ K/s. In these measurements, there exists one peak with peak maximum temperature of nearly 160 K as shown in figure 4.27. For the analysis of the obtained curves, it is necessary to determine the type of the trapping kinetics in the TSC process [101]. The type of the trapping kinetics is determined by the comparison of the magnitudes of capture cross sections S_t and S_r of the trapping and recombination centers. For first order kinetics $S_t \ll S_r$, slow retrapping occurs in the TSC experiments. In this case, electrons (holes) excited thermally from the traps have much greater probability for recombining with holes (electrons) than of being retrapped. Therefore, the concentration of the charge carriers trapped in the defect centers have no any effect on the peak maximum temperature of the TSC curve. The magnitude of the current measured in the experiments is only changed with the variation of concentration of the charge carriers. Fast retrapping case occurs in the case of $S_t \gg S_r$. In the fast retrapping, electrons (holes) are retrapped before recombination takes place. Therefore, these retrapped charge carriers take role in the TSC process more than one time. The TSC curves corresponding to fast retrapping are shifted to higher temperatures. Also, peak position and shape of the TSC curve changes with the concentration of filled traps. For this purpose, the initial concentration of the charge carriers in the trapping centers was changed by illuminating the sample for different times (0-600 sec) at low temperature (figure 4.27). As shown from the TSC curves in the figure, the shape of the spectra and peak maximum temperature values remain invariable. This behavior indicates that the observed trapping center may be considered under the first order kinetics condition. Inset of figure 4.27 shows the dependence of peak maximum currents on illumination time for observed peak. It is revealed that trapping center is filled completely after nearly 600 sec. Therefore, the illumination time for TSC experiments on $\text{Ga}_{0.75}\text{In}_{0.25}\text{Se}$ crystal was taken as 600 sec.

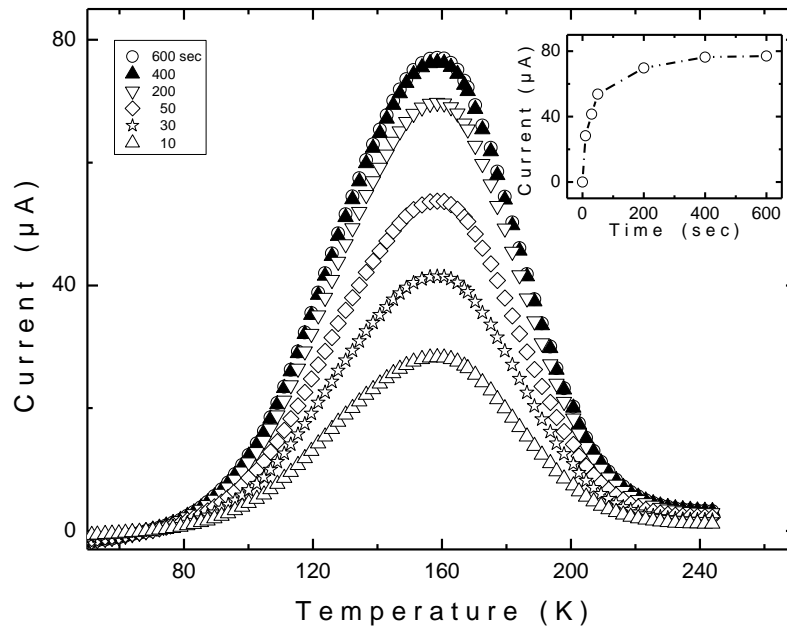


Figure 4.27. TSC spectra of $\text{Ga}_{0.75}\text{In}_{0.25}\text{Se}$ crystal for various illumination times. Inset: the dependence of peak maximum current on illumination time. The dash-dotted lines are only guides for the eye.

The type of the charge carriers taking part in the TSC experiments was also determined by illuminating only one contact of the sample. Figure 4.28 shows the TSC curves of $\text{Ga}_{0.75}\text{In}_{0.25}\text{Se}$ crystals measured for forward and reverse bias conditions for the observed trapping center. In this experimental technique, the contact on the illuminated surface of the crystal was connected to the positive or negative terminals of the applied voltage and TSC experiments were carried out for both cases. The illumination of crystal surface creates both types of charge carriers. But, only one type of carriers is driven along the whole field zone, while the opposite type is collected very quickly depending on the bias voltage. Only the illuminated terminal type carrier is trapped throughout the excitation. It was revealed from the figure 4.28, that when the polarity of the illuminated contact is positive, TSC curve intensity was highest. That means holes are distributed in the sample and then trapped. Consequently, observed peak can be characterized as hole trap.

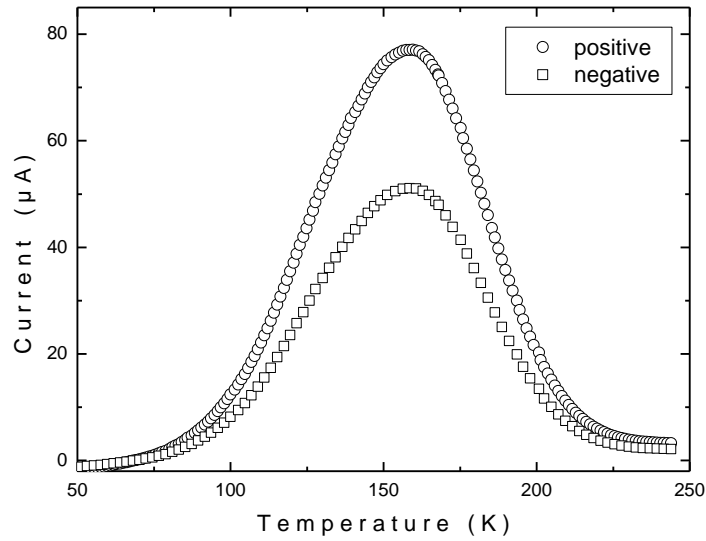


Figure 4.28. Typical experimental TSC curves of $\text{Ga}_{0.75}\text{In}_{0.25}\text{Se}$ crystal under opposite bias voltage. Circles and stars represent the experimental data obtained at illumination of positive and negative contacts, respectively.

ii. Determination of activation energy

There are several methods to determine the activation energies of the trapping centers. Among these methods, we have used the curve fitting, initial rise, peak shape and differential analysis methods. When the curve fitting method was applied on the TSC curve for one trapping center case, a good fit of the theoretical consideration to the experimental data was obtained (Figure 4.29). The fitting process was successfully accomplished for the case of slow retrapping according to equation 2.75. This also suggests that retrapping is negligible for the trap of $\text{Ga}_{0.75}\text{In}_{0.25}\text{Se}$ crystal studied in the present work. The solid line in figure 4.29 shows the data for a heating rate of 0.8 K/s fitted with one peak having activation energy of $E_t = 62$ meV (table 4.4).

As a second analysis technique, we have used the initial rise method which is independent of the recombination kinetics. This method is based on the theoretical fact that the TSC is proportional to $\exp(-E_t/kT)$ when the charge carriers are thermally excited from the traps [50]. Therefore, when the initial portion of the TSC curve is analyzed, the plot of $\ln(I)$ versus $1/T$ gives a straight line with a slope of $(-E_t/k)$. Figure 4.30 shows this plot with its linear fit given as a solid line. The activation energy of the trap calculated from this slope was found as 61 meV (Table 4.4).

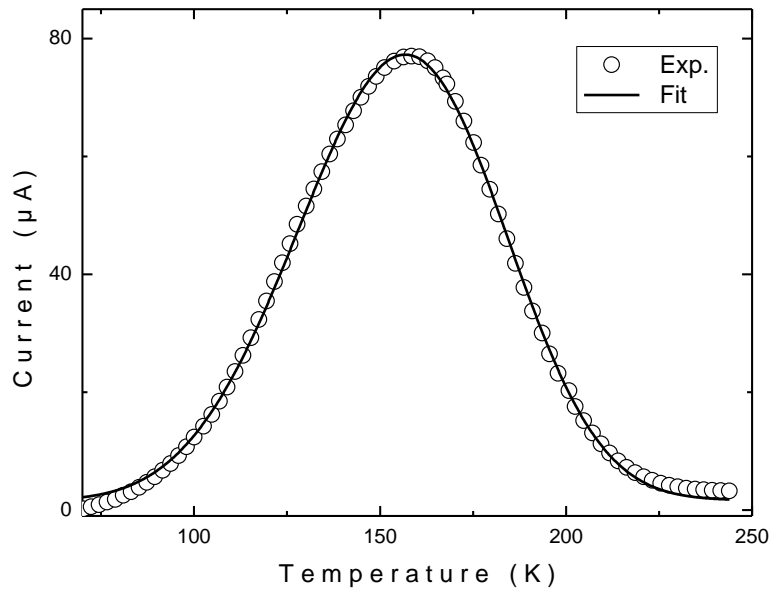


Figure 4.29. Experimental TSC spectrum of Ga_{0.75}In_{0.25}Se crystal with heating rate of 0.8 K/s. Open circles are experimental data. Solid curve shows the fit to the experimental data.

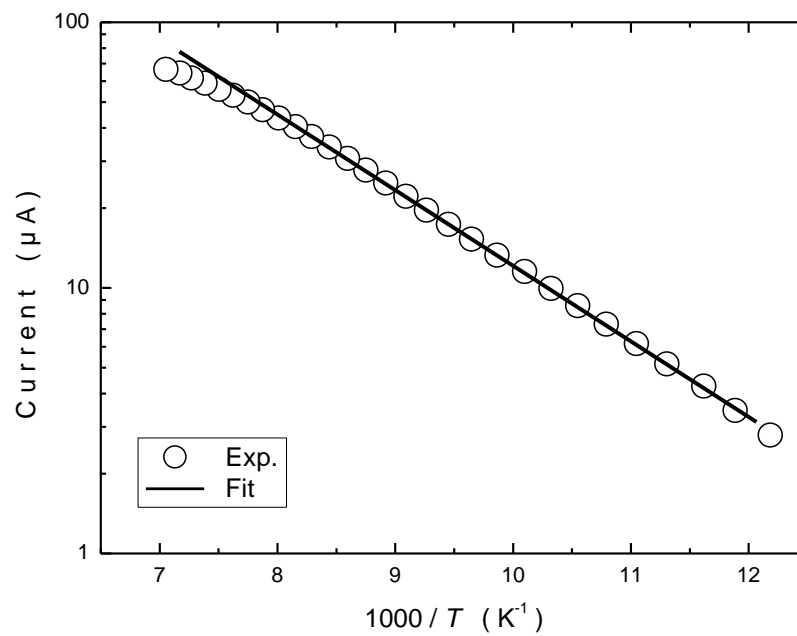


Figure 4.30. Thermally stimulated current vs. $1000/T$. The circles present the experimental data and the line represents the theoretical fit using initial rise method.

Table 4.4. The activation energy (E_t), capture cross section (S_t), attempt-to-escape frequency (ν) and concentration of observed trap of $\text{Ga}_{0.75}\text{In}_{0.25}\text{Se}$ crystal from TSC measurements.

T_m (K)	E_t (meV)			S_t (cm ²)	ν (s ⁻¹)	N_t (cm ⁻³)
	Curve fitting method	Initial rise method	Peak shape method			
156.8	62	61	65	1.0×10^{-25}	2.30	1.4×10^{17}

TSC glow curve has also been analyzed using peak shape method which depends on the analysis of the low and high half-intensity temperatures of the TSC curve. The averaged value of calculated E_t , E_δ and E_w using equations 2.90, 2.91 and 2.92 for the observed peak is found as 65 meV (Table 4.4). The characteristic parameter μ_g value for the trap in $\text{Ga}_{0.75}\text{In}_{0.25}\text{Se}$ crystal was calculated as 0.45 which is closer to the value of 0.42 suggested for the slow retrapping process. This closeness is also another indication of the first order kinetics for the trap level of $\text{Ga}_{0.75}\text{In}_{0.25}\text{Se}$ crystal.

As a last method, we have applied the differential analysis method on the observed peaks. Figure 4.31 shows the graph of the first derivative of the logarithmic current with respect to temperature. Activation energy of the observed trap was calculated using the slope of the tangent (α_m) at $T = T_m$ of the first derivative of the TSC curve. As can be seen from the figure, the derivative is equal to zero at $T_m = 156.7$ K with a tangential slope of $\alpha_m = -1.26 \times 10^{-3}$. The corresponding activation energy of this α_m value was calculated using equation 2.95 as $E_t = 63$ meV.

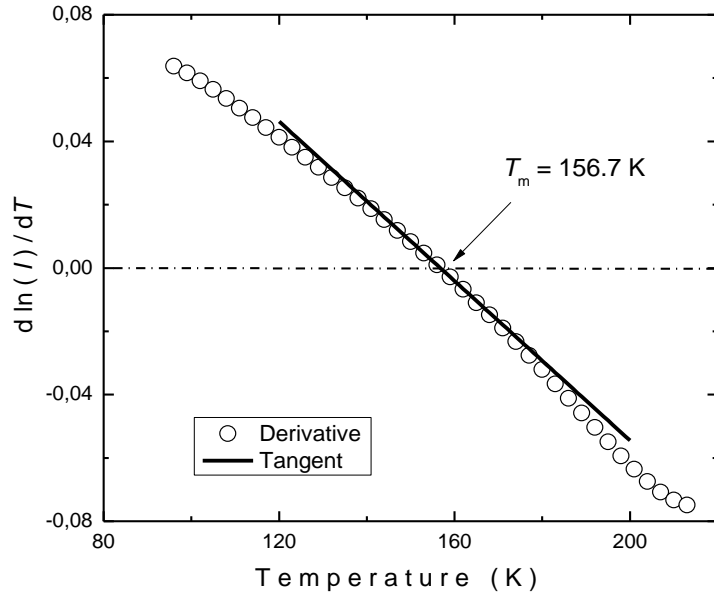


Figure 4.31. Derivative of the thermally stimulated current. Open circles are experimental data and the line is the tangent at $T_m = 156.7$ K.

iii. *Determination of capture cross section and concentration of traps*

Curve fitting parameters can also be used to calculate the capture cross section (S_t), attempt-to-escape frequency (ν) and concentration (N_t) of the traps. Equations 2.72 and 2.77 relating the parameter B' can be combined to calculate the attempt-to-escape frequency. Then the capture cross section of the trap can be found using equation 2.86. Table 4.4 shows the results of the calculations in which hole effective mass of $m_h = 0.14 m_o$ reported for GaSe crystal [100] was used. The small value of the capture cross section justifies the assumption of first order kinetics.

The concentration of the trap (N_t) and photoconductivity gain G were calculated using the relations 2.87 and 2.88, respectively. The photoconductivity decay is nearly exponential after termination of light pulse at $t = t_0$. The carrier lifetime τ was determined from the corresponding output voltage expressed as [56]

$$V_{ph} = V_{pho} + D \exp(-t / \tau), \quad (4.7)$$

where V_{pho} is the voltage at $t = \infty$ and D is a constant. Figure 4.32 represents the experimental data (circles) and its theoretical fit (solid line) obtained using equation 4.7. The carrier lifetime was found as 0.11 ms from the output of the fitting program. The photoconductivity gain corresponding to this value was calculated as 6.9 from equation 2.84, using $V = 3$ V and $\mu = 210$ cm²/Vs [100]. Then, concentration of the observed trap was evaluated as $N_t = 1.4 \times 10^{17}$ cm⁻³ (Table 4.4).

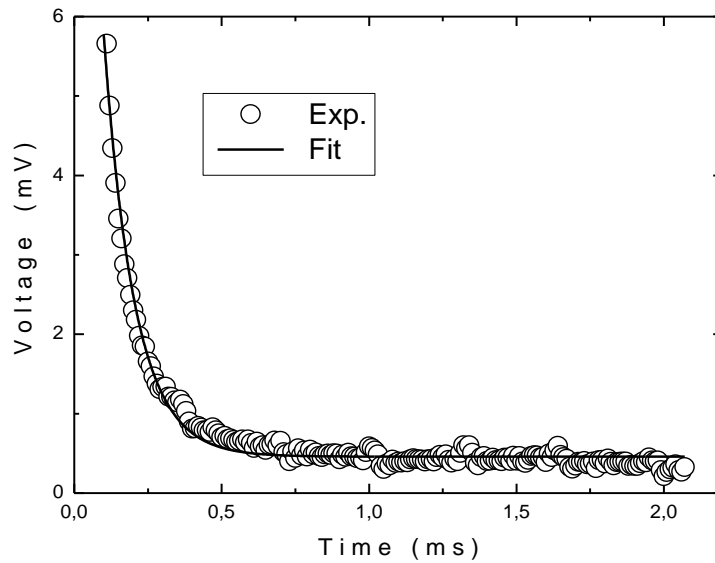


Figure 4.32. Photoconductivity decay curve for Ga_{0.75}In_{0.25}Se crystal. Open circles are experimental data. Solid line shows the fit to the experimental data.

4.11 Thermoluminescence Measurements

i. *Determination of the minimum excitation time*

Figure 4.33 shows the TL curves of Ga_{0.75}In_{0.25}Se crystal observed in the temperature range of 10–200 K for different illumination times [102]. Since TL experiments do not represent any peak above 200 K, this range was not given in the graphs presented in the work. The

obtained curve at constant heating rate of 1.0 K/s reveals the existence of at least three distinctive peaks. There are a few methods to find the exact number of these centers and their luminescence parameters. However, before applying these methods, the order of the kinetics in the TL process should be determined. The theoretical approach and experimental methods are different for first (slow retrapping) and second (fast retrapping) order kinetics as mentioned in chapter 2. The dependency of the TL glow curve on excitation time helps to understand the type of the kinetics as mentioned in the results of thermally stimulated current measurements. As can be seen from the figure 4.33, observed TL glow curves for different illumination times differ with regard to peak intensity, but their peak temperature positions do not change. This is an important indicator of slow retrapping process. Moreover, the dependency of intensity on excitation time reveals that defect centers are completely filled for illumination times between 300 and 600 sec illumination time. Therefore, the crystal was illuminated for 600 sec in all thermoluminescence measurements.

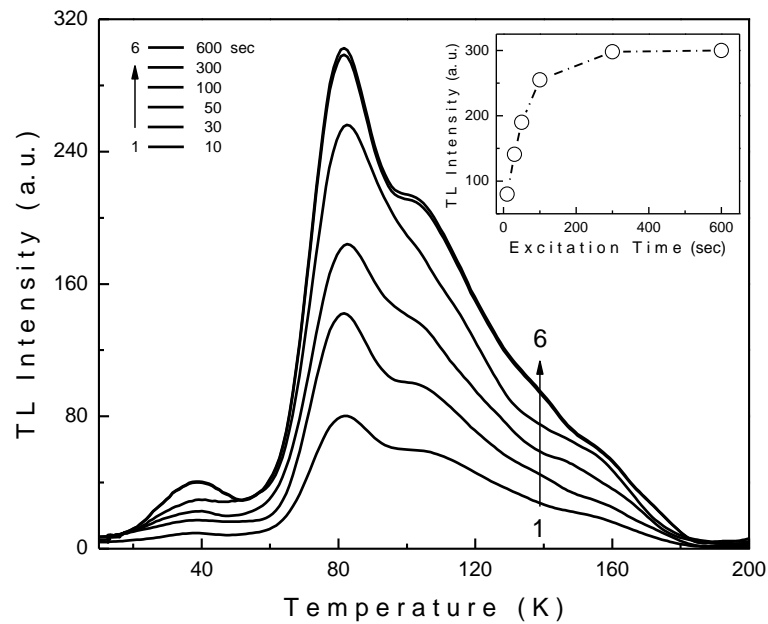


Figure 4.33. TL curves of $\text{Ga}_{0.75}\text{In}_{0.25}\text{Se}$ crystals for different illumination times at a constant heating rate $\beta = 1.0$ K/s. Inset: Maximum value of TL intensity as a function of illumination time. The dash-dotted line is only guide for the eye.

ii. Determination of activation energy

In the determination of activation energies, curve fitting, initial rise and different heating rate methods were used for the observed TL curves.

The curve fitting method was applied to the experimental glow curve under the light of the expression 2.75. Curve fitting method revealed that there appear four different defect centers with activation energies of 9, 45, 54 and 60 meV (Figure 4.34). The dashed-dot lines below the experimental data (open circles) represent the each defect center's own glow curves (deconvoluted peaks). Peak maximum temperatures, activation energies, capture cross sections and attempt-to-escape frequencies of the defects centers obtained from the curve fitting method are presented in table 4.5.

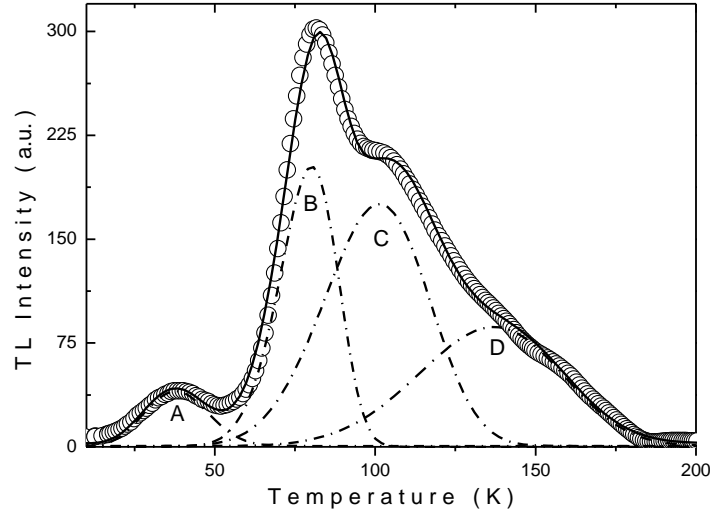


Figure 4.34. Experimental TL curve of $\text{Ga}_{0.75}\text{In}_{0.25}\text{Se}$ crystal with heating rate $\beta = 1.0$ K/s and decomposition of this curve into four separate peaks. Open circles are experimental data. Dashed curves represent decomposed peaks. Solid curve show total fit to the experimental data.

At this point, the comparison of calculated activation energies with those determined from TSC and PL analysis should give essential assessment to relate these luminescence techniques. TSC measurements demonstrated that one hole trapping center exists at 62 meV. This level is also observed in TL analysis with $E_{\text{TD}} = 60$ meV in the glow curve. However, three additional defect centers (A, B and C) also appear in TL measurements. The reason of not observing these centers in the TSC experiments can be because of the large dark currents in $\text{Ga}_{0.75}\text{In}_{0.25}\text{Se}$ crystal having low resistivity. Moreover, it may be informative to compare the present TL outcomes with previous results obtained from PL spectroscopy measurements on $\text{Ga}_{0.75}\text{In}_{0.25}\text{Se}$ crystals in the temperature range of 10–300 K. Trap levels of 10 and 12 meV were revealed from the temperature dependency of the PL intensity and photoconductivity measurements, respectively. These energies are very close to the level located at 9 meV found in the TL analysis. Taking into consideration the errors, these energies can be assigned to the same level.

As a second method, the initial rise method, valid for both of slow and fast retrapping processes, was applied. Figure 4.35 shows the convenient plots and linear fitted lines (according to equation 2.89) with their resulting activation energies. The calculated values of 8, 41, 53 and 55 meV were in good agreement with values obtained from curve fitting method (Table 4.5).

Table 4.5. The activation energy (E_t), capture cross section (S_t) and attempt-to-escape frequency (ν) of observed traps in $\text{Ga}_{0.75}\text{In}_{0.25}\text{Se}$ crystal from TL measurements.

Peak	T_m (K)	E_t (meV)				S_t (cm^2)	ν (s^{-1})
		Curve fitting method	Initial rise method	Heating rate method	After thermal cleaning		
A	37.8	9	8	–	–	7.2×10^{-25}	0.7
B	80.2	54	53	53	–	4.6×10^{-23}	193.0
C	101.4	45	41	–	48	9.5×10^{-25}	6.3
D	137.0	60	55	–	59	3.5×10^{-25}	4.3

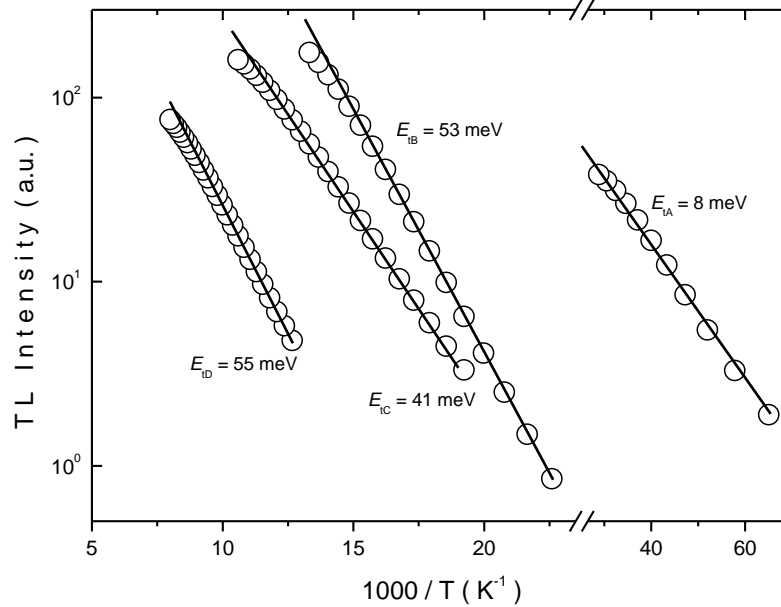


Figure 4.35. TL intensity vs. $1000/T$ for observed peaks in TL spectra of $\text{Ga}_{0.75}\text{In}_{0.25}\text{Se}$ crystal. Open circles are experimental data and solid lines are the fitted straight lines.

The reliability of the curve fitting method results introducing the number of defect centers as four can be verified using an experimental technique which separates the overlapped peaks. For this separation purpose, thermal cleaning process is used in the TL measurements. In this method, the sample illuminated at low temperature ($T_0 = 10$ K) is heated up to a cleaning temperature ($T_{cl.}$) value which empties some of the initial defect levels. Then the sample is cooled to initial low temperature and re-heated to higher temperature without any additional excitation. By this way, some of the initial defect levels are emptied throughout the process occurring between T_0 and $T_{cl.}$ temperatures. The TL curve obtained after re-heating the sample includes all the luminescence properties belonging to the remaining distributed traps. We have performed many experiments for different $T_{cl.}$ temperatures and revealed that first two peaks empty for $T_{cl.} = 45$ K. The TL glow curve obtained after thermal cleaning process is given in figure 4.36. It can be easily seen that this curve belongs to the combination of remaining peaks C and D. We have also applied curve fitting method on this glow curve (inset of figure 4.36). The results of curve fitting method on C- and D-peaks before and after the thermal cleaning were in good agreement with each other (Table 4.5).

The effect of heating rate on the TL curve is also investigated using heating rates (β) between 0.2 and 1.0 K/s (figure 4.37). Behavior of the TL curve according to the change of heating rate can be used to calculate the activation energy of the traps [103]. In this method, the plot of $\ln(T_m^2 / \beta)$ versus $1/T_m$ gives a straight line with a slope of E_t / k . In the inset of figure 4.37, this plot obtained using the T_m values of the most intensive peak in TL curves for different heating rates is represented. As a result of linear fit of the plot, corresponding activation energy was found as 53 meV. It should be noted, that the T_m values of the most intensive peak in TL curve and deconvoluted peak B curve are very close to each other (see figure 4.34). For this reason 53 meV energy calculated from the different heating rate method can be attributed to the activation energy of peak B.

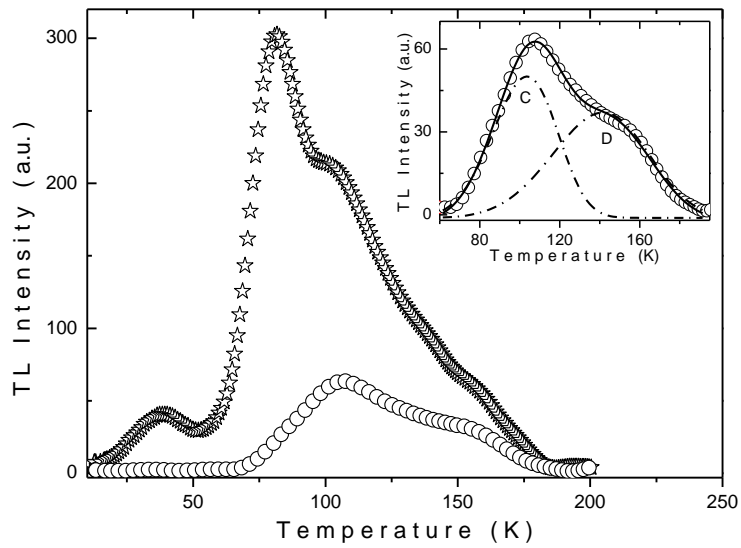


Figure 4.36. Experimental TL glow curves of $\text{Ga}_{0.75}\text{In}_{0.25}\text{Se}$ crystal before (stars) and after (circles) thermal cleaning for a heating rate of $\beta = 1.0$ K/s. Inset: Experimental TL curve after thermal cleaning and decomposition of this curve into two separate peaks. Open circles are experimental data. Dashed curves represent decomposed peaks. Solid curve show total fit to the experimental data.

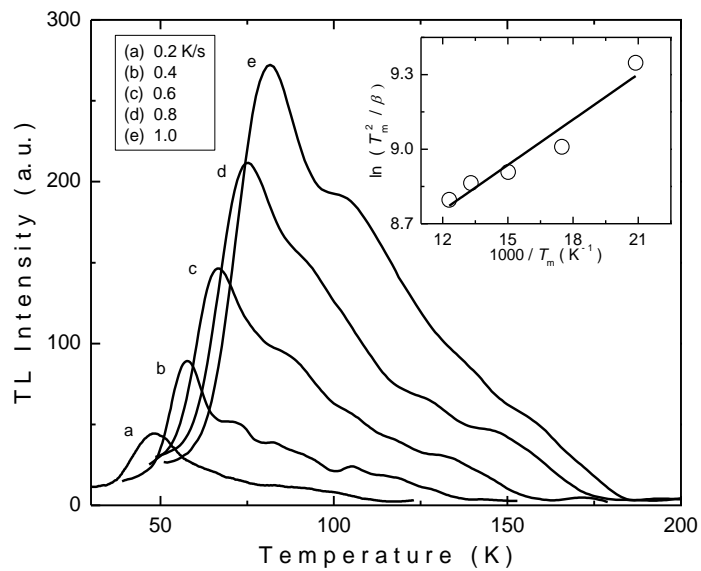


Figure 4.37. Experimental TL curve of $\text{Ga}_{0.75}\text{In}_{0.25}\text{Se}$ crystal with different heating rates. Inset: $\ln(T_m^2/\beta)$ versus $1000/T_m$ for different heating rates. Open circles are experimental data and solid line shows the theoretical fit to the experimental data.

CHAPTER 5

CONCLUSION

In the present thesis, an important mixed crystals, $\text{Ga}_{0.75}\text{In}_{0.25}\text{Se}$ which is formed from the restricted combination of GaSe and InSe semiconductor crystals was characterized by means of structural, optical and electrical measurements. The applied techniques were x-ray diffraction and energy dispersive spectral analysis for structural characterization, visible and infrared reflectivity and transmittance, ellipsometry, Raman spectroscopy and photoluminescence for optical characterization and dark electrical resistivity, space-charge-limited current and photoconductivity for electrical characterization. Furthermore, the trapping centers in the undoped $\text{Ga}_{0.75}\text{In}_{0.25}\text{Se}$ single crystals were studied using thermally stimulated current and thermoluminescence measurements. The obtained results of each experimental methods were compared with those of GaSe crystal to understand how the addition of In atoms changes the characteristic properties of the GaSe.

Energy dispersive spectroscopy experiments were carried out in the energy range of 0-9 keV. As a result of the analysis, the atomic composition ratio of the constituent elements (Ga : In : Se) in the crystal was found out as 39.8 : 11.3 : 48.9, respectively. The crystal system, Miller indices and lattice parameters of the crystal structure of $\text{Ga}_{0.75}\text{In}_{0.25}\text{Se}$ were obtained from the analysis of the x-ray diffraction experiment. The lattice parameters of the orthorhombic unit cell were found to be $a = 0.62365$, $b = 0.52206$ and $c = 1.59194$ nm. The effect of addition of In atoms to GaSe compound on the crystal structure was revealed by comparing the obtained results with those of GaSe given in the literature. This comparison indicated that addition of In atoms to GaSe compound transforms the structure of the mixed crystal $\text{Ga}_{0.75}\text{In}_{0.25}\text{Se}$ from hexagonal to orthorhombic with above given lattice parameters.

The optical constants of $\text{Ga}_{0.75}\text{In}_{0.25}\text{Se}$ single crystals were found via the transmission and reflection measurements in the 380–1100 nm spectral region. The analysis of the absorption data at the room temperature showed the existence of indirect transitions in the crystal with energy band gap of 1.89 eV. In the literature, the band gap energies of GaSe and InSe were found approximately as 2.0 and 1.2 eV, respectively. When the obtained result for $\text{Ga}_{0.75}\text{In}_{0.25}\text{Se}$ single crystal was compared with those of previous studies, it is seen that band gap energy value is in the expected region of 1.2 – 2.0 eV and closer to that of GaSe crystal. Temperature dependence of the transmission measurements were also performed in the 10-300 K region. Measurements revealed the shift of the absorption edge toward lower energy as temperature is increased from 10 to 300 K. The rate of change of the indirect band gap of the crystal was found as $\gamma = -6.2 \times 10^{-4}$ eV/K from the theoretical relation giving the band gap energy as a function of temperature. The absolute zero value of the band gap energy was calculated as $E_{gi}(0) = 2.01$ eV from the same analysis. The refractive index values found in the wavelength range of 650–1100 nm decrease from 3.15 to 3.03. The long wavelength refractive index 3.03 calculated for $\text{Ga}_{0.75}\text{In}_{0.25}\text{Se}$ single crystals showed a good consistency with the refractive index values $n = 3$ for InSe and $n = 2.92$ for GaSe given in the literature. The Wemple-DiDomenico single-effective-oscillator model applied to refractive index dispersion data was used to determine the oscillator energy (E_{so}), dispersion energy (E_d), and zero-frequency (n_0) refractive index. The oscillator parameters were calculated as $E_{so} = 4.60$ eV, $E_d = 34.21$ eV and $n_0 = 2.9$. The real (ϵ_1)

and imaginary (ϵ_2) parts of the dielectric constant were also calculated from the refractive index and extinction coefficient in the 380–1100 nm spectral region.

The optical characterization of $\text{Ga}_{0.75}\text{In}_{0.25}\text{Se}$ crystal was extended by carrying out the ellipsometry measurements the 1.2–6.0 eV spectral region to get detailed information about the optical constants, real and imaginary parts of the pseudodielectric function, pseudorefractive index and pseudoextinction coefficient. Moreover, the critical point analysis of the second derivative spectra of the dielectric constant in the above band gap region were accomplished to get comprehensive information about the interband transitions in the electronic band structure of $\text{Ga}_{0.75}\text{In}_{0.25}\text{Se}$ crystal. Analysis revealed the presence of four critical points (CP) with energies of 3.16, 3.53, 4.05 and 4.53 eV. The CP energies of $\text{Ga}_{0.75}\text{In}_{0.25}\text{Se}$ crystal was found to be slightly smaller than those of GaSe given in literature. This is thought to be an expected result, since the band structure of GaSe crystal changes and consequently band gap energy decreases with the addition of In atoms.

The infrared reflectivity and transmittance and Raman scattering in $\text{Ga}_{0.75}\text{In}_{0.25}\text{Se}$ layered crystals were investigated in the frequency ranges of 100–400, 400–4000 and 25–500 cm^{-1} , respectively. The frequencies of transverse (ν_T) and longitudinal (ν_L) optical phonons were determined as 209 and 243 cm^{-1} , respectively, from the maxima of the function of the imaginary part of the dielectric constant (ϵ_2) and the function of energy losses $\text{Im}(1/\epsilon)$, respectively. Moreover, the high- and low-frequency refractive indices were determined as 2.42 ($\nu = 400 \text{ cm}^{-1}$) and 3.09 ($\nu = 100 \text{ cm}^{-1}$), respectively, with maximum value of $n = 5.95$ corresponding to the frequency $\nu = 206 \text{ cm}^{-1}$. In the Raman spectroscopy measurements, six lines with frequencies of 41, 136, 210, 242, 305 and 480 cm^{-1} were observed in the spectrum. The latter line with frequency of 480 cm^{-1} may be assigned to the overtone of mode with frequency of 242 cm^{-1} . The two lines with frequencies of 210 and 247 cm^{-1} , revealed in the Raman spectrum, were attributed to the TO and LO branches of the polar mode, respectively. The infrared transmittance spectrum of $\text{Ga}_{0.75}\text{In}_{0.25}\text{Se}$ crystal showed minimas at 421, 443, 480, 511 and 540 cm^{-1} which are considered as caused by the two-phonon absorption. The bands in IR spectrum with frequencies of 421 and 480 cm^{-1} were attributed to the overtones of modes with frequency of 210 and 242 cm^{-1} observed in the Raman spectrum of $\text{Ga}_{0.75}\text{In}_{0.25}\text{Se}$ crystal.

Photoluminescence measurements were carried out as a function of temperature and excitation laser intensity on $\text{Ga}_{0.75}\text{In}_{0.25}\text{Se}$ single crystals. Two emission bands centered at 613 nm (2.02 eV, A-band) and 623 nm (1.99 eV B-band) were observed at $T = 7 \text{ K}$ at constant laser excitation intensity of 1.40 W cm^{-2} . The excitation intensity ($0.06\text{--}1.40 \text{ W cm}^{-2}$) and temperature dependence ($7\text{--}59 \text{ K}$) analysis performed on the PL spectra of A- and B- bands revealed that observed emissions are interpreted as transitions from two donor levels to a single acceptor level located at 0.01 eV above the valence band. The energies of donor levels were calculated from the band energy positions of the bands as 0.11 and 0.15 eV for A- and B-bands, respectively. Since the studied samples were not intentionally doped, the revealed acceptor and donor levels are considered to come out from the uncontrolled impurities and/or defects produced during the crystal growth.

The dark electrical resistivity measurements were carried out on $\text{Ga}_{0.75}\text{In}_{0.25}\text{Se}$ crystals in the temperature range of 150–300 K. The room temperature value of the resistivity (ρ) was found as $2.2 \times 10^3 \text{ }\Omega\text{cm}$. In the studied temperature range, the resistivity activation energy was found as 0.10 eV. This energy value showed a good agreement with the result obtained in PL measurements. The I - V measurements revealed that both ohmic and space-charge-limited (SCL) characters exhibit in the 180–300 K range. The analysis on the SCL region indicated the energy of the trap level as 0.11 eV which is consistent with the results obtained from PL (0.11 eV) and dark resistivity (0.10 eV) measurements. Photoconductivity measurements were performed at different light intensities in the range of $9.8\text{--}81.1 \text{ mWcm}^{-2}$ and in the temperature range of 150–300 K. The photocurrent-illumination intensity relation showed that the behavior of the photoconductivity is sublinear recombination. Moreover, analysis on the dependence of photocurrent on temperature at different illumination intensities revealed the photocurrent energy as 12 meV.

The defect levels in $\text{Ga}_{0.75}\text{In}_{0.25}\text{Se}$ single crystals were studied by means of thermally stimulated current (TSC) and thermoluminescence (TL) measurements. TSC measurements

performed in the temperature range of 10–300 K with constant heating rate of $\beta = 0.8$ K/s revealed that there exists one hole trapping center at 62 meV energy level. The results of the various activation energy determination methods (curve fitting, initial rise, peak shape and differential analysis methods) were agree with each other. Since the analysis of the experimental TSC curve gave reasonable results under the model that assumes slow retrapping, the retrapping process was negligible for the observed trap level. As the crystals studied are not intentionally doped, the observed levels are thought to exist due to the presence of defects created during the growth of crystals and/or unintentional impurities. The capture cross section of the trap was calculated to be 1.0×10^{-25} cm². Also the concentration of the trap was estimated to be 1.4×10^{17} cm⁻³.

Thermoluminescence measurements were also carried out in the low temperature range of 10–300 K with different heating rates. The observed TL curves have been analyzed using curve fit, initial rise and different heating rate methods. Four trapping centers with activation energies of 9, 45, 54 and 60 meV were found from the results of the analysis. The trapping center at 60 meV was also observed in the TSC measurements with 62 meV activation energy. The reason of not observing the other three centers in TL results can be due to the large dark currents in Ga_{0.75}In_{0.25}Se crystal having low resistivity. Moreover, taking into consideration the errors, trapping center at 9 meV observed in TL analysis can be considered as the same level observed in PL result with 10 meV level. The studied Ga_{0.75}In_{0.25}Se crystals were not intentionally doped. Therefore, the existence of these trapping centers can be referred to the defects, created in the growth process of crystals, and/or unintentional impurities. The experimental applications and consistency of the slow retrapping theory with experimental curve showed that the first order of kinetics is the dominant case in the TL measurements. The capture cross sections and attempt-to-escape frequencies of the observed trap levels were also calculated.

REFERENCES

- [1] G. Saintonge and J. L. Brebner, *Can. J. Phys.* **62**, 730 (1984).
- [2] R. H. Tregold and A. Clark, *Sol. Stat. Commun.* **7**, 1519 (1969).
- [3] J. C. J. M Terhell, *Prog. Cryst. Growth Charact. Mater.* **7**, 55 (1983).
- [4] A. Chevy, A. Kuhn and M. S. Martin, *J. Cryst. Growth* **38**, 118 (1977).
- [5] A. Seyhan, O. Karabulut, B. G. Akinoğlu, B. Aslan and R. Turan, *Cryst. Res. Technol.* **40**, 893 (2005).
- [6] J. V. Mc Canny and R. B. Murray, *J. Phys. C* **10**, 1211 (1977).
- [7] M. K. Anis, *J. Crystal Growth* **55**, 465 (1981).
- [8] E. Mooser, *Physics and Chemistry of Materials with Layered Structures*, Riedel, Dordrecht (1976).
- [9] A. Kuhn, A. Chevy and R. Chevalier. *Phys. Stat. Sol. (a)* **31**, 469 (1975).
- [10] O. Karabulut, *Structural, Electrical and Optical Characterization of N- and Si-implanted GaSe Single Crystal Grown by Bridgman Method*, Ph.D Thesis, Middle East Technical University, 2003.
- [11] E. Aulich, J.L. Brebner and E. Mooser, *Phys. Stat. Sol. (b)* **31**, 129 (1969).
- [12] S.G. Choi, D.H. Levi, C. Martinez-Tomas and V. Munoz Sanjose, *J. Appl. Phys.* **106**, 053517 (2009).
- [13] N.M. Gasanly, A. Aydinli, H. Ozkan and C. Kocabas, *Mat. Res. Bul.* **37**, 169 (2002).
- [14] A. Aydinli, N.M. Gasanly and K. Goksen, *Phil. Mag. Lett.* **81**, 859 (2001).
- [15] N.M. Gasanly, A. Aydinli and O. Salihoglu, *Cryst. Res. Technol.* **36**, 295 (2001).
- [16] C. Manfredotti, A. M. Mancini, R. Murri, A. Rizzo and L. Vasanelli, *II Nuovo Cimento B* **39**, 257 (1977).
- [17] C. De Blassi, G. Micocci, A. Rizzo and A. Tepore, *Physical Review B* **27**(4), 2429 (1983).
- [18] S. G. Choi, D.E. Aspnes, A.L. Fuchser, C. Martinez-Tomas, V. M. Sanjose and D.H. Levi, *Appl. Phys. Lett.* **96**, 181902 (2010).
- [19] M. Kundakci, B. Gurbulak, S. Dogan, A. Ates and M. Yildirim, *Appl. Phys. A* **90**, 479 (2008).
- [20] B. Abay, H. Efeoglu and Y.K. Yogurtcu, *Mat. Res. Bulletin* **33**, 1401 (1998).
- [21] G. Micocci, A. Rizzo and A. Tepore, *J. Appl. Phys.* **54**, 1924 (1983).

- [22] S. Shigetomi and T. Ikari, *J. Appl. Phys.* **88**, 1520 (2000).
- [23] Yasuo Iwamura, Makoto Moriyama and Naozo Watanabe, *Jpn. J. Appl. Phys.* **30**, L42 (1991).
- [24] N.B. Singh, D.R. Suhre, V. Balakrishna, M. Marable, R. Meyer, N. Fernelius, F.K. Hopkins and D. Zelmon, *Progress in Crystal Growth and Characterization of Materials* **37**, 47 (1998).
- [25] G.B. Abdullaev, K.R. Allakhverdiev, M.E. Karasev, V.I. KOnov, L.A. Kulevskii, N.B. Mustafaev, P.P. Pashinin, A.M. Prokhorov, Yu. M. Starodumov and N.I. Chapliev, *Sov. J. Quantum Electron* **19**, 494 (1989).
- [26] Y.Z. Lu, X.B. Wang, X.W. Zhu, X.L. Zhang, D.L. Zuo and Z.H. Cheng, *J. Appl. Phys.* **107**, 093105 (2010).
- [27] A.G. Kyazym-zade, A.A. Agaeva, V.M. Salmanov and A.G. Mokhtari, *Tech.Phys.* **52**, 1611 (2007).
- [28] L. Gousskov, A. Gousskov, M. Hajjar, L. Soonckindt and C. Llinares, *Physica B & C* **99**, 291 (1980).
- [29] G. L. Belenkii, M. O. Godzhaev, N. T. Mamedov, E. Y. Salaev and R. A. Suleimanov, *Phys. Status Solidi (a)* **53**, 137 (1979).
- [30] E. A. Vinogradov, N. M. Gasanly, A. F. Goncharov, B. M. Dzhavadov and N. N. Melnik, *Sov. Phys. Solid State* **21**, 1572 (1979).
- [31] V. I. Tagirov, N. M. Gasanly, B. M. Dzhavadov, M. A. Sobeikh and V. M. Salmanov, *Phys. Status Solidi (a)* **47**, K157 (1978).
- [32] A. Karatay, C. Aksoy, H. G. Yaglioglu, A. Elmali, U. Kurum, A. Ates and N. M. Gasanly, *J. Opt.* **13**, 075203 (2011).
- [33] R. de L. Kronig and W. G. Penney, *Proc. Roy. Soc. (London)* **A130**, 499 (1930).
- [34] B. G. Yacobi, *Semiconductor Materials; An Introduction to Basic Principles*, Kluwer Academic, New York (2003).
- [35] C.Kittel, *Introduction to Solid State Physics*, Wiley, New York (1971).
- [36] W. L. Bragg, *Proceedings of the Royal Society of London Series A* **17**, Part I, 43 (1913).
- [37] B. D. Cullity, *Elements of X-ray Diffraction*, Addison-Werley Publishing Company (1978).
- [38] S. M. Sze, *Physics of Semiconductor Devices*, John Wiley and Sons, New York (1981).
- [39] T. S. Moss, G. J. Burrell and B. Ellis, *Semiconductor Opto-Electronics*, John Wiley & Sons, New York (1973).
- [40] J. I. Pankove, *Optical Processes in Semiconductors*, Prentice Hall, New Jersey (1971).
- [41] S. H. Wemple and M. DiDomenico, *Phys. Rev. B* **3**, 1338 (1971).
- [42] S. H. Wemple and M. DiDomenico, *Phys. Rev. Lett.* **23**, 1156 (1969).
- [43] A. K. Walton and T. S. Moss, *Proc. Phys. Soc.* **81**, 509 (1963).

- [44] F. Yakuphanoglu, A. Cukurovali and I. Yilmaz, *Physica B: Condensed Matter* **351**, 53 (2004).
- [45] M. Fox, *Optical Properties of Solids*, Oxford University Press, London (2001).
- [46] H. Fujiwara, *Spectroscopic Ellipsometry Principles and Applications*, John Wiley & Sons, New York (2007).
- [47] E. Hecht, *Optics*, 4th ed., Reading, MA: Addison–Wesley (2002).
- [48] S. Adachi, *Optical Properties of Crystalline and Amorphous Semiconductors*, Kluwer Academic, New York (1999).
- [49] S. W. S. McKeever, *Thermoluminescence of solids*, Cambridge Uni. Press, Cambridge (1985).
- [50] R. Chen and Y. Kirsh, *Analysis of Thermally Stimulated Processes*, Pergamon Press, Oxford (1981).
- [51] J.T. Randall and M.H.F. Wilkins, *Proc. Roy. Soc. (London)* **A 184**, 366 (1945).
- [52] R.R. Haering and E.N. Adams, *Phys. Rev.* **117**, 451 (1960).
- [53] G.F.J. Garlick and A.F. Gibson, *Proc. Roy. Soc. (London)* **60**, 574 (1948).
- [54] N. S. Yuksek, N. M. Gasanly, and H. Ozkan *Semicond. Sci. Technol.* **18**, 834 (2003).
- [55] N. M. Gasanly, A. Aydınli, N.S. Yuksek and O. Salihoglu, *Appl. Phys. A* **77**, 603 (2003).
- [56] C. Manfredotti, R. Murri, A. Quirini and L. Vasanelli, *Phys. Stat. Sol. (a)* **38**, 685 (1976).
- [57] R. Bube, *Photoelectronic Properties of Semiconductors*, Cambridge University Press, Cambridge (1992).
- [58] M. Castagne, J. Bonnafe, J. Romestan and J.P. Fillard, *J. Phys. C: Solid State. Phys.* **13**, 5555 (1980).
- [59] P. Y. Yu and M. Cardona, *Fundamentals of Semiconductors*, Springer, Berlin (1995).
- [60] T. Taguchi, J. Shirafuji and Y. Inuishi, *Phys. Stat. Sol. (b)* **68**, 727 (1975).
- [61] D. E. Cooper, J. Bajaj and P. R. Newmann, *J. Cryst. Growth* **86**, 544 (1988).
- [62] Z. C. Feng, A. Mascarenhas and W. J. Choyke, *J. Lumin.* **35**, 329 (1986).
- [63] Q. Kim and D. W. Langer, *Phys. Stat. Sol. (b)* **122**, 263 (1984).
- [64] T. Schmidt, K. Lischka and W. Zulehner, *Phys. Rev. B* **45**, 8989 (1992).
- [65] A. Bauknecht, S. Siebentritt, J. Albert and M. Ch. Lux-Steiner, *J. Appl. Phys.* **89**, 4391 (2001).
- [66] E. Zacks and A. Halperin, *Phys. Rev. B* **6**, 3072 (1972).
- [67] D. G. Thomas, J.J. Hopfield and W.M. Augustiniak, *Phys. Rev. A* **140**, 202 (1965).

- [68] P.J. Dean and Lyle Patrick, *Phys. Rev B* **2**, 1888 (1970).
- [69] M. Lax, *J. Phys. Chem. Solids* **8**, 66 (1959).
- [70] Y. P. Varshni, *Physica* **34**, 149 (1967).
- [71] C. J. Hwang, *Physical Review* **180**, 827 (1969).
- [72] D.K. Schroder, “*Semiconductor Material and Device Characterization*”, John Wiley and Sons, New York, 1990.
- [73] J.G. Simmons, “*DC Conduction in Thin Films*”, London, 1971.
- [74] M. A. Lampert, *Phys. Rev.* **103**, 1648 (1956).
- [75] G.G. Roberts and F.W. Schmidlin, *Phys. Rev.* **180**, 785 (1969).
- [76] M.A. Lampert and P. Mark, “*Current Injection in Solids*”, Academic Press, 1970.
- [77] N.F. Mott and R.W. Gurney, “*Electronic Processes in Ionic Crystals*”, Oxford University Press, New York, 1964.
- [78] V. Capozzi, G. Mariotto, N. Montagna, A. Cingolani and A. Minafra, *Phys. Stat. Sol. (a)* **40**, 93 (1977).
- [79] L. J. van der Pauw, *Philips Research Reports*, **13**, 1 (1958).
- [80] M. Isik and N.M. Gasanly, *J. Phys. Chem. Sol.* **72**, 768 (2011).
- [81] A. I. Malik, Z. D. Kovalyuk, N. T. Savitskii and V. B. Baranyuk, *Sov. Phys. Semicond.* **12**, 1433 (1978).
- [82] M. Isik and N.M. Gasanly, *Cryst. Res. Technol.* **47**, 530 (2012).
- [83] B. Celustka, A. Persin and D. Bidjin, *J. Appl. Phys.* **41**, 813 (1970).
- [84] R. Letoullec, N. Piccioli, M. Mejatty and M. Balkanski, *Nuovo Cimento B* **38**, 159 (1977).
- [85] M. Isik, S.S. Cetin, N. M. Gasanly and S. Ozcelik, *Solid State Commun.* **152**, 791 (2012).
- [86] M. Grandolfo, F.Somma and P. Vecchia, *Phys. Rev. B* **5**, 428 (1972).
- [87] M. Piacentini, C.G. Olson, A. Balzarotti, R. Girlanda, V. Grasso and E. Doni, *Nuovo Cimento B* **54**, 248 (1979).
- [88] F. Meyer, E.E. de Kluizenaar and D. den Engelsens, *J. Opt. Soc. Am.* **64**, 529 (1973).
- [89] S. Adachi and Y. Shindo, *J. Appl. Phys.* **71**, 428 (1992).
- [90] S.Yu. Sarkisov, V.V. Atuchin, T.A. Gavrilova, V.N. Kruchinin, S.A. Bereznaya, Z.V. Korotchenko, O.P. Tolbanov and A.I. Chernyshev, *Russ. Phys. J.* **53**, 346 (2010).
- [91] N. Kuroda and Y. Nishina, *Physica B+C* **105**, 30 (1981).

- [92] K. Allakhverdiev, T. Baykara, S. Ellialtioglu, F. Hashimzade, D. Huseinova, K. Kawamura, A. M. Kulibekov, S. Onari, *Mat. Res. Bulletin* **41**, 751 (2006).
- [93] A. Mercier and J. P. Voitchovsky, *Solid State Commun.* **14**, 757 (1974).
- [94] J. C. Irwin, R. M. Hoff, B. P. Clayman and R. A. Bromley, *Solid State Commun.* **13**, 1531 (1973).
- [95] R. M. Hoff and J. C. Irwin, R. M. A. Lieth, *Can. J. Phys.* **53**, 1606 (1975).
- [96] V. Riede, H. Neumann, Hoang Xuan Nguyen and H. Sobotta, *Phys. Status Solidi (b)* **104**, 277 (1981).
- [97] V. Riede, H. Neumann, F. Levy and H. Sobotta, *Phys. Status Solidi (b)* **109**, 275 (1982).
- [98] M. Isik and N. M. Gasanly, *Opt. Mat.* **35**, 414 (2013).
- [99] M.I. Kolinko, I.V. Kityk and A.S. Krochuk, *J. Phys. Chem. Sol.* **53**, 1315 (1992).
- [100] G. Ottaviani, C. Canali, F. Nava, Ph. Schmid, E. Mooser, R. Minder and I. Zschokke, *Solid State Commun.* **14**, 933 (1974).
- [101] S. Ozdemir, N. M. Gasanly and M. Bucurgat, *Phys. Stat. Sol. (a)* **196**, 422 (2003).
- [102] M. Isik, E. Bulur and N.M. Gasanly, *J. Alloy. Compd.* **545**, 153 (2012).
- [103] R. Chen and S.W.S. McKeever, *Theory of Thermoluminescence and Related Phenomena*, World Scientific, Singapore (1997).

CURRICULUM VITAE

PERSONAL INFORMATION

Surname, Name: Işık, Mehmet
Nationality: Turkish (TC)
Date and Place of Birth: 31 May 1981 , Kadirli/OSMANİYE
Marital Status: Married
Phone: +90 312 586 8299
e-mail: misik@atilim.edu.tr

EDUCATION

Degree	Area	Institution	Year
BS	Physics	Boğaziçi University	2004
MS	Physics	Middle East Technical University	2008

WORK EXPERIENCE

Year	Institution	Position
2005-2008	Atilim University	Teaching Assistant
2008-2013	Atilim University	Instructor

PUBLICATIONS

1. “Trap Distribution in $TlInS_2$ Layered Crystals from Thermally Stimulated Current Measurements”
M. Isik, K. Goksen, N. M. Gasanly and H. Ozkan, *J. Korean Phys. Soc.* **52**, 367 (2008).
2. “Deep Traps Distribution in $TlInS_2$ Layered Crystals”
M. Isik, N. M. Gasanly and H. Ozkan, *Acta Phys. Pol. A* **115**, 732 (2009).
3. “Trapping centers and their distribution in $Tl_2Ga_2Se_3S$ layered single crystals”
M. Isik and N. M. Gasanly, *J. Phys. Chem. Solids* **70**, 1048 (2009).
4. “Thermally Stimulated Current Measurements in undoped Ga_3InSe_4 single crystals”
M. Isik and N. M. Gasanly, *J. Phys. Chem. Solids* **72**, 768 (2011).
5. “Trapping center parameters in In_6S_7 crystals”
M. Isik and N. M. Gasanly, *Physica B: Condensed Matter* **406**, 2650 (2011).
6. “Optical Constants of Layered Structured $Ga_{0.75}In_{0.25}Se$ Crystals from the Ellipsometric Measurements”
M. Isik, S.S. Cetin, N. M. Gasanly and S. Ozcelik, *Solid State Commun.* **152**, 791 (2012).

7. "Determination of Optical Parameters of $Ga_{0.75}In_{0.25}Se$ Layered Crystals"
M. Isik and N. M. Gasanly, *Cryst. Res. Technol.* **47**, 530 (2012).
8. "Absorption Edge and Optical Constants of $Tl_2Ga_2S_3Se$ Crystals from Reflection and Transmission, and Ellipsometric Measurements"
M. Isik and N. M. Gasanly, *Physica B: Condensed Matter* **407**, 2229 (2012).
9. "Ellipsometry Study of Interband Transitions in $TlGaS_{2x}Se_{2(1-x)}$ Mixed Crystals ($0 \leq x \leq 1$)"
M. Isik and N. M. Gasanly, *Opt. Commun.* **285**, 4092 (2012).
10. "Spectroscopic ellipsometry study of above-band gap optical constants of layered structured $TlGaSe_2$, $TlGaS_2$ and $TlInS_2$ single crystals"
M. Isik, N. M. Gasanly and R. Turan, *Physica B: Condensed Matter* **407**, 4193 (2012).
11. "Low-temperature Thermoluminescence in Layered Structured $Ga_{0.75}In_{0.25}Se$ Single Crystals"
M. Isik, E. Bulur and N.M. Gasanly, *J. Alloy. Compd.* **545**, 153 (2012).
12. "Dielectric functions and interband critical points of anisotropic chain structured $TlSe$ single crystals"
M. Isik and N.M. Gasanly, *J. Appl. Phys.* **112**, 083526 (2012).
13. "Interband transitions in gallium sulfide layered single crystals by ellipsometry measurements"
M. Isik, N. M. Gasanly and R. Turan, *Physica B: Condensed Matter* **408**, 43 (2013).
14. "Optical constants and interband transitions of anisotropic layered structured Tl_2GaInS_4 crystals by spectroscopic ellipsometry"
M. Isik, N.M. Gasanly and R. Turan, *J. Alloy. Compd.* **549**, 179 (2013).
15. "Low-temperature Thermoluminescence in Layered Structured $TlGaS_2$ Single Crystals"
M. Isik, E. Bulur and N.M. Gasanly, *J. Lumin.* **135**, 60 (2013).
16. "Temperature and excitation intensity tuned photoluminescence in $Ga_{0.75}In_{0.25}Se$ Crystals"
M. Isik, I. Guler and N.M. Gasanly, *Opt. Mat.* **35**, 414 (2013).
17. "Infrared and Raman scattering spectra of layered structured Ga_3InSe_4 crystals"
M. Isik, N.M. Gasanly and F. Korkmaz, *Physica B: Condensed Matter.* **412**, 61 (2013).

INTERNATIONAL CONFERENCES

1. **M. Isik**, N.M. Gasanly and H. Ozkan "Thermally stimulated current study of traps distribution in $Tl_2Ga_2Se_3S$ layered crystals" Condensed Matter Physics Conference of Balkan Countries, Muğla University, Muğla, Turkey (2008).
2. **M. Isik**, N.M. Gasanly and H. Ozkan, "Determination of Trapping Parameters in $Tl_2Ga_2Se_3S$ Layered Crystals from Thermally Stimulated Current Measurements" 26. International Physics Congress, Bodrum, Turkey (2009).
3. **M. Isik**, N.M. Gasanly and I. Guler, "Determination of Trapping Parameters in In_6S_7 Single Crystals from Thermally Stimulated Current Measurements" 28. International Physics Congress, Bodrum, Turkey (2011).

4. **M.Isik**, N.M.Gasanly and I.Guler, "*Low Temperature Photoluminescence in Ga_{0.75}In_{0.25}Se layered single crystals*" 29. International Physics Congress, Bodrum, Turkey (2012).
5. **M.Isik**, N.M.Gasanly and E.Bulur, "*Thermally stimulated current and thermoluminescence measurements on Ga_{0.75}In_{0.25}Se layered single crystals*" 29. International Physics Congress, Bodrum, Turkey (2012)

NATIONAL CONFERENCES

1. **M.Isik**, K.Goksen, N.M.Gasanly and H.Ozkan, "*Determination of Trapping Parameters in TlInS₂ Layered Crystals from Thermally Stimulated Current Measurements in the low Temperature*" 14. Yoğun Madde Fiziği Toplantısı, Hacettepe Üniversitesi, Ankara (2007).
2. **M.Isik**, N.M.Gasanly and H.Ozkan, "*Thermally Stimulated Current Measurements in TlInS₂ Layered Crystals in the 100-300K Temperature Range*" 15. Yoğun Madde Fiziği Toplantısı, Bilkent Üniversitesi, Ankara (2008).
3. **M.Isik**, N.M.Gasanly and H.Ozkan, "*Determination of Trapping Parameters in Tl₂Ga₂Se₃S Layered Crystals from Thermally Stimulated Current Measurements*" 16. Yoğun Madde Fiziği Toplantısı, Gazi Üniversitesi, Ankara (2009).
4. **M.Isik**, T.Yildirim, N.M.Gasanly and H.Ozkan, "*Thermally Stimulated Current Measurements in In₃S₅ Crystals*" 17. Yoğun Madde Fiziği Toplantısı, Ankara Üniversitesi, Ankara (2010).
5. **M.Isik** and N.M.Gasanly, "*Katkılanmamış Ga₃InSe₄ tek kristallerinde ısıtılarak akım ölçümleri*" 18. Yoğun Madde Fiziği Toplantısı, Orta Doğu Teknik Üniversitesi, Ankara (2011).